ABSTRACT

Title of Dissertation: MATHEMATICAL MODELING OF LATERALIZATION

AND ASYMMETRIES IN CORTICAL MAPS

Svetlana Levitan, Doctor of Philosophy, 1999

Dissertation directed by: Professor James A. Reggia
                            Applied Mathematics Program

Recent experimental work in neurobiology has defined asymmetries and lateralization in the topographic maps found in mirror-image regions of the sensorimotor cerebral cortex. However, the mechanisms underlying these asymmetries are currently not established, and in some cases are quite controversial. In order to explore some possible causes of map asymmetry and lateralization, several neural network models of cortical map lateralization and asymmetries based on self-organizing maps are created and studied both computationally and theoretically. Activation levels of the elements in the models are governed by large systems of highly nonlinear ordinary differential equations (ODEs), where coefficients change with time and their changes depend on the activation levels. Special metrics for objective evaluation of simulation results (represented as paired receptive field maps) are introduced and analysed. The behavior of the models is studied when their parameters are varied systematically and also when simulated lesions are introduced into one of the hemispheric regions. Some very sharp transitions and other interesting phenomena have been found computationally. Many of these computationally observed phenomena are explained by theoretical analysis of total hemispheric activation in a simplified model. The connection between a bifurcation point of the system of ODEs and the sharp transition in the model's computational behavior is established. More general understanding of topographic map formation and changes under various conditions is achieved by analysis of activation patterns (i.e., ω-limit sets of the above system of ODEs). This is the first mathematical model to demonstrate spontaneous map lateralization and asymmetries, and it suggests that such models may be generally useful in better understanding the mechanisms of cerebral lateralization. The mathematical analysis of the models leads to a better understanding of the mechanisms of self-organization in the topographic maps based on competitive distribution of activation and competitive learning.

MATHEMATICAL MODELING OF LATERALIZATION

AND ASYMMETRIES IN CORTICAL MAPS

by

Svetlana Levitan

Dissertation submitted to the Faculty of the Graduate School of the
University of Maryland at College Park in partial fulfillment
of the requirements for the degree of
Doctor of Philosophy
1999

Advisory Committee:

    Professor James A. Reggia, Chairman/Advisor
    Professor Jeffery M. Cooper
    Professor Royal B. Kellogg
    Professor V.S. Subrahmanian
    Professor Peter Wolfe

TABLE OF CONTENTS

LIST OF TABLES

LIST OF FIGURES

Chapter 1

Introduction

1.1 Motivations

The human brain consists of two *hemispheres*, and in most people one hemisphere can perform better on some tasks than the other. This is called *hemispheric specialization*. For example, usually the left hemisphere is dominant/specialized for control of hand movements (which is why most people are right handed, since each hemisphere controls the opposite side of the body) and for language. Conversely, the right hemisphere is dominant/specialized for facial expression and processing of spatial information. The term *lateralization* refers to one hemisphere being more specialized for a specific task than the other, as in these examples. Its causes and mechanisms are not well understood and are a subject of active research. Possible causes of lateralization include some anatomical asymmetries of the two hemispheres, biochemical differences, and the influence of the bundle of fibers connecting the two hemispheres, the *corpus callosum*. Whether the callosal influence is mostly excitatory (positive) or inhibitory (negative) is also not clear. Fig. 1.1 (taken from the online Webster dictionary [137]) shows one hemisphere of a split human brain, including the cross-section of corpus callosum. Better understanding of the causes, mechanisms and effects of brain lateralization can be very useful for biomedical applications, medicine, robotics, and other areas.

This dissertation focuses on studying a mathematical model of some aspects of the cerebral cortex as a means of obtaining a better understanding of some hypothesized causes of lateralization. The *cerebral cortex* is the convoluted layer of gray matter over the outside of the cerebral hemispheres (see Fig. 1) [1]. The cerebral cortex is the part of the brain most closely associated with cognition (language, memory, etc.). Of direct relevance to the research described here is that several sensory and motor *maps* are found across the surface of the cerebral cortex. Cortical maps are the parts of the cerebral cortex that represent some aspect of the environment in a topology-preserving fashion. Figure 1.2 (taken from [59]) shows schematically primary sensory and motor maps in the human brain. Every part of human body surface is represented in corresponding regions of sensory and motor cortex. For each body part this representation is continuous, but different parts take up different areas of cortex. Areas of cortex corresponding to hands and face, especially lips, are relatively large, while the areas representing body trunk are quite small. Stimulation of a particular body part will activate corresponding somatosensory cortex region, and activation of a motor
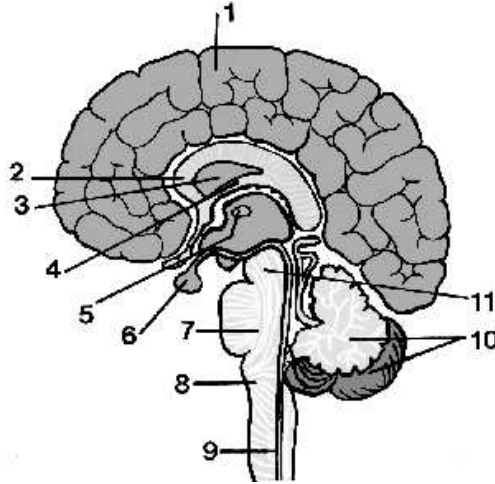
Figure 1.1: Human brain viewed medially after vertical midline sectioning: 1 cerebral hemi-sphere, 2 corpus callosum, 3 ventricle, 4 fornix, 5 thalamus, 6 pituitary gland, 7 pons, 8 medulla oblongata, 9 spinal cord, 10 cerebellum, 11 midbrain. Picture taken from [137].

cortex region will cause muscle contraction in the corresponding body part.

The goal of this research is to create a neural model of cortical map lateralization and asymmetry and to use it to examine possible causes and mechanisms of lateralization and the role of corpus callosum, both in the intact model and during recovery from a lesion (damage). Past work on understanding brain lateralization has largely focused on empirical research involving humans and animals. The concept of using mathematical/computational models of hypothesized mechanisms of lateralization is relatively new, and while some work has been done (see Chapter 2), this field is in its infancy. The intent is that the kind of theoretical work described here will complement experimental work on lateralization (which remains, after more than a century, very active) by critically examining in detail the implications of theories about its underlying mechanisms.

1.2   Accomplishments

This thesis describes a study with recurrently-connected neural models consisting of two hemispheric regions interacting via a simulated corpus callosum. The models are intended only as an abstract representation of two interacting cortical regions. The goal is to examine how these regions might influence map formation in one another. While the models are sim-plified from reality, they do capture some important neurobiological constraints: the model hemispheric regions have a spatial organization, their interconnections are roughly homotopic (each element is connected to the symmetric one and its neighbors), and they self-organize using unsupervised (Hebbian) learning. Activations of individual elements (of which the hemispheric regions are comprised) are governed by coupled nonlinear ordinary differential equations (ODEs), where coefficients (called weights) change with time and their changes depend on the activation levels. Simulation results are represented as pairs of receptive field maps. Special measures are introduced for numerical evaluation of the map organization,
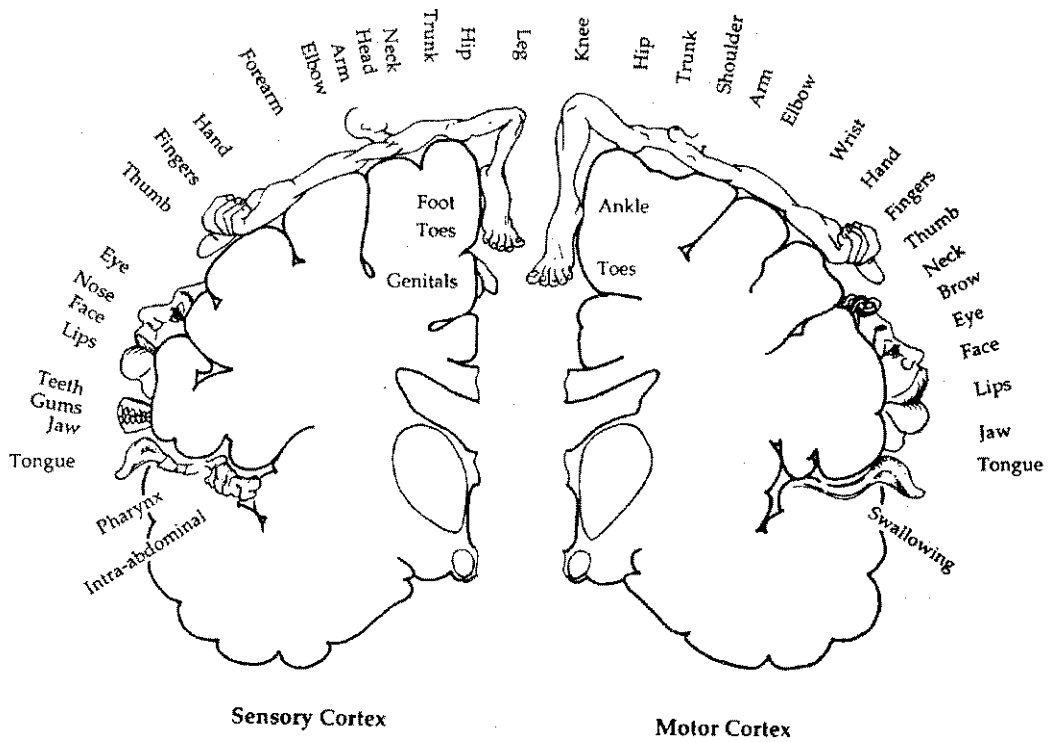
Figure 1.2: Diagram of the area of sensory and motor cortex devoted to different portions of the body. Each part of the human body is represented by a corresponding area in sensory and motor cortex in a topography-preserving fashion. This figure shows a vertical cross-section of a brain, through the sensory cortex for the left hemisphere and the motor cortex for the right one. Body parts represented by specific cortical regions are drawn and named next to them. Picture taken from [59].

lateralization, and mirror symmetry. Mathematical properties of those measures are proved.

Systematic variations of the models were studied through computer simulations. With each simulation the underlying assumptions about cortical region asymmetry and callosal excitatory/inhibitory strength were varied, and conditions resulting in map asymmetries were determined. The initial hypotheses were that map lateralization and asymmetries would arise from all of the underlying hemispheric asymmetries that were examined (cortical region size, excitability, plasticity, etc.), and that map lateralization and asymmetries would gradually occur as callosal connections became progressively more inhibitory. The actual situation proved to be more interesting, with only some factors causing persistent lateralization, and the existence of a sharp transition between callosal strengths leading to lateralization.

Many of these computationally observed phenomena are explained by theoretical analysis of total hemispheric activations in a simplified model. The connection between a bifurcation point of the system of ODEs and the sharp transition in the model's computational behavior is established. More general understanding of topographic map formation and changes under various conditions is achieved by analysis of activation patterns (i.e., ω-limit sets of the above system of ODEs). It is shown how the activation patterns forming in the cortical regions at the beginning of training can predict the map organization after training. Factors affecting the activation patterns are also discussed.

This is the first mathematical model to demonstrate spontaneous map lateralization and asymmetries, and it suggests that such models may be generally useful in better understanding the mechanisms of cerebral lateralization. The mathematical analysis of the models leads to a better understanding of the mechanisms of self-organization in the topographic maps based on competitive distribution of activation and competitive learning.

1.3 Overview

Chapter 2 provides some general background information on brain lateralization, cortical maps and their neural models, and then describes the S1 simulator which was used as a basis for the model in this study. Lateralization and asymmetries in the brain have been a subject of research in biology, psychology, cognitive science, and other disciplines for over a century. However, computer models of this phenomenon have appeared only recently and are very limited. Since this study deals with models of cortical maps, a brief review of previous models of cortical maps is also given. The S1 simulator is described in detail, including its architecture, connectivity, activation and learning rules, as well as visualization and interpretation of its results using a special software package `tmap`.

Chapter 3 describes a new model called S2 simulator, including its architecture, connectivity, activation dynamics, and learning rule. The model consists of two cortical regions interconnected by a simulated corpus callosum and receiving input from a single input layer. Activation levels of cortical elements (of which the cortical regions consist) are governed by a large system of nonlinear ODEs. The weights on connections from the input layer to the cortical regions (which serve as coefficients in the above system of ODEs) are initialized randomly and then change periodically based on the cortical activations. These changes are called *learning*. The chapter also explains how the numerical simulations were organized and

their results evaluated. The approach similar to the one used for the S1 simulator allows a quick qualitative estimate of map formation and lateralization. However, objective quantitative estimates are needed for a systematic study of simulation results with the S2 simulator. Metrics for objective topographic map organization, lateralization and mirror symmetry are introduced, and their properties analyzed. The metrics estimate map organization for each individual cortical region, lateralization and mirror symmetry for map pairs. Important mathematical properties of the metrics are proved.

Chapter 4 presents simulation results for a symmetric S2 model as well as for several cases when some asymmetries have been introduced into the model. For each model asymmetry dependence of map organization, lateralization, and mirror symmetry on callosal influences are studied systematically. Analysis of the results shows that not all asymmetries cause lateralization, and for most model variations there are sharp transitions in organization, lateralization and mirror symmetry values as functions of the callosal strength.

Chapter 5 contains results of the lesioning simulations and some analysis of them. Lesions are used to model the effects of brain damage resulting from an accident or a stroke. Lesions are introduced into the model by clamping activation levels for some cortical elements to zero. The effects of lesions on map formation are studied both acutely (immediately after the lesion) and chronically (after a retraining period), again for excitatory and inhibitory callosal connections. The effect of diaschisis (reduction in activation of the other hemisphere after a unilateral lesion) is observed with an excitatory corpus callosum. But participation of the other hemisphere in recovery after the lesion is mostly pronounced with inhibitory interhemispheric connections.

Chapter 6 presents another bihemispheric model of cortical maps called the S4 simulator. This model uses the same activation and learning rules as the S2 simulator but allows independent inputs to the two cortical regions from the contralateral sensory surfaces. This is closer in architecture to much of real primary sensory cortex. The model allows two different ways of computing receptive fields, and also the overlap of training inputs sent to the two cortical regions can be controlled. The effects of different degrees of training input overlap are studied, along with the effects of varying callosal influences on the map formation in the presence of various model asymmetries. Simulation results show that the most interesting phenomena occur when the training inputs are kept symmetric, so that the model is equivalent to the S2 simulator. This gives support to the previous model.

Mathematical analysis of the above (and some other) models is given in Chapter 7. First, it describes the results of theoretical analysis of the S1 simulator and similar models obtained by previous researchers. Then it explains the sharp transitions demonstrated in Chapters 4 and 6, and helps to understand better the topographic map formation in the models. For a slightly simplified S2 model, a system of linear ordinary differential equations (ODE) for total hemispheric activations is obtained and analysed. In most cases the system has one fixed point, which is asymptotically stable for excitatory and slightly inhibitory callosal connections, and asymptotically unstable for strongly inhibitory connections. The explanation of the effects of this change on map formation is given. Deeper analysis of activation patterns helps to explain some cases not explained by the first approach. It is shown how activation patterns observed in the cortical regions in the beginning of training can predict weight and map organization after training, and how the activation patterns

depend on model parameters.

Chapter 8 contains concluding remarks and suggestions for future work in this area.

Chapter 2

Background

To place the research in this dissertation in the context of related previous work, a brief summary of several issues is given. The experimental work on hemispheric asymmetries and lateralization that motivates this modeling is described, and some previous mathematical models of lateralization and cortical maps are characterized, establishing the novelty of the results presented here.

2.1   Hemispheric Asymmetries and Lateralization

Several behavioral cerebral asymmetries exist in humans, e.g., unilateral hemispheric dominance for language tasks, handedness, visuospatial processing, emotion and its facial expression, olfaction and attention [59, 120, 104, 36]. Much of the evidence for such qualitative and quantitative asymmetries came from studies of deficits in stroke and trauma patients, from special procedures applied to normal subjects and "split-brain" patients following commisurotomy [46], and from functional imaging studies of higher cortical functions and perceptual tasks [25]. There is enormous plasticity of the brain with respect to functional asymmetries. For example, left hemispherectomy in infants can result in the right hemisphere becoming remarkably skilled in language functions [39].

A distinction relevant to this research is that between individual and population lateralization. *Individual lateralization* refers to the fact that a specific function is asymmetrically supported by the two hemispheres. *Population lateralization* refers to the fact that not only is individual lateralization of a function occurring, but the lateralization tends statistically to favor one hemisphere over the other in a population. In this study we are concerned exclusively with individual lateralization.

While the above hemispheric specializations are well known, their underlying *causes* are not well understood. Some potentially relevant factors include hemispheric anatomical asymmetries [48, 81], higher-order dendritic branching [114], the ratio of gray matter to white matter [53], important neurotransmitters such as dopamine and norepinephrine [126], and the threshold for motor evoked potentials [82].

Another potential factor is hemispheric interactions via the largely homotopic connections of the corpus callosum [66, 98]. It is unclear at present whether the predominant influence of the corpus callosum is excitatory or inhibitory. For example, an excitatory in-

fluence is suggested by the cellular components involved (mainly pyramidal cell to spiny cell connections that are presumably excitatory), transcallosal diaschisis, and split-brain experiments [66, 134]. An inhibitory influence is suggested by the occurrence of lateralization, directly measured inhibitory transcallosal effects, and transcranial magnetic stimulation studies [34, 72, 125, 45, 87].

While lateralization and functional cortical asymmetries have been most prominently associated with higher cortical functions (language, spatial information processing, etc.), it has recently been demonstrated electrophysiologically that *topographic maps* in primary sensory and motor cortex also exhibit a rich range of patterns of individual lateralization and asymmetry [17, 92]. Topographic cortical maps are regions of the cortical surface that represent some aspect of the environment (visual space, body surface, etc.) in a topology-preserving fashion. In other words, they literally form detailed, two-dimensional mappings of various sensory input or motor output spaces [70, 127].

In one recent study with more than 100 animals, it was found that somatosensory, auditory and visual map asymmetries are almost always present in an individual animal's primary sensory cortex, even in the context of bilateral stimuli [17]. These map asymmetries were classified as qualitative (complete lateralization; 40% of animals), quantitative (partial lateralization; 30%), topographic (no lateralization but asymmetric spatial distributions or mosaic patterns; 10%), and quantitative-plus-topographic (lateralization and asymmetric spatial distribution; 20%). The dependence of asymmetries on callosal connectivity was shown by the fact that callosal sectioning generally caused a partial or complete loss of map asymmetries. Figure 2.1 (from [17]) illustrates direct and inverse dominance zones in several sensory regions of cortex.

In another series of experiments with six adult squirrel monkeys, detailed primary motor cortex forelimb maps were found to be both larger and more complex in the hemisphere opposite the preferred hand [92]. The causes of these map asymmetries are not known.

2.2 Past Computational Models

Neural models are a promising approach for developing a theoretical understanding of brain function and its disruption by stroke. In recent years neural models have increasingly been adopted to study neurological, neuropsychological and psychiatric disorders, with two international meetings being held on this subject at the University of Maryland since 1995 [108, 110].

2.2.1 Previous Neural Models of Hemispheric Interactions

While there have been many previous neural models of cerebral cortex, very few have examined aspects of hemispheric interactions via callosal connections. One model demonstrated that oscillatory activity in one hemisphere could be transferred to the other via interhemispheric connections [3, 4]. Another demonstrated that inhibitory callosal connections produced slower convergence and different activity patterns in two simulated hemispheres [35]. Additionally, a pair of error backpropagation networks were trained to learn a set of input-
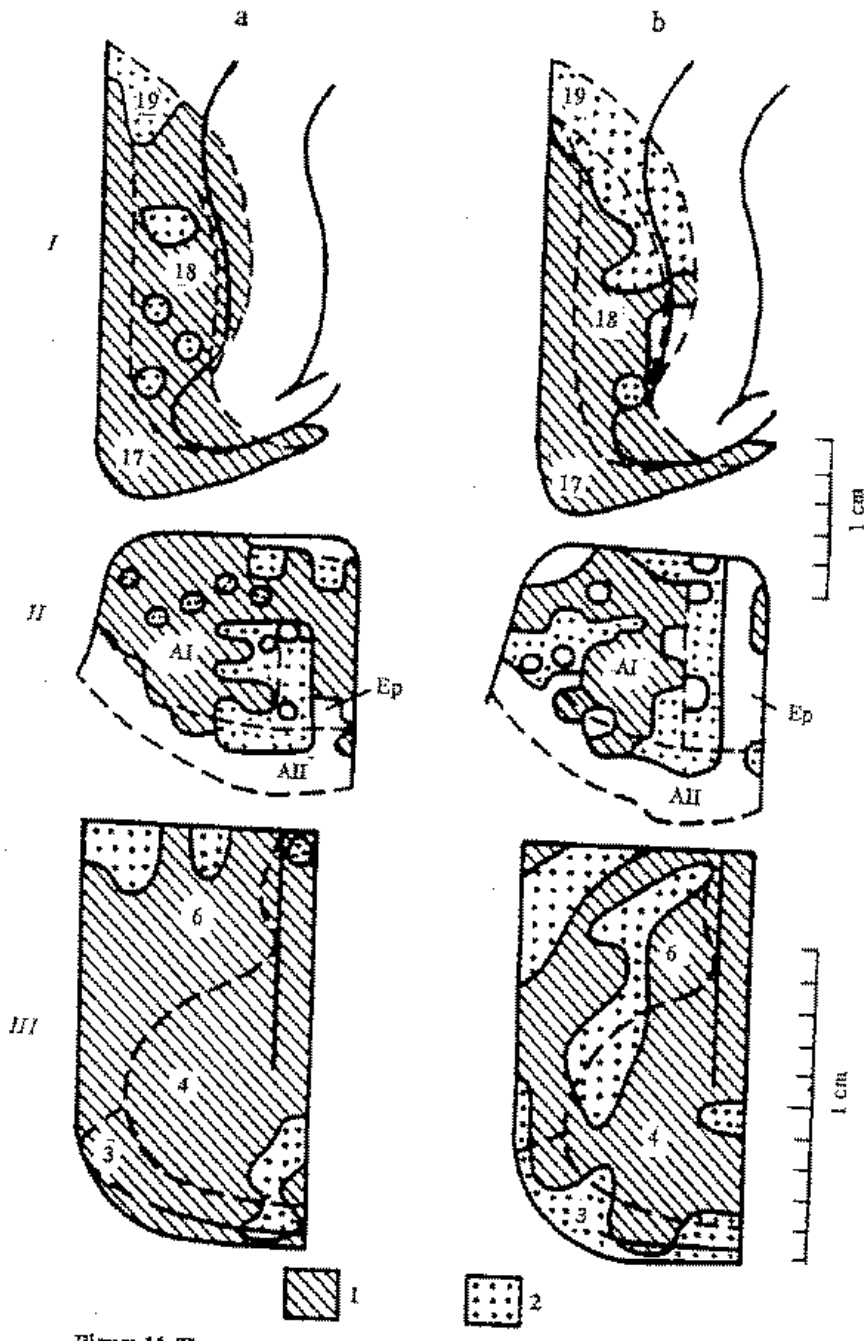
Figure 2.1: The topography of direct and inverse dominance zones in different cortical areas in cats before (a) and after (b) corpus callosum section. 1,2 – direct and inverse dominance zones; *I* – visual, *II* – auditory, *III* – sensorimotor cortical areas. All pictures display mosaic patterns. This picture is taken from [17].

9

output associations simultaneously, and it was shown that slow interhemispheric connections were not critical for short output times [112]. None of these previous neural models of hemispheric interactions examined the central issues in this research: lateralization of functionality through synaptic weight changes (learning), and the interhemispheric effects of simulated focal lesions. None of these past models incorporates the spatial organization of neocortex in their structure, the networks being fully/randomly connected (e.g., there could be no concept of cortical maps or focal lesions in these models). Other studies have related simulation results to their implications for lateralization, but did not actually model two hemispheric regions interacting via callosal connections [75, 24]. A recent mixture-of-experts backpropagation model examined how unequal receptive field sizes in two networks could lead to their specialization for learning spatial relations, but did not incorporate callosal connections or represent cortical spatial relationships [67].

Finally, there has been one symbol processing model of lateralization [76]. This model is neither a neural model nor a brain model. It does not demonstrate spontaneous lateralization of functionality (i.e., it starts with assumed partial lateralization), does not examine the interhemispheric effects of focal lesions, and does not represent cortical structure at all.

Thus, these past studies have generally not looked directly at how lateralization or asymmetry of functions can arise spontaneously. An exception is a couple of recent computational models developed in our research group in parallel with this study: of single word reading lateralization [109] and of letter identification by left and right simulated visual cortices [115]. In contrast to the work described in this dissertation, these were supervised learning models and they did not consider map lateralization.

2.2.2   Previous Models of Cortical Maps

Several neural network models of cortical maps have been described in the literature. None of these models involves multiple maps interacting via callosal connections, nor do they examine issues of lateralization or map asymmetry.

Von der Malsburg's model

One of the first computational models of cortical maps is the model of line orientation feature cells in visual cortex by von der Malsburg [129]. His model produces clusters of cortical cells that respond to similarly oriented input lines as a result of learning. Von der Malsburg showed that orientation sensitive cells develop when competitive learning was used. At the time, this was a major advance over previous thinking that genetically-predetermined, fixed strength connections are necessary to generate orientation sensitive cells [63].

Von der Malsburg's model simulates certain neurons found in cat and monkey primary visual cortex (area 17) [63, 64]. These neurons are selectively sensitive to line orientations, respond in clusters to stimuli, and form a computational map with respect to the ordering of the orientations of the visual line stimuli. His network had random weights initially and was trained using a competitive learning rule. This self-organizing network has the advantages of needing far less genetically encoded information for its construction, a high initial degree of plasticity, and an ability to adapt to a changing environment at any stage

in its development. The initial plasticity is necessary to explain studies with young kittens where their visual cortical behavior was clearly affected by their environment [61, 20, 21]. The ability to continuously adapt has obvious advantages and seems to occur in mammalian sensory cortical maps [68].

Kohonen's Self-Organizing Maps

Kohonen has done extensive research on the principles of map formation in artificial neural networks [74]. He showed that only a few basic principles are necessary for topographic map formation. The most basic ingredient is a two-dimensional layer of nodes with a neighborhood relationship which is usually defined in terms of lateral connectivity between the nodes. This can sometimes be viewed as a tessellation of a two-dimensional surface with the nodes at the vertices. The neighborhood relationship is important because the definition of a topographic map is that neighboring nodes must have similar responses to input stimuli. In other words, neighboring map nodes must have similar receptive fields (a node's receptive field is a region of a sensory surface in which input stimuli elicit a response in the node), and that similar input stimuli generate similar responses in the output layer. The second ingredient is an activation rule for the output-layer nodes which generates similar responses for a node when that node is presented with similar input stimuli. The third ingredient is a learning rule which enables neighboring nodes to learn to have similar responses to input stimuli. The fourth ingredient is a lateral interaction mechanism among neighboring nodes which forces them to learn to have similar responses to input stimuli. The last ingredient, which is only necessary in order to have a globally consistent topographic map, is a mechanism for smoothing out the topographic map between local neighborhoods.

In order for a learning rule to insure that output-layer nodes have similar responses to similar input stimuli, a measure of similarity for input stimuli must be defined. The two most common measurements of similarity for vector stimuli are the Euclidean distance between the vector endpoints and the angle between the vectors as measured by the normalized dot product. The activation rule must insure that for each node similar input stimuli produce similar responses. The learning rule must insure that a node which learns for a given input stimulus will in the future be more responsive to similar input stimuli and less responsive to dissimilar input stimuli. Thus, a node must learn for the input stimuli to which it responds.

In order to have a topographic map, neighboring nodes must have similar responses to any given input stimulus. To achieve this, neighboring nodes must have similar incoming weight vectors which is accomplished by having neighboring nodes learn for highly overlapped sets of input stimuli. Excitatory lateral connections between neighboring cortical nodes can help them to learn for many of the same input stimuli, so their incoming weight vectors become similar.

The Biologically Oriented Models of Pearson, Grajski, Obermayer

The Pearson model is constructed of two two-dimensional layers: an input layer representing the hand, and an output layer representing a portion of S1 somatosensory cortex [101]. Nodes in the hand layer project in a divergent but topographically ordered fashion to the

cortical layer. Nodes in the cortical layer model actual neurons, excitatory and inhibitory. The excitatory cortical nodes are the only ones receiving direct input from the land layer, inhibitory cortical nodes provide indirect lateral inhibition between the excitatory cortical nodes. The spread of activation is governed by a typical noncompetitive activation rule, but the learning rule is essentially competitive.

In the Pearson model the hand layer is subdivided into glabrous and dorsal regions, each cortical node receives connections from both types of regions. There is also learning on the excitatory connections between cortical nodes. The network is trained with small contiguous rectangular patches. Tight, stable clusters of cortical nodes tend to form after training. The model is able to account for experimental data that shows intermingled glabrous and dorsal cortical regions.

The Pearson model is able to show some topographic map refinement with training, and map reorganization in response to repeated finger stimulation. One of the drawbacks of the Pearson model is that topographic map formation is not measured or plotted in a very accurate way.

The Grajski model focuses on accounting for the "inverse magnification rule", which states that there is an inverse relationship between cortical magnification and receptive field size [52]. The cortical magnification of a skin region is the area of the cortical region which responds to the stimulation of a unit area of skin within the given skin region. The receptive field size of a cortical neuron is the area of the skin region which, when any portion of that skin region is stimulated, causes the cortical neuron to alter its response/activation level. The model shows how the dynamic instances of the inverse magnification rule can be accounted for with learning.

The Grajski model is similar to the Pearson model in structure and connectivity, but the hand layer is not divided into glabrous and dorsal regions, and there is an additional intermediate "subcortical" layer. The subcortical layer is used to increase the area of projection from the hand layer to the cortical layer and to allow the subcortical layer to dynamically affect the cortical inputs. The model uses a typical noncompetitive activation mechanism and a version of competitive learning. Again, no accurate plot of the detailed structure of the topographic map is provided.

The Grajski model is used to perform three types of simulations: topographic map refinement, topographic map reorganization due to repetitive finger stimulation, and topographic map reorganization due to a focal cortical lesion. The model maintains the inverse magnification rule for both topographic map reorganizations. However, in order for the model to achieve map reorganization after a focal cortical lesion, Grajski and Merzenich have to resort to randomizing all remaining weights and enhancing cortical excitation, so the reorganization is not spontaneous.

The Obermayer model [93] is a more general noncompetitive activation model explicitly based on the work of Kohonen. It has full connectivity between its two layers: hand layer and cortical layer. That allows greater flexibility for topographic map formation, but the absence of an initial coarse map makes learning more difficult.

A major weakness of Kohonen topographic networks in general, and the Obermayer model in particular, is the reliance on so called "shortcuts" (global operations) in place of actual

activation dynamics. Another weakness for brain modeling is that the required full connectivity between the input and output layers is not neurophysiologically plausible. For the Obermayer model, an output (cortical) node is designated the "winner" for a specific input stimulus if the dot product of the input vector and the winner's incoming weight vector is the largest dot product of the input vector with each of the input nodes' incoming weight vectors (note that this is a global, neurophysiologically-implausible operation). Lateral connections are then postulated (but not implemented) that would generate a Gaussian activation response of fixed amplitude and width (the width also slowly decreases with time) regardless of the actual inputs to the cortical nodes. No activation dynamics are given or modeled to account for this response behavior; the desired activation levels are simply instantiated in the cortical layer. This places a heavy burden on the postulated global lateral interactions for which no implementation has ever been demonstrated. The Gaussian activation response might be a reasonable approximation of a localized central-excitation, peristimulus-inhibition response, which has been implemented with lateral excitatory and inhibitory interactions, but the very large initial width and the slow decrease in width over time of the Gaussian activation response have yet to be implemented with lateral interactions. Regardless of these modeling approximations, results from Kohonen topographic networks still provide intuition for analyzing realistic models of topographic neural networks.

The Obermayer model also generalizes the Kohonen plotting technique for topographic maps in a way very similar to the plotting techniques developed for the competitive activation S1 model (described in section 3.1). The Obermayer model plots the center of each cortical node's incoming weight vector as a point and connects the points of neighboring cortical nodes with lines. The Obermayer model also calculates a weighted width of the cortical nodes' incoming weight vectors similar to the competitive activation S1 width definition, but does not plot these widths as is done for the competitive activation S1 model. The Obermayer model shows that, when contiguous patches are used as input, complete topographic map formation often takes place but that sometimes topographic defects in the map are present. The defects are a result of local conflicts in the map which are not smoothed out by the initial global processing. The Obermayer model uses both analysis and simulations to show that the width of cortical nodes' incoming weight vectors (and correspondingly the size of their receptive fields) is proportional to both the size of the input patches and the final size of the central-excitation activation response.

Other Recent Models of Cortical Maps

A self-organizing model of motor-control and sensorimotor maps was developed and studied recently [31, 30]. The maps developed clusters of elements responsible for each of the six "muscles" of a simulated arm. The alignment of clusters and their reorganization after a simulated lesion were studied both computationally and analytically. But this work didn't consider topographic maps or lateralization.

Finally, a self-organizing model of topographic maps (S1 simulator) using competitive distribution of activation was developed by Sutton, Reggia, and others [123, 124]. In contrast with the models described in this thesis, the S1 model has a single cortical region. It is the subject of the next section.
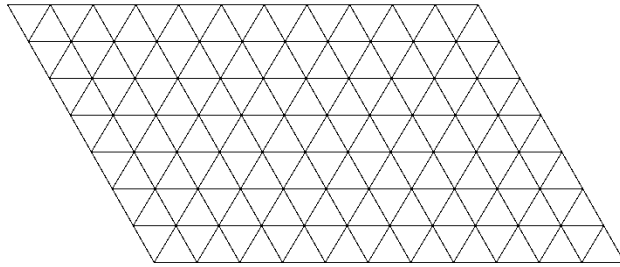
Figure 2.2: Internal structure (hexagonal tessellation) of the sensory surface and the cortical region. Each vertex represents a node. Each node's six nearest neighbors are equidistant.

2.3   S1 Simulator

The Neural Modeling group at the Department of Computer Science at UMCP has developed an artificial neural network model of topographic maps which has been shown to reproduce not only map refinement from initial very coarse topographic representation, but also map plasticity exhibited under certain conditions, such as repetitive stimulation of a small area or lesions of sensory[1] or cortical regions [5, 6, 33, 123, 124, 133]. The model (called the S1 simulator) is built on the ideas of self-organization, competitive distribution of activation and competitive learning. The *bihemispheric* models studied in this dissertation are based in part on extending ideas from the S1 simulator, so it is described in detail here (following [123]).

The competitive activation S1 model is a crude representation of a portion of the sensory surface and primary somatosensory (body sensation) cortex. The model assumes the existence of a coarse initial topographic map from the sensory surface to the cortex (due to limited topographic connectivity between the sensory surface and the cortex). This initially coarse map is then tuned by training the model with various inputs. The resulting well-tuned topographic map becomes smooth and regular.

2.3.1   Connectivity

The model consists of two separate layers of nodes representing the sensory surface and the cortex. The input layer has no lateral connections and is assumed to have a well-defined topographic organization with respect to the sensory inputs. However, input nodes are more than just relays because they competitively distribute their output, and the weights from sensory to cortical nodes are adaptive. The cortical layer is treated as a two-dimensional sheet of nodes which are connected laterally in a regular fashion (Fig. 2.2). All cortical nodes have similar cortico-cortical and sensory-cortical connections. This is accomplished by connecting together the opposite edges of the two-dimensional cortical sheet to form a

---

[1]Technically this was viewed as representing the *thalamus*, a sensory way station along the afferent pathway from body surface to cortex [124]. For simplicity, I will refer to this layer consistently as the "sensory layer" or "input layer" in the following.

torus, which is done to eliminate edge effects. The cortical nodes represent cortical columns; a cortical column being a group of cooperating cells within a small volume element in cerebral cortex.

The competitive activation S1 model has two kinds of connections: sensory-cortical and cortico-cortical. Each input node sends connections to a different topographically defined subset of the cortical nodes (Fig. 2.3). Each cortical node sends connections to its six nearest neighbors (Fig. 2.2). All connections in S1 model are excitatory and competitive.
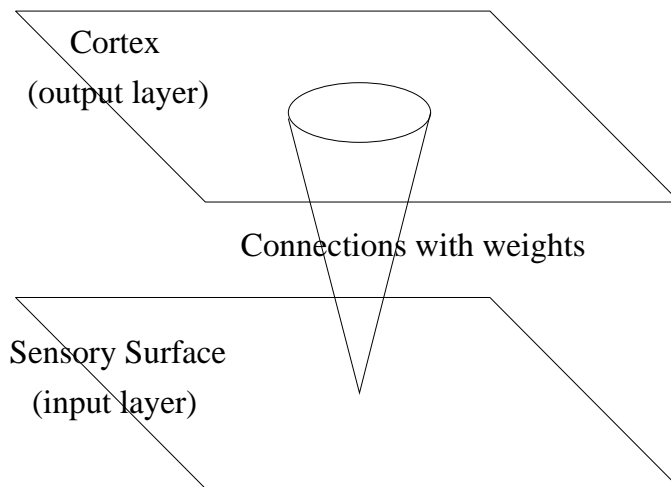
Figure 2.3: Topographical projection of sensory-cortical connections from one input node in the sensory surface to the cortical layer in the $S1$ simulator. Each sensory node sends activation to the corresponding cortical node and its neighbors within a certain radius. The weights on connections from the sensory surface to cortex change during learning.

Using the same number of nodes and the same hexagonal structure for sensory and cortical layers produces a one-to-one correspondence between input and cortical nodes and allows the use of a notion of "hexagonal radius". An input node normally connects to its corresponding cortical node and its neighbors within hexagonal radius of 4. The weights on these connections are initialized randomly: with probability 1/2 a weight is assigned the minimum weight value (0.0001); otherwise, the weight is randomly chosen with a uniform probability from the range between the minimum and maximum weight values. Each cortical node connects to its neighbors at hexagonal radius 1, and the weights on these connections are assumed to be equal.

2.3.2   Activation Rule

Competitive distribution of activation was first described in [105]. Its essence is described below.

The update rule chosen for the competitive activation S1 model is designed to keep the activation level bounded between zero and a specified maximum value Max. The activation

a_j of cortical node j is governed by the differential equation

$$\frac{d}{dt}a_j(t) = c_s a_j(t) + (Max - a_j(t))in_j(t) \tag{2.1}$$

where c_s is a self-connection constant (usually negative, also called self-inhibition); the outputs of sensory nodes, via the weighted afferent connections, as well as the outputs of other cortical nodes, via intracortical connections, are included in the $in_j(t)$ term: $in_j(t) = \sum_j outs_{ji}(t) + \sum_k outc_{ki}(t)$. The activation of sensory node j is also determined by (2.1), but for sensory nodes the $in_j(t)$ term only represents the input from sensory receptors.

The output dispersal rule for S1 model sensory surface is

$$outs_{ji}(t) = c_p \left(\frac{w_{ji}(t)(a_j(t) + q)}{\sum_k w_{ki}(t)(a_k(t) + q)} \right) a_i(t) \tag{2.2}$$

where the constant q is a small positive number which serves two purposes: it varies the competitiveness of the output rule and prevents the denominator in (2.2) from ever being zero, even when all $a_k(t)$ are zero. For the cortex the output dispersal rule is similar, but since all weights on lateral connections between nearest neighbors are equal, we have:

$$outc_{ji}(t) = c_{lf} \left(\frac{a_j(t) + q}{\sum_k (a_k(t) + q)} \right) a_i(t) \tag{2.3}$$

2.3.3   Unsupervised Learning

Learning in the Neural Networks usually proceeds by updating weights on connections between elements and falls into one of the three categories: supervised learning, reinforcement learning, and unsupervised learning. The term "supervised learning" refers to the situation when a neural network must learn a number of given input-output pairs, and then it can generalize by finding an appropriate output for a new input. Reinforcement learning happens when the network's response to each input receives some kind of a grade, but no correct output is specified. Finally, unsupervised learning (often also called self-organization) means that a network must discover some features or categories in the data it receives and find an appropriate output for each input without any additional information (i.e. without a "teacher").

The S1 simulator uses unsupervised learning for map formation. One way of implementing unsupervised learning is Hebbian learning. The term "Hebbian learning" refers to a method which increases the weights on connections between active elements. It is based on the hypothesis by Hebb [56] that in a real brain a connection between two firing neurons gets stronger. This method works well, but has one serious drawback: it allows weights to grow without bounds. There are several modifications of the method, intended to keep the weights bounded, including Oja's rule [95], Linsker's, Yuille's, and others [60].

Competitive learning rule [60, p.220] increases the weights between active input and output elements and decreases the weights on connections from inactive input to active output elements, so that the entire weight vector remains normalized in some norm.

Input stimuli in the form of hexagonal patches of radius 1 with centers located randomly on the sensory surface are used to drive the self-organization. Input stimuli are induced on the thalamic layer by providing input to specific sensory nodes. Since there are no lateral connections in the sensory layer, this leads to activation of only the nodes receiving positive input, i.e. the nodes in a hexagonal patch of radius 1. Input stimuli of larger radius are also possible.

After the activation in both layers converges to a stable distribution, sensory-cortical weights are updated according to the competitive learning rule

$$\Delta w_{ji} = \epsilon(a_i - w_{ji})a_j \tag{2.4}$$

where ϵ is the *learning rate*.

Initially, a randomly generated incoming weight for each cortical node is normalized so that $\sum_i w_{ji} = 7$, provided that input patches of radius 1 are used. Then, after an update according to (2.4), the total change in the incoming weight for the cortical element j is

$$\sum_i \Delta w_{ji} = \epsilon \sum_i (a_i - w_{ji})a_j = \epsilon a_j (\sum_i a_i - \sum_i w_{ji}) = \epsilon a_j (7 - 7) = 0 \tag{2.5}$$

Thus, the weights remain normalized.

2.3.4 Receptive Field Calculation and Representation

The *receptive field* of a cortical element is the set of sensory elements that, when stimulated, affect that cortical element's activation. In order to study and visualize topographic map formation in S1 model the following quantitative approach to evaluating receptive fields was used by Sutton [123]. A cortical node's receptive field is defined to be that node's responses to the sensory point stimulus set (which is taken to accurately reflect the topography of the sensory surface). This is measured by a procedure where every sensory node is stimulated, one node at a time using an input of 1.0, and the cortical response is recorded.

In order to compute the center and width of the receptive field, the sensory point stimuli are given explicit x, y coordinates. The uniform tesselation of the cortical layer and the fact that the input layer has a one-to-one correspondence with the cortical layer imposes a relative coordinate system on the sensory nodes. The distance between nearest neighbors is defined to be one "unit". The coordinates are always assigned so that the sensory node corresponding to the cortical node whose receptive field is being computed is at the origin. The x-axis is aligned so that one of the nearest neigbors of the node has coordinates (1,0). The following formulas are used to determine the center, width in the x dimension, width in the y dimension, and the total response of the receptive field for cortical node j:

$$tr_j = \sum_i a_{ji} \ , \tag{2.6}$$

$$cx_j = \left(\sum_i x_i a_{ji} \right) / tr_j \ , \quad cy_j = \left(\sum_i y_i a_{ji} \right) / tr_j \ , \tag{2.7}$$

$$rx_j = \sqrt{\left(\sum_i (x_i - cx_j)^2 a_{ji} \right) / tr_j} \ , \quad ry_j = \sqrt{\left(\sum_i (y_i - cy_j)^2 a_{ji} \right) / tr_j} \ , \tag{2.8}$$

where a_{ji} is the activation level of cortical node j when a point stimulus is applied at sensory node i, tr_j is the total response of cortical node j summed over all of the sensory point stimuli, x_i and y_i are the coordinates of sensory node i, cx_i and cy_i are the coordinates for the center of cortical node j's receptive field, and rx_j, ry_j are the horizontal and vertical "radii" of cortical node j's receptive field. The coordinates of the receptive field represent locations in the sensory layer.

The receptive fields are used to measure topographic map formation. The cortical connectivity defines a two-dimensional ordering of the cortical nodes and the cortical receptive field centers define a two-dimensional ordering of the cortical responses. A topographic map is plotted by placing points at the computed centers of the receptive fields and connecting any two points which represent cortical nodes which are nearest neighbors.
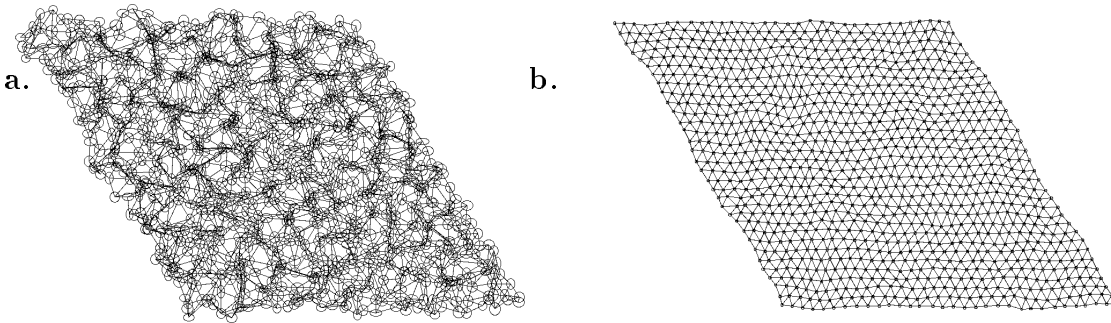
Figure 2.4: Some results from the S1 simulator. Receptive field maps **a.** before training and **b.** after training. The map before training is uneven, and receptive field sizes (represented by ellipses) are large. After training the map is smooth and receptive fields become small.

This approach to representing map organization is illustrated in Fig. 2.4, produced by a software graphics package `tmap` implemented by C.Lynne D'Autrechy and later modified by David Montgomery. Specifically, each of the two pictures in Fig. 2.4 plots the centers of receptive fields of a cortical region in the space of the sensory surface (i.e., it is *not* a picture of the cortical regions involved). For example, the vertices (nodes) in the right picture represent the centers of the receptive fields of the cortical region after training plotted in the space of the sensory surface in Fig. 2.3. Each pair of receptive field centers (vertices) of nearest neighbor cortical elements is connected by a line segment, so there are six line segments for each vertex. The entire grid in this picture shows that a fairly organized map is present in the cortical region (i.e., the sensory surface projects in a smooth fashion onto the two-dimensional cortex surface), the typical result found after learning is complete. In contrast,

Fig. 2.4a illustrates a case before training, when the connection weights are random and no organized regions are present. Also, in both pictures in Fig. 2.4, each vertex is encircled by a small ellipse centered on the vertex that indicates the relative x and y radii of the receptive fields computed as described above. Along with regular receptive field locations, small receptive fields (e.g., Fig. 2.4b) generally indicate highly organized map regions, while larger ones (e.g., Fig. 2.4a) indicate poor map formation.

Chapter 3

Basic S2 Model and Research Methods

This chapter describes a bihemispheric model of cortical maps called the S2 model, experimental methods and baseline parameter set, and the metrics used to evaluate results of the simulations.

3.1 The S2 Model

3.1.1 Connectivity

The methods used in the S1 model of a single hemisphere self-organizing map [6, 124] described in Chapter 2 were adopted to a two-hemisphere model. The S2 model consists of two cortex regions interconnected via a corpus callosum, and receiving input connections from a two-dimensional sensory surface, as shown in Fig. 3.1. Each hemispheric region or cortical layer represents a small patch of cerebral cortex. The model cortices are two–dimensional, with individual elements representing cortical columns. These elements hexagonally tessellate the cortex, with each element having excitatory connections to its six nearest neighbors. Each cortical element connects via the corpus callosum to those elements lying within a certain hexagonal radius R_{cc} of the element homotopic to it in the opposite hemisphere. In most of our simulations the sensory surface and both cortical sets have the same number of elements. Each sensory element sends input to its two corresponding cortical elements, one in each of the hemispheres, and their neighbors within certain radii R_L and R_R. As is often done in simulations of this sort to avoid edge effects, the opposite edges of a hemispheric region are connected (forming a torus).

The model architecture (with a single sensory surface) minimizes the likelihood that asymmetries in input stimuli themselves would lead to lateralization/asymmetries in maps (i.e., as opposed to intrinsic hemispheric asymmetries or callosal influences). This model can only be related to cortical regions receiving bilateral inputs, such as visual cortex for midline retinal areas [122, 96, 44], or to special experimental situations where matched bilateral input stimuli are used [17]. Later in this dissertation (chapter 6), a model with two sensory surfaces is considered.

Unsupervised competitive learning occurs on the connections from sensory surface S to the left and right cortical sets L and R. Weights on these connections are initialized with
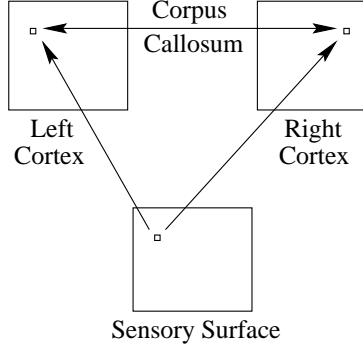
Figure 3.1: The model of two interacting cortical regions.

random values between 0.0001 and 1.0. Sensory stimuli in the form of random seven-element hexagonal patches of activation are applied to drive the self–organization of the model.

3.1.2   Activation Rule

Activation and learning rules from S1 model were adopted for two hemispheres connected by a corpus callosum. A real–valued activation level $a_i^L(t)$ is associated with the ith element of the left cortical region, $a_i^R(t)$ with the right homotopic element, and $a_i^S(t)$ with the corresponding element of the sensory surface. Just the equations for the left hemisphere are given; those for the right are analogous. Activation $a_i^L(t)$ is governed by:

$$da_i^L/dt = in_{Li}^+(M - a_i^L) + (c_s + in_{Li}^-)a_i^L \qquad (3.1)$$

where $c_s < 0$ is a self-inhibition constant, $M > 0$ is the maximal activation level, and initial activation levels are all zero. With an inhibitory corpus callosum,

$$in_{Li}^+ = \sum_j c_{ij}^{LL} a_j^L + \sum_k c_{ik}^{LS} a_k^S, \qquad (3.2)$$

$$in_{Li}^- = \sum_m c_{im}^{LR} a_m^R. \qquad (3.3)$$

The sums in (3.2) range over the six immediate neighbors j in the same cortical hemisphere, and over elements k in the sensory surface that send input to i. Index m in inhibitory input in_{Li}^- ranges over elements in the opposite hemisphere within radius R_{cc} of the element homotopic to i. When the corpus callosum is excitatory, the callosal term $\sum_m c_{im}^{LR} a_m^R$ instead is added into in_{Li}^+, and self-inhibition is increased to prevent excessive hemispheric activation using $in_{Li}^- = -2.6K$, where K is the *callosal connection strength*.

Note that biological callosal *connections* are presumably excitatory, as discussed in Chapter 2, but the resultant transcallosal *influences* of one hemisphere on the other have often been argued to be inhibitory or competitive [34, 38, 72]. The parameter K reflects this resultant influence.

A "Mexican Hat" pattern of lateral interactions occurs in biological cortex and is widely used in neural models of self-organizing maps [74]. As in earlier models, this is achieved by having each sensory element competitively distribute its output among the receiving cortical elements, and each cortical element among its nearest neighbors, using

$$c_{ik}^{LS} = c_p^L \frac{w_{ik}^L(a_i^L + q)}{\sum_n w_{nk}^L(a_n^L + q)}, \qquad c_{ij}^{LL} = c_{lf}^L \frac{a_i^L + q}{\sum_n (a_n^L + q)}. \tag{3.4}$$

Here q is a small constant (0.0001), c_p^L and c_{lf}^L are the *input sensitivity* and *lateral feedback* constants for the left hemisphere, and the sums in the denominators are over all elements of one hemisphere connected to the given source of activation. Such competitive distribution of activation has repeatedly been shown in the past to produce Mexican Hat activation patterns and topographic map formation similar to those produced by inhibitory connections [105, 6, 124].

Intercortical connections work in a similar manner. Callosal strength to the left from the right hemisphere is designated as K^{LR}, and to right from left as K^{RL}, using just K when these are the same as is usually the case. For inhibitory callosal connections $(K < 0)$, we use

$$c_{im}^{LR} = K^{LR}(\sum_n a_n^L + q)^{-1}.$$

to normalize total callosal signal. For excitatory corpus callosum $(K > 0)$, the influence of the opposite hemisphere is distributed competitively, with K^{LR} playing the role of c_p^L in (3.4):

$$c_{im}^{LR} = K^{LR} \frac{a_i^L + q}{\sum_n (a_n^L + q)}. \tag{3.5}$$

3.1.3 Learning Rule and Receptive Field Calculation

Learning occurs only on the connections from the sensory surface to the cortical regions. Self–organization proceeds according to an unsupervised learning rule

$$\Delta w_{ik}^L = \epsilon_L(a_k^S - w_{ik}^L)a_i^L, \quad \Delta w_{ik}^R = \epsilon_R(a_k^S - w_{ik}^R)a_i^R, \tag{3.6}$$

where ϵ_L, ϵ_R are the left and right hemisphere *learning rates*.

Receptive fields for the cortical nodes in S2 simulator are calculated very similarly to S1 simulator. Again, sensory nodes are activated, one at a time, and responses in both cortical sets are recorded. Then the responses in the left cortical set are used to compute the receptive fields for the cortical elements in that set using formulas (2.6)–(2.8), and similarly in the right.

3.2   Experimental Methods

The procedure followed in the computer simulations reported in the following chapter consists of the following stages:

1. weights on sensory-cortical connections are initiated randomly;

2. the following is repeated thousands of times:

   (a) a randomly centered hexagonal patch of radius 1 (or 2 for the S4 simulator described in Chapter 6) is applied as input to the sensory surface;

   (b) activations in the sensory surface and both cortices change starting from 0 according to the ODEs (3.1) until they reach a stable pattern;

   (c) sensory-cortical weights are updated according to the learning rule (3.6);

3. point stimuli are applied to the sensory surface (each node, one at a time) and cortical responses are recorded as described in 2.3.4;

4. receptive fields are computed (and may be plotted for visualization of results);

5. measures of organization, lateralization and mirror symmetry are computed.

Using the two hemispheric region model described above, several series of simulations were performed while parameters were varied systematically. For a baseline parameter set the values shown in Table 3.1 were used. One parameter at a time was altered and the

symbol	meaning	baseline value
size	number of elements in a cortical set	16x16
K^{LR}, K^{RL}	callosal strengths from R to L and back	varies
K	callosal strength when $K^{LR} = K^{RL} = K$	varies
c_p^L, c_p^R	input sensitivity in L and R	1.0
c_{lf}^L, c_{lf}^R	lateral feedback in L and R	0.6
c_s	self-inhibition constant	-2.0
M	maximal activation constant	3.0
R_{cc}	radius of corpus callosum connections	5
R_L, R_R	radii from S to L and R	3
ϵ_L, ϵ_R	learning rates for L and R	0.01

Table 3.1: Baseline Parameter Values; L and R denote left and right cortex, S sensory surface.

resulting map organization, lateralization, and asymmetry were studied for callosal strengths K ranging from -4 (strongly inhibitory) to +3 (strongly excitatory). Roughly 30 simulations were performed for each model asymmetry, and about 40 simulations were done for the

symmetric case. The program was implemented in programming language C, and simulations were run on Sun SPARCstations.

Model variations described below where callosal connections were effectively absent (K=0, or very small K values) are most consistent with much of primary sensorimotor cortex which has sparse callosal connections, while model variations with larger callosal weights and receiving matched bilateral input stimuli are most consistent with axial/midline sensory cortex which has significant callosal connections. For maximal comparability, the same seed for random weight generation was used in most runs. This seed was chosen as causing the least lateralization in the symmetric case in numerous simulations with different seeds. However, all major findings were verified by additional simulations with several different seeds.

3.3   General Nature of Bihemispheric Maps

We now consider some specific examples of maps occuring with the S2 model, both to make subsequent discussion more concrete, and for reference to make the metrics introduced in the next section more intuitive.

Fig. 3.2 shows representative examples of the maps observed during simulations with versions of the S2 model. Each part of Fig. 3.2 presents a pair of images indicating the topographic maps for a pair of corresponding symmetric cortical regions like those illustrated in Fig. 3.1.

Maps in Fig. 3.2 involve equal size cortical regions (both 16 x 16) except for (j) where the right cortical region is smaller (12 x 12). The smaller right region in Fig. 3.2j is evident in that more vertices are plotted in the left picture. Inspection of these pairs of maps shows that in some cases maps are *disorganized bilaterally*, as in Fig. 3.2a–c. In other cases, the maps are well *organized bilaterally* (Fig. 3.2d), or on just one side (Fig. 3.2g,h). Finally, in some cases maps may form *mosaic patterns* that divide up the sensory surface in complementary ways as occurs experimentally [17], either in roughly equal (Fig. 3.2e) or quite unequal shares (Fig. 3.2f,i,j).

3.4   Metrics

In addition to visual inspection of the resulting maps, the degree of cortical map organization, lateralization and mirror symmetry were measured using metrics described in our joint work [2]. Objective quantitative estimates of map organization, lateralization, and symmetry are necessary for a systematic study of the effects of various model parameters on map formation and lateralization. Although objective in nature, these measures have been shown to correlate fairly well with subjective estimates (see Discussion at the end of this Chapter). Briefly, the measures are:

Organization measure: indicates the degree of topographic map formation in a single hemispheric region on a 0 (no map forms) to 1 (nearly perfect map) scale.

Lateralization measure: ranges from -1, indicating complete map formation on the left and no map on the right, to 1 indicating the opposite.
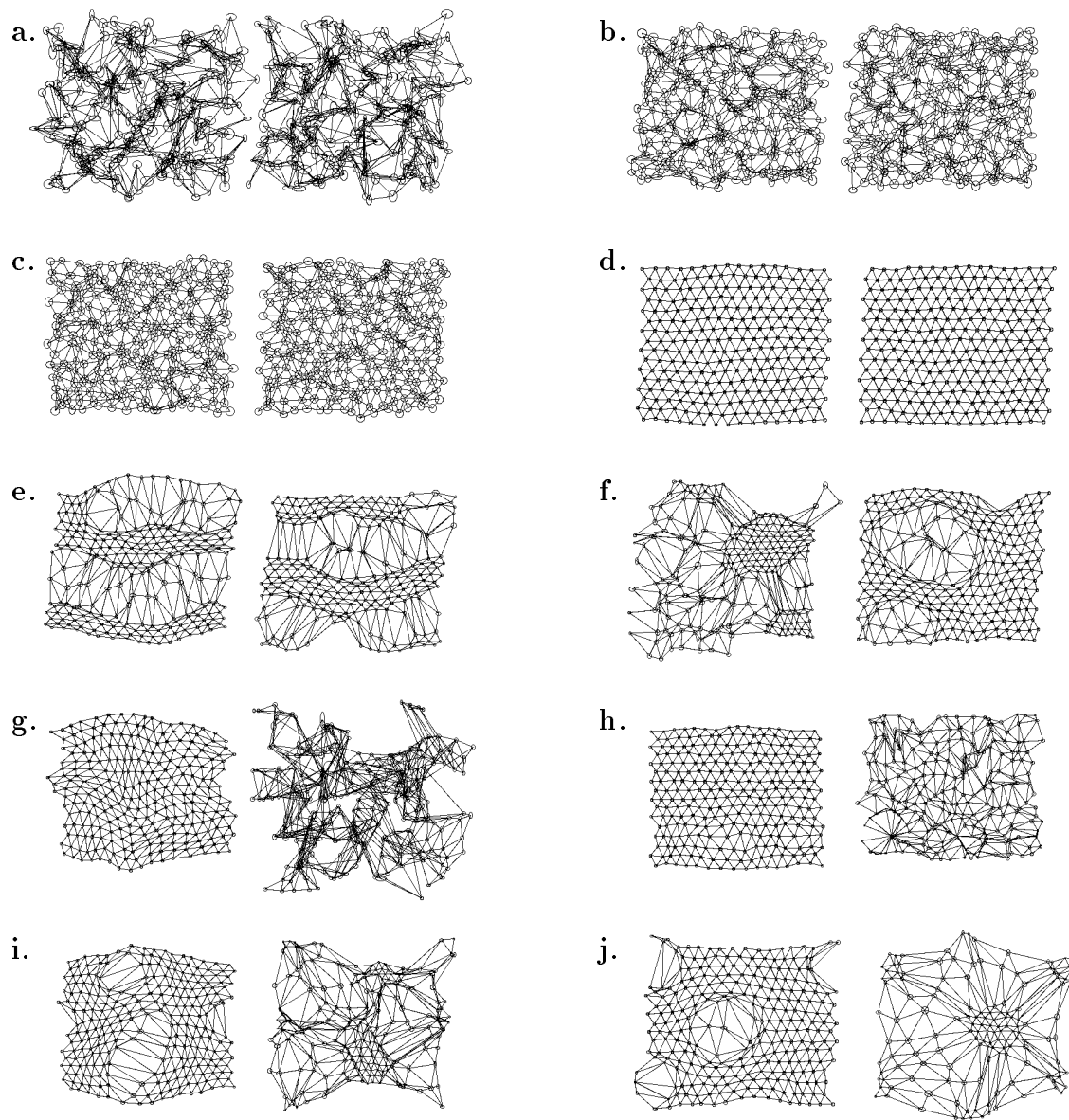
Figure 3.2: Pairs of cortical maps **a–i** are equal sized: **a, b, c** unorganized, pre-training; **d** organized and symmetric; **e, f** complementary mosaics; **g, h, i** asymmetric: left more organized than right; **j** the left hemisphere has more elements and is better organized.

Mirror symmetry measure: ranges from 1 for a pair of cortical maps covering the same regions in the sensory surface, to -1 for complementary maps covering different regions.

The above measures are computed as follows. For each cortical element n, a map M is described by the offsets of its receptive field center $(cx(n), cy(n))$ from the ideal position in a perfectly organized map, by the receptive field radii $(rx(n), ry(n))$, and the "total response" $(tr(n))$. These quantities are defined in equations (2.6)–(2.8).

Two different approaches to measuring a map's organization are considered here. They evaluate map organization from different points of view and work best in different situations. One evaluates the map's "smoothness" and gives high organization values to the maps where neighboring elements have very close offsets and radii. This is called the "sigmoid differential". It normally produces results similar to people's estimates of the degree of organization (see below), but sometimes it does not work well with the S2 model. For instance, in an unusual situation where one hemisphere does not get any activation at all, then its receptive fields have offsets 0 and radii 0, so the map looks like an ideal map (but with no ellipses) and gets an unappropriate organization value of 1, while in fact the weights have not organized at all, and if some activation could be induced in the hemisphere (e.g., by removing intense callosal inhibition), then it would be obvious that there is no organization.

The second approach, called "organized area", is based on the observation that the organized regions of a map usually consist of small triangles whose vertices have small receptive field radii and high total response values (the latter would help to avoid giving a high organization value to the "empty" map just described). So the idea is to add together the areas of such triangles (assuming that the total area is 1).

The two measures produce similar results for some maps, but differ significantly for others. We are using one or the other depending on which works best in a particular case. Normally, the sigmoid differential measure works fine. However, when simulated lesions (damage) are introduced into one cortical area, and it is desirable to measure recovery from it, this approach gives counterintuitive results. Lesioning studies are described in detail in Chapter 5, so here only a short explanation is given. Recovery from a lesion happens when the cortical elements on the boundary of damaged area shift and enlarge their receptive fields to cover the sensory region previously covered by their dead neighbors. This may make the whole map look less smooth, so the sigmoid differential measure would decrease, when in fact the organization measure should increase. The organized area measure works much better in this case.

Below the formulas for the two measures are given.

The "differential square distance" between two immediate neighbors n and n' is computed as

$$|(n, n')|^2 = (cx(n') - cx(n))^2 + (cy(n') - cy(n))^2 + (rx(n') - rx(n))^2 + (ry(n') - ry(n))^2.$$

The *sigmoid differential organization measure* $||M||_S$ for map M is then computed as

$$||M||_S = \frac{1}{N} \sum_{\text{all M-nodes } n} \text{sigmoid}_{\tau,s} \left(\sum_{\text{all neighbors } n' \text{ of } n} |(n, n')|^2 \right)^{\frac{1}{2}}$$

Table 3.2: Values of Quantitative Measures for the Maps in Fig. 3.2

| map | sigmoid diff. (SD) | | organized area | | lateralization | mirror |
	left	right	left	right	based on SD	symmetry
a	0.01	0.01	0.04	0.04	0.0	undefined
b	0.25	0.28	0.48	0.57	0.03	-0.28
c	0.59	0.61	0.74	0.77	0.02	0.13
d	0.98	0.99	1.0	1.0	0.01	1.0
e	0.62	0.64	0.38	0.36	0.02	-1.0
f	0.47	0.78	0.20	0.67	0.31	-1.0
g	0.83	0.07	1.0	0.06	-0.76	-0.88
h	0.96	0.32	0.95	0.0	-0.64	-1.0
i	0.82	0.29	0.61	0.08	-0.53	-1.0
j	0.83	0.37	0.55	0.12	-0.46	-0.99

where $\mathrm{sigmoid}_{\tau,s}(x) = (1 + e^{-2s(x-\tau)})^{-1}$. Parameters τ and s were chosen to approximate human estimates of organization values for various maps [2].

The *organized area measure* $||M||_A$ is computed as the sum of areas of all triangles (formed by triples of immediate neighbor elements) having sufficiently small perimeter, sufficiently small radii of receptive fields at all three vertices, and sufficiently large total responses in all three vertices. The area is normalized so that the total area for an ideal map is 1.0.

A simple difference of the organization values for right and left cortical maps (using any of the two organization measures described) gives a *lateralization measure*: $\mathrm{Lat}(L, R) = ||R|| - ||L||$.

The degree of *mirror symmetry* is estimated using a measure of the overlap of organized regions $\mathrm{oreg}(L)$ in the left map L and $\mathrm{oreg}(R')$ in the mirror image R' of the right map R (those organized regions are the unions of the triangles used for the organized area measure described above). Areas of the intersection $(\mathrm{oreg}(L) \cap \mathrm{oreg}(R'))$, union and symmetric difference $(\mathrm{oreg}(L)\Delta\mathrm{oreg}(R'))$ of the above regions are used to define

$$\mathrm{map\_overlap}(L, R) = \frac{\mathrm{area}(\mathrm{oreg}(L) \cap \mathrm{oreg}(R')) - \mathrm{area}(\mathrm{oreg}(L)\Delta\mathrm{oreg}(R'))}{\mathrm{area}(\mathrm{oreg}(L) \cup \mathrm{oreg}(R'))}$$

The intersection term measures the overlap of the organized regions, while the symmetric difference term measures the discrepancy between these regions. When no organized regions exist, map overlap is undefined.

Table 3.2 gives the values of the quantitative measures for the maps shown in Fig. 3.2. For example, maps in Figs. 3.2a–d show increasing individual organization, while in each case the lateralization measure does not exceed 0.03, indicating that significant lateralization has not occurred. Significant lateralization is measured with many of the other map pairs shown, and is of greatest magnitude for Fig. 3.2g (lateralization = -0.72). The two maps in Fig. 3.2d are mirror images of each other (mirror symmetry = 1.0), while those in

Figs. 3.2e,f are complementary, representing largely disjoint portions of the sensory surface (mirror symmetry = -1.0).

3.5   Properties of the Metrics

The above metrics have some important properties (first described in our joint paper [2]):

Theorem 3.5.1. *The organization measures described above (sigmoid differential and organized area) satisfy the following properties:*

1. *size independence: only the organization per processing element is measured.*

2. *spatial homogeneity: if a map M is given and a new map M' is obtained from M by any distance–preserving geometric transformation of the map associated with the reference locations of the elements of M, then M and M' have the same organization measure.*

Proof. Property 1 is enforced by explicitly defining sigmoid differential organization as an average value over all elements and by normalizing the total area of an ideal map to be 1.0. Property 2 follows from the fact that the expressions used in the definitions of the organization measures are independent of the particular nodes' (or triples) locations, depending only on the values cx, cy, rx, ry, tr.   □

Theorem 3.5.2. *Lateralization measure $\mathrm{Lat}(L, R)$ satisfies the following properties:*

1. *antisymmetry:*
$$\mathrm{Lat}(M, N) = -\mathrm{Lat}(N, M);$$

2. *zero property:*
$$\mathrm{Lat}(M, M) = 0;$$

3. *monotonicity: for a fixed $||L||$ it is a strictly increasing function of $||R||$;*

4. *boundedness: the maximal value of $\mathrm{Lat}(L, R)$ is 1 and it is achieved only when $||L|| = 0$ and $||R|| = 1$, the minimal value is -1 achieved for $||L|| = 1$ and $||R|| = 0$.*

Proof.   Properties 1-3 follow from the definition of the lateralization measure as the difference of two organization measures. The last property also uses the fact that the organization measures are bounded between 0 and 1, which combined with properties 1 and 3 completes the proof.   □

Finally, for the symmetry measure

Theorem 3.5.3. *For maps N and M, the measure $sym(M, N) = map\_overlap(M, N)$ (if it is defined) satisfies the following three properties.*

1. invariance under left-right interchange:

$$sym(M, N) = sym(N, M)$$

2. equal shift independence: if $\tilde{M}$ and $\tilde{N}$ are obtained from M and N by adding the same constant dx to all the cx entries of M and N' (here N' is the mirror image of the map N), and another constant dy to all the cy entries of M and N, then:

$$sym(\tilde{M}, \tilde{N}) = sym(M, N)$$

3. normalization:

$$sym(M, M) = 1 \qquad\qquad\qquad\qquad (3.7)$$

Proof. Property 1 follows from the symmetry of the operators $\cap$, $\cup$, and Δ. Property 2 follows from the fact that under the above conditions the organized regions $oreg(M)$ and $oreg(N')$ have the same shift, and hence the areas of their intersection, union and symmetric difference don't change. (3.7) is a consequence of the fact that if $M = N$, then $M\Delta N$ is empty and so has area 0, and also $M \cup N = M = M \cap N$. $\qquad\qquad\square$

3.6   Discussion

The methods of computation and visualization of cortical receptive fields presented in the last chapter provide a very convenient way for representing simulation results. It is usually quite easy to estimate the results qualitatively by simply looking at the maps. However, such qualitative estimates are not sufficient for a systematic rigorous study of map formation in a bihemispheric model. Objective quantitative measures are needed for such study. The metrics for map organization, lateralization, and mirror symmetry developed in this chapter have all the desired properties. On one hand, the metrics have the mathematical properties that one would expect of such measures. On the other hand, their computed values tend to correspond also to subjective estimates of what these values should be. On ten sample pairs of maps presented to nine people (graduate students and faculty from the University of Maryland) [2], computing the metrics described above produces results which are very close to the average values of human estimates. A quantitative assessment of the closeness of the fit between human measurements and those produced by the measures is obtained by representing each measure by the vector whose coordinates are the measurement values produced by that measure for a given set of test examples. The mean absolute distances between the vector representing the human scores and the vectors representing the measures is then computed. The mean absolute distance between two vectors $v, w \in \mathbb{R}^N$ is defined by: $\|v - w\|_1 = \frac{1}{N} \sum_{k=1}^{n} |v_k - w_k|$ Thus, the mean absolute distance between two measures approximates the average difference, in absolute value, between the scores produced by the two measures for an arbitrarily chosen input map. The results are summarized in Table 3.3. Left and right hemisphere distances are given separately for each organization measure, while a single distance is given for lateralization measure corresponding to each of the organization

Table 3.3: Mean absolute distances to human scores: Organization and Lateralization.

Measure	Organization		Lateralization
	Left	Right	
$\|M\|_S$	0.04	0.03	0.03
$\|M\|_A$	0.09	0.10	0.06
$\|M\|_H$	*	*	0.04

measures. The last line gives the mean absolute distance between average human lateralization values and the lateralization values computed as difference of the human estimates of right and left organization values ($\|M\|_H$).

Finally, the value of mean absolute distance for mirror symmetry measure was 0.11 when two pairs of completely unorganized maps were excluded (recall that the symmetry measure is not defined for unorganized maps).

Thus, all the mean absolute distances are quite low, indicating good agreement of the metrics descibed in this chapter with subjective estimates.

Chapter 4

Results from the S2 Model

This chapter describes results of the simulations with the S2 model. For various model asymmetries, callosal influences have been varied systematically from strongly inhibitory to strongly excitatory, and resulting organization, lateralization, and mirror symmetry recorded. In the symmetric case (when all model parameters except random initial weights were symmetric) no lateralization is observed for any callosal strength, and a very sharp transition in organization and mirror symmetry appears near $K = -1.4$. For most asymmetric cases, sharp transitions occur in lateralization as well, with most lateralization appearing with strongly inhibitory callosal influences.

4.1 Symmetric Hemispheric Regions

Before considering various hemispheric asymmetries, simulations with a symmetric version of the model where the two hemispheric regions were identical except for the initial random weights were done. Complete topographic maps similar to those in Fig. 3.2d form in both hemispheres when corpus callosum connections are excitatory, absent, or weakly inhibitory. However, as callosal inhibition becomes stronger there is a sharp transition at roughly K = -1.4 from two complete maps to two complementary mosaic pattern maps similar to those in Fig. 3.2e. Fig. 4.1 shows how the organization, lateralization and symmetry measures vary as the callosal strength K is systematically altered. Since the organization values on the left and right are essentially the same, lateralization is very close to zero for *all* values of K.

As seen in Fig. 4.1a, initial organization values are close to 0 for $K < -1$, but grow noticeably for positive K. This happens because inhibitory callosal connections "push" the receptive fields of corresponding cortical elements away from each other and hence from their ideal location in a perfectly organized map, while excitatory callosal connections "pull" the receptive fields of corresponding cortical elements closer to each other and to their ideal locations, thus making the pretraining maps look more organized. Fig. 3.2a–c show pretraining maps for $K = -2$, $K = 0$ and $K = 2$ in the symmetric case.
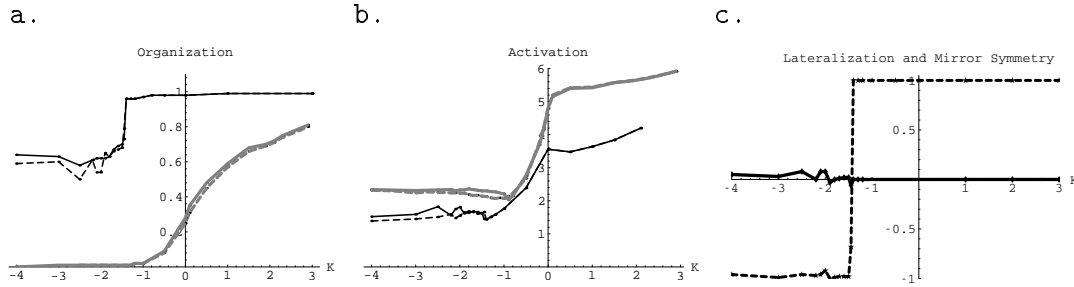
Figure 4.1: Symmetric hemispheric regions (except for random initial weights). **a.** Organization of left and right maps as a function of callosal strength K. Black lines – after training, gray lines – before training; solid lines - right hemisphere, dashed – left. **b.** Activation in the two hemispheres. **c.** Lateralization and mirror symmetry after training. Solid line - lateralization, dashed line - mirror symmetry.

4.2 Asymmetric Versions of the Model

4.2.1 Asymmetric Cortical Excitability

Asymmetric cortical excitability has been associated experimentally with functional lateralization [82] and regionally may be implied by asymmetries in various neurotransmitter levels [126]. In the S2 model, the learning rule is such that the higher the activation in one hemisphere, the faster it should self-organize. Conversely, a hemisphere that gets very little or no activation cannot effectively learn a good topographic map. Several parameters of the model can cause different excitability in the two hemispheres. Fig. 3.2h,i show sample maps resulting from a small difference in input sensitivity or lateral feedback (in both cases the left hemisphere is more active). Fig. 4.2 summarizes the results of simulations when the two hemispheres had only a slightly different input sensitivity favoring the left: $c_p^L = 1.05$ and $c_p^R = 1.0$. For approximately $K > -1.2$, symmetric highly organized maps always formed without lateralization (similar to Fig. 3.2d). For $K < -1.2$ however, strong lateralization to the left always occurred, usually with mosaic patterns like those in Fig. 3.2i. Similar results were obtained with mildly asymmetric maximal activation constants M_L and M_R, and with small asymmetries in lateral feedback strengths c_{lf}^L and c_{lf}^R. Small differences in the strength of corpus callosum inhibition also caused significant lateralization. With fixed $K^{LR} = -2$, for example, when $K^{RL} < K^{LR}$ complete lateralization to the left occurred, and for $K^{RL} > K^{LR}$, the opposite occurred.

4.2.2 Asymmetric Hemispheric Sizes

Experimentally-measured differences in hemispheric region sizes have been associated with function lateralization to the larger hemispheric region [48, 92]. To examine how asymmetric hemispheric region size influences lateralization, simulations were run with the two
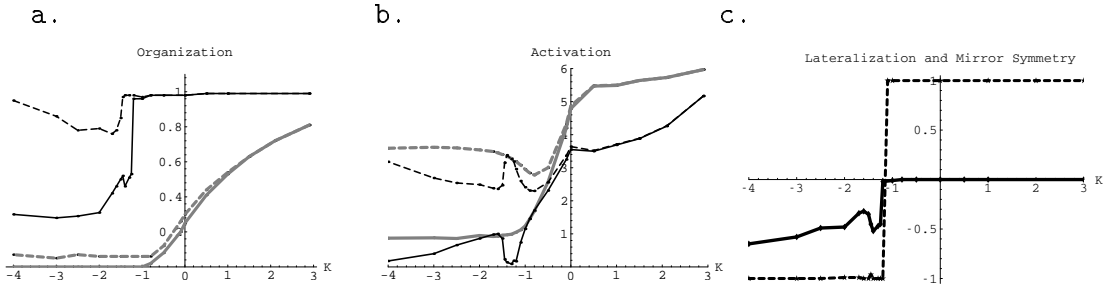
Figure 4.2: Results with asymmetric input sensitivity ($c_p^L = 1.05$, $c_p^R = 1.0$). Same notation as in Fig. 4.1. The left hemisphere clearly dominates for roughly $K < -1.2$: its post-training organization is higher than the organization on the right. Activation on the left is much higher than the right, which is the main reason for the lateralization.

hemispheric regions having different numbers of elements: the left having 16x16 elements, the right 12x12, for a total of 256 vs. 144 elements. Fig. 4.3 shows the results as callosal
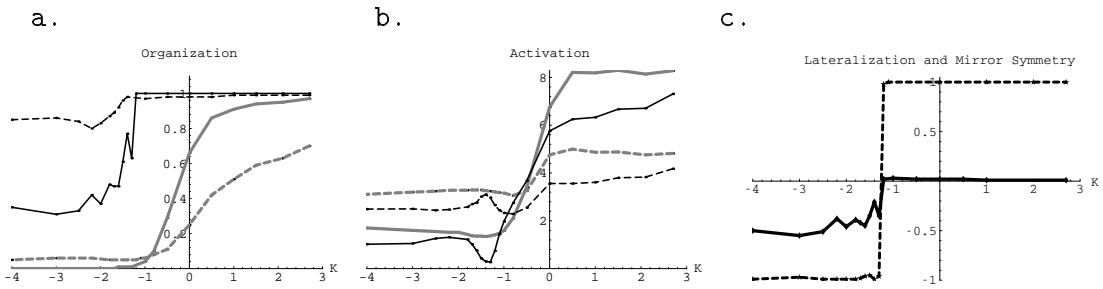
Figure 4.3: Simulation results for two hemispheric regions differing only in their numbers of elements (left larger). Same notation as in Fig. 4.1.

strength is varied. For excitatory, absent or mildly inhibitory callosal strengths (roughly $K > -1.2$), both hemispheres formed highly organized and symmetric maps. For strongly inhibitory callosal strengths ($K < -1.2$), marked map lateralization occurred, with a much better organized map in the larger left region, and with complementary maps. Fig. 3.2j shows a typical example of the maps found under these latter conditions.

Fig. 4.3b shows quite clearly that when inhibition is strong (roughly $K < -1.2$), the *initial* activation on the left was much higher than on the right. To remove this potentially biasing factor, callosal inhibition strength was adjusted so that the inhibition from left to right was slightly weaker than inhibition from right to left. A 5% difference produced nearly equal initial activations on both sides for $K < -1$. The effect of this adjustment is demonstrated in Fig. 4.4. Lateralization is smaller, but is still present for sufficiently strong inhibition ($K < -1.5$), and the maps formed under these conditions remain complementary.

a. Organization

b. Activation

c. Lateralization and Mirror Symmetry
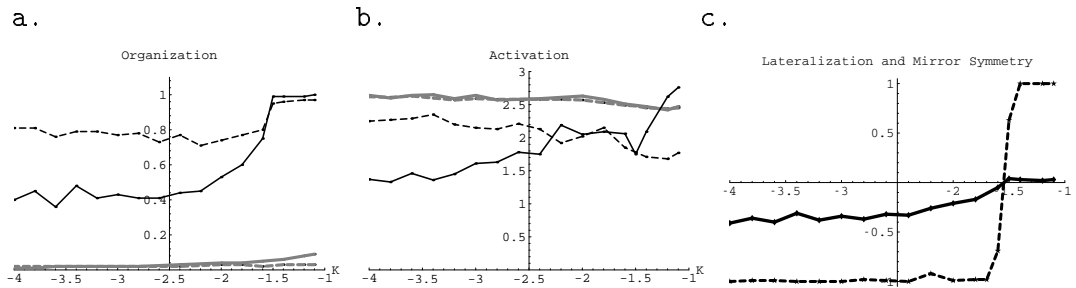
Figure 4.4: Results for the two hemispheric regions with different numbers of elements, when the initial activations are equal. Same notation as Fig. 4.1.

4.2.3 Asymmetric Learning Rates

Another possible cause of lateralization is a difference in synaptic plasticity in the two hemispheres. The biological existence of asymmetric plasticity is suggested by asymmetric hemispheric neurotransmitters [126], and directly indicated by asymmetric synaptogenesis during development and early life [7]. Simulations were also run where all parameters of the two hemispheres were the same except initial random weights and the learning rates (left 0.01, right 0.001). Figs. 4.5 and 4.6 display simulation results for brief (16,000 inputs) and long-term (123,000 inputs) training, showing that initially the hemisphere with a higher learning
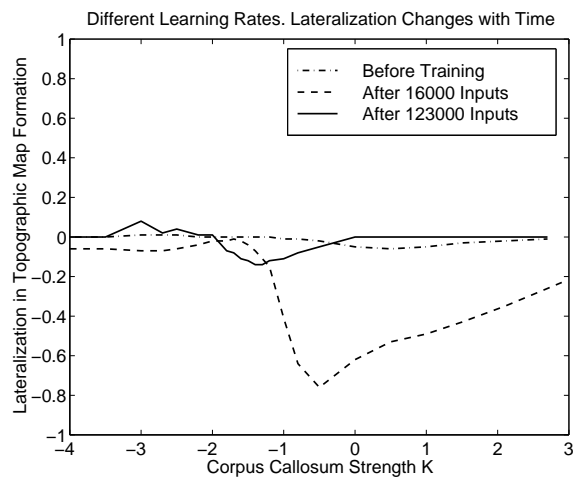
Figure 4.5: Lateralization as a function of K with asymmetric learning rates. Lateralization is significant for $K > -1$ after brief training, but subsequently essentially vanishes.

rate organizes faster. However, after sufficiently long training, the difference in organization values becomes much smaller. For this type of simulations, much more transient lateralization occurs with excitatory and weak inhibitory callosal connections than with strongly inhibitory ones. For example, Fig. 4.7 shows that for $K = -3$ both hemispheres learn very slowly, while for $K = 0$ the one with higher learning rate learns much faster than the other.
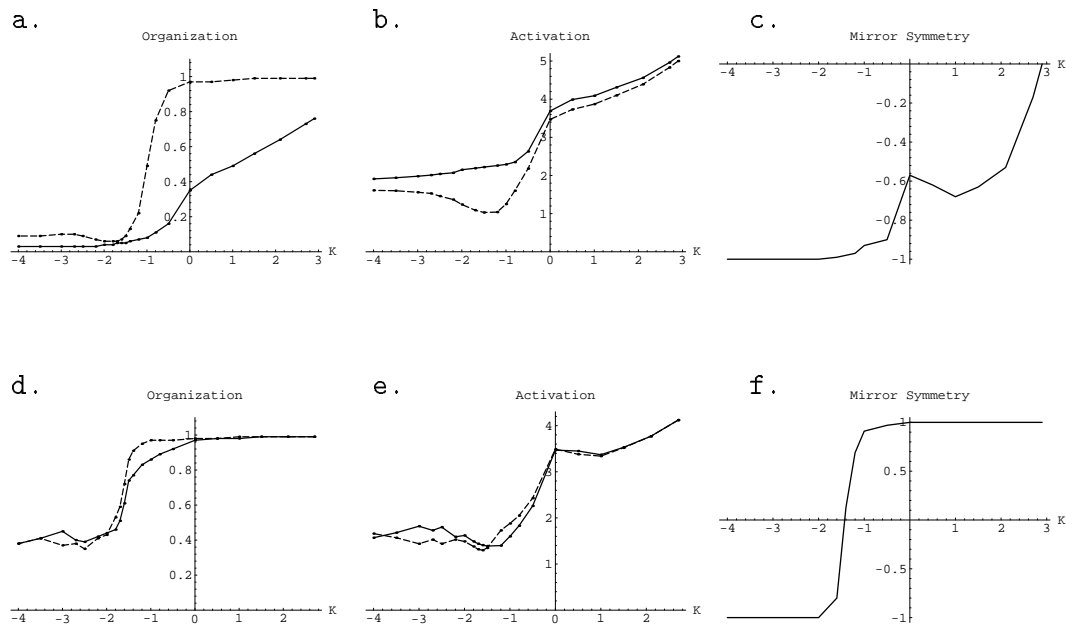
Figure 4.6: Results for the two hemispheres with different learning rates after about 16,000 (**a–c**) and 123,000 (**d–f**) training inputs. Solid lines in (**a,b,d,e**) correspond to the right hemisphere with learning rate 0.001, the dashed lines to the left hemisphere with learning rate 0.01. After 16000 inputs the left hemisphere is dominant for $K > -1.4$. After very long training the two hemispheres achieve about the same organization levels. Pretraining organization and activation are as in Fig. 4.1.

These results differ from those with the asymmetries examined above in that the lateralization that occurs is more pronounced for $K > -1.4$. Given the asymmetry in learning rates, transient lateralization to the left would generally be expected for *all* values of K: the larger left learning rate would cause its map to organize more quickly, but the slower right side would eventually catch up. The issue then is why transient lateralization does *not* occur with a strongly inhibitory corpus callosum. The reason is that, in general, as a map organizes the mean activation level in its hemispheric region falls (e.g., Fig. 4.1 in the symmetric case). Lateralization does not occur with strongly inhibitory callosal connections here because the higher learning rate on the left is largely cancelled by simultaneously lower mean activation levels on the left that slow learning (see Fig. 4.6). These asymmetric mean activation levels are not present for less inhibitory K for the reasons discussed in Sec. 7.3.
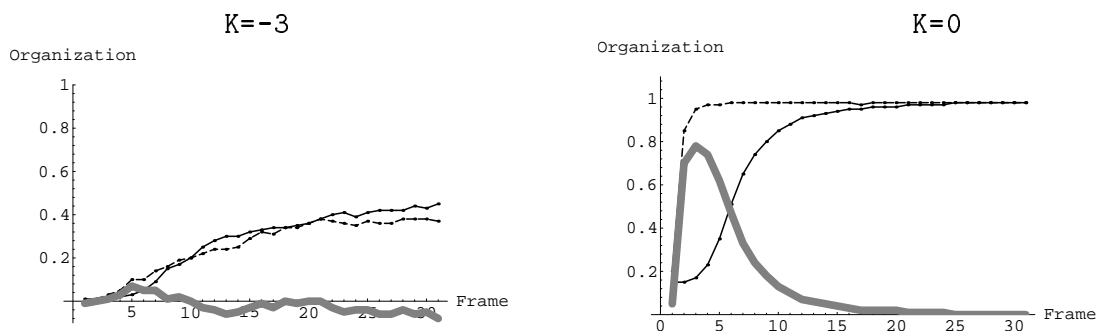
Figure 4.7: Organization with different learning rates during training (learning curves). One frame corresponds to 4096 inputs. Solid black line – right hemisphere, dashed line – left hemisphere (with higher learning rate). The thick gray line shows the difference between organizations in the two hemispheres. For $K = -3$ the difference is small, for larger values of K it first becomes large, but vanishes after longer training.

4.2.4 Asymmetric Sensoricortical Radii

Different connectivity patterns can also lead to lateralization in the model. For example, Fig. 4.8 plots organization, activation, lateralization and mirror symmetry, and Fig. 3.2g shows the maps after training, when different sensoricortical radii are used (left radius 3, corresponding to 37 connections; right radius 4, or 61 elements.). This provides an example where the hemisphere with lower activation levels became better organized. This surprising result is due to asymmetries in the activation patterns in the two cortical regions with inhibitory callosal connections. An example of such activation patterns is shown in Fig. 4.9. The pretraining hemispheric response to a small input patch is broken up into multiple cortical activation areas on the right by the intercortical inhibition from the more compact response on the left. Since good map formation requires learning in a compact neighborhood, the fractured activation patterns prevent map formation on the right.

36
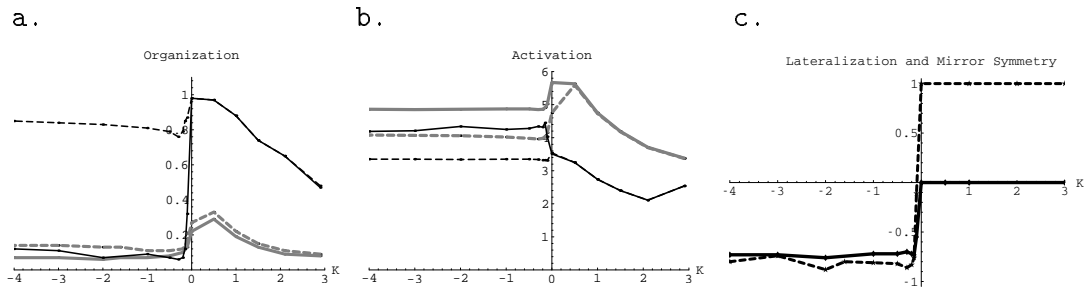
Figure 4.8: Results with different connection radii from S to L (3) and R (4) while callosal radius is 1. Same notation as in Fig. 4.1. For $K < 0$ post-training organization in the left hemisphere is quite high while in the right hemisphere organization does not change almost at all. At the same time activation is higher in the right hemisphere. For $K > 0$ organization and activation in both hemispheres decrease as K increases due to strong self-inhibition.
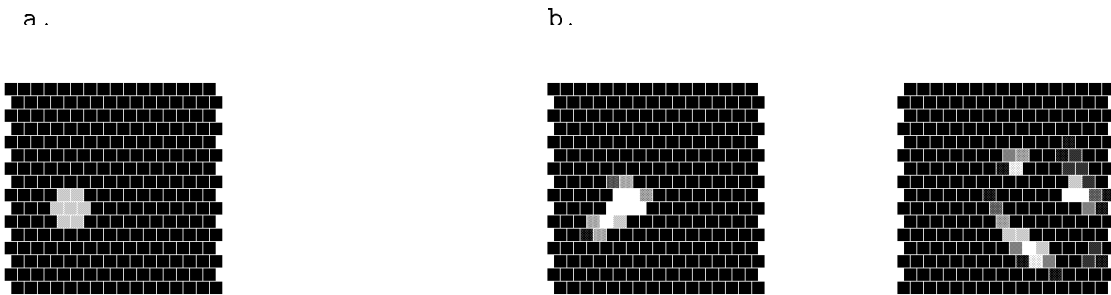
Figure 4.9: Activation in the (**a**) sensory surface and (**b**) the two cortical regions when radii are as in Fig. 4.8. Black rectangles denote elements with no activation, lighter rectangles mean higher activation. The activation in the left cortical region is concentrated at one location, while in the right it is dispersed, preventing map formation. $K = -2$.

4.3 Discussion

The results of the simulations presented in this chapter are summarized in Fig. 4.10 and are as follows. First, when callosal connections were absent ($K = 0$), in every case complete, mirror symmetric maps ultimately formed in both hemispheric regions without significant lateralization. This finding is consistent with experimental data suggesting that lateralization and complementary mosaic maps arise due to hemispheric interactions, even in regions like auditory cortex with bilateral afferent pathways and receiving matched bilateral input stimuli [17]. Second, a sharp transition in model behavior was observed depending on callosal strength. For excitatory, absent or weakly inhibitory callosal strengths, complete and symmetric mirror-image maps typically appeared in both hemispheric regions. In contrast, with stronger inhibitory callosal connections, partial to complete map lateralization tended to occur, and the maps in each hemispheric region often became complementary (resembling mosaic patterns observed experimentally [17]). These results, along with those of the

37
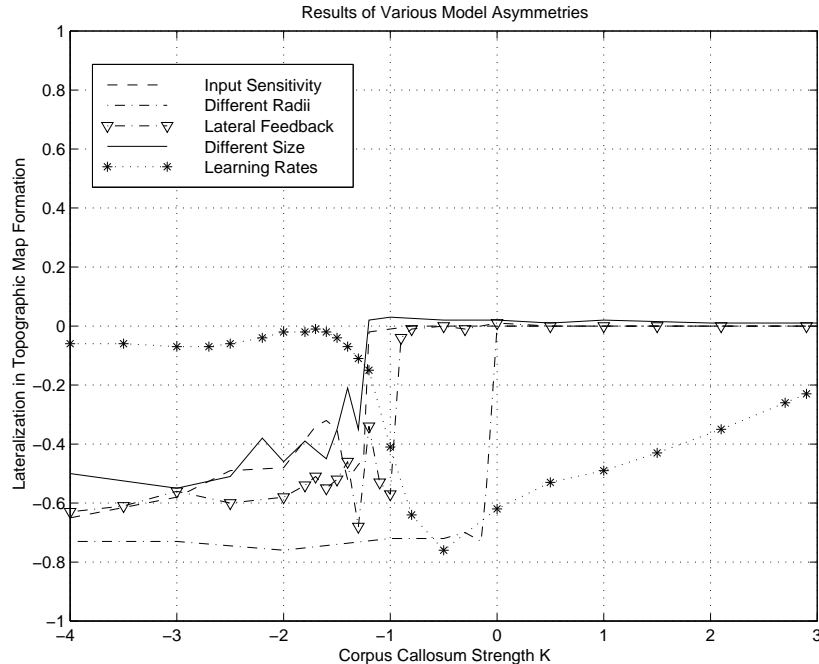
Figure 4.10: Lateralization as a function of K for various types of asymmetry. Lateralization is significant for most asymmetries when $K < -1$, but for different radii it is large when $K < -0.1$, and for different learning rates it is transiently larger for $K > -1$.

earlier phoneme sequencing model [109], provide support for the hypothesis that the corpus callosum plays a functionally inhibitory role [72, 34].

Third, lateralization occurred readily toward the side having a larger cortical region, higher excitability, or more focused input connectivity. These factors produced lateralization more or less independently. This suggests that biological lateralization may be a multifactorial process, consistent with the phoneme sequencing model and consistent with arguments that current experimental data does not support the concept of a single underlying factor causing human behavioral lateralization [59, pp. 54–64]. These results are also consistent with the general concept that initial small quantitative differences in hemispheric regions can ultimately give rise to qualitative differences. Finally, it was observed that asymmetric synaptic plasticity had only a transitory effect on lateralization of map formation. In contrast, asymmetric plasticity in the phoneme sequencing model [109] led to marked, persistent functional lateralization. The difference occurs because map formation here is based on an unsupervised learning rule, whereas it was controlled by an error-correction process in the earlier phoneme sequencing model (once one hemisphere learned to control phoneme sequencing, the error dropped to zero and the other hemisphere stopped learning). The key implication here is that for biological lateralization the effects of asymmetric synaptic plasticity may vary dramatically depending on whether supervised or unsupervised learning is involved.

While the work described here has been primarily motivated by recent experimental studies demonstrating lateralization and asymmetries in cortical sensory maps, note in con-

clusion that it may have more general applicability. For example, viewed in an abstract sense, these results may relate to the diversification of interconnected cortical regions in the same hemisphere, such as those described in [43].

Chapter 5

Results of Lesioning the S2 Simulator

This chapter examines the effects of sudden, localized damage to one of the map regions in the S2 model. Map reorganization after a *lesion* (damage) is of interest for a number of reasons. For example, a model that not only works the same as the real system being modeled, but also reacts to and recovers from damage in the same way, is more convincing than a model which fails to respond similarly to damage. Further, the simulated focal lesions here can be viewed as modeling *ischemic stroke*. An ischemic stroke is a sudden death of a localized region of brain due to loss of blood flow and thus oxygen to that region. The diffuse lesions might be viewed as simulating damage in diffuse cortical diseases, e.g., Alzheimer's disease. In the following, background information on the effects of stroke on the other, intact hemisphere is given, along with a brief summary of previous neural models of stroke. Experimental methods are described, including the ten variations of the S2 model used for the lesioning study. Finally, results of lesioning simulations with the ten model variations, where size and shape of the lesion were varied systematically, are presented and discussed.

5.1   Background

Since the effects of a simulated lesion on the two model hemispheres are considered in this chapter, it is useful to briefly consider the biomedical data on the effects of stroke on the two hemispheres, and previous neural models of stroke.

5.1.1   Interhemispheric Effects of Ischemic Stroke

A stroke is a complex pathophysiological event [111]. Most relevant to this research is that, acutely following a hemispheric stroke, there is an immediate depression of neural activity, metabolism and cerebral blood flow contralaterally in the intact hemisphere [42, 90]. Such changes are referred to as *transcallosal diaschisis*. Their severity is proportional to the severity of the damage and they persist for roughly three to four weeks after a stroke. It is often accepted that transcallosal diaschisis is responsible for part of the clinical deficit in stroke [90]; including sensorimotor findings ipsilateral to the infarct [28], although this view has been challenged [22]. A presumably important mechanism responsible for transcallosal diaschisis is loss of excitatory inputs to otherwise intact contralateral cortex, although other

neurophysiological phenomena appear to be contributing factors [90]. Animal models have demonstrated that the contralateral effects of an acute hemispheric infarct are reduced or abolished by prior sectioning of the corpus callosum [71, 88]. The presumptive mechanism of focal depression of the contralateral hemisphere is thus widely presumed to be loss of facilitation (deafferentation) via the corpus callosum.

The importance of hemispheric interactions during recovery from aphasia (impaired language) following left hemisphere language area damage is underscored by evidence that the right hemisphere plays a crucial role in the language recovery process in adults. Early evidence came from observations that recovery from aphasia due to a left hemisphere lesion would relapse when a new, mirror-image right hemisphere lesion occurred [77]. Subsequently, a series of studies has provided evidence of substantial right hemisphere responsibility for language recovery after left hemisphere strokes, using a wide variety of methods [72, 73, 99, 100, 117, 118]. During the last decade further evidence has come from several functional imaging studies, showing that recovered aphasics have increased activation in the right hemisphere in areas largely homotopic to the left hemisphere's language zones [132, 94, 27], but some of these studies have questioned how well these changes correlate with the recovery process [8, 57, 58]. As a result, the issue is currently controversial and an active area of experimental investigation for which modeling provides a new investigative technique.

5.1.2   Previous Neural Models of Stroke

Early models of damage to neural networks were based on abstract associative memories (e.g., [135, 51]). More recent spatially-oriented neural models have been used to study acute focal cortical lesions, including work at the University of Maryland [108, 50, 119, 111, 124]. This past research has generally examined only unilateral cortical regions and local adaptation, and most often has looked at local post-lesion map reorganization. An exception is some recent work on visual information processing where both left and right hemispheric regions have been simulated [103, 91], and then one hemispheric region removed/isolated to simulate unilateral neglect phenomena. However, these latter studies have not modeled hemispheric interactions via the corpus callosum, the effects of underlying hemispheric asymmetries, or variable lesion sizes, as is done here. To our knowledge, neither these nor any other previous modeling studies have investigated how the contralateral intact hemisphere might participate in recovery, nor how underlying cortical asymmetries and callosally-mediated hemispheric interactions might influence the recovery process.

As mentioned above, one of the important features of S1 simulator was its ability to react correctly to changes in the environment, in particular, to cortical lesions. In this study the effects of various model parameters on the extent of damage and recovery from a one-sided cortical lesion on the other intact cortical region in the bihemispheric S2 model are considered.

41

5.2   Experimental Methods

The goal of this study is the analysis of the effects of various model features (including model asymmetry, callosal influences, size and shape of the lesion) on the extent of damage and recovery from a one-sided cortical lesion on both sides of the S2 model.

To evaluate organization and lateralization of lesioned maps it is more convenient to use the organized area measure instead of sigmoid differential measure used in the previous chapter. The former measure works better in representing damage and recovery from lesions, since during recovery the "smoothness" of a map may suffer, making sigmoid differential organization lower, while in fact the area covered by the relatively good topographic map increases.

In addition to the organization, lateralization and mirror symmetry measures described above, for the lesioned model *mean activation* of each cortical region was computed by dividing the total activation in that region caused by all possible single-element input stimuli by the number of cortical elements. When simulated lesions were present, the mean activation in the lesioned region could be computed in two ways: by dividing the total activation by the total number of elements, or only by the number of intact (unlesioned) elements remaining. The graphs in this chapter and Table 5.2 show both of these quantities.

Lesions were introduced into the model after the initial training was completed and some kind of cortical maps formed in both cortical regions. For the lesioning experiments described here, ten variations of the basic model were used, as summarized in Table 5.1. These variations represent four different types of hemispheric asymmetry: symmetric (no hemispheric asymmetry except initial random weights), size 256/144 (left hemisphere has 16x16 elements and right has 12x12), excitability 1.05/1.0 (using notation from (Levitan & Reggia, 1998) $c_p^L = 1.05$, $c_p^R = 1.0$), connectivity: radii of connections from input layer 3/4 (each element of the input layer sends activation to 37 cortical elements on the left and to 61 elements on the right). Both positive (excitatory) and negative (inhibitory) callosal connections were used for each type of asymmetry, and in some cases two different strengths of inhibitory connection were used because they had produced qualitatively different results in the intact model (see previous section). As a result of these variations, prelesion lateralization (usually to the left) varied from none (0.0) to almost complete (−0.84) in the ten model variations, as listed in Table 5.1 . The table also shows organization (organized area), lateralization, mean activation, and mirror symmetry measures in the corresponding intact models.

Each lesion was introduced into the intact model by literally clamping to zero a randomly selected subset of elements in one hemispheric region (diffuse lesion) or a parallelogram-shaped contiguous subset of the region (focal lesion). Lesions of different sizes were done independently, not progressively.

We describe the general nature of the lesions in topographic maps, what is meant by map recovery during simulations, and the results of simulations in which lesion size and shape were systematically varied.

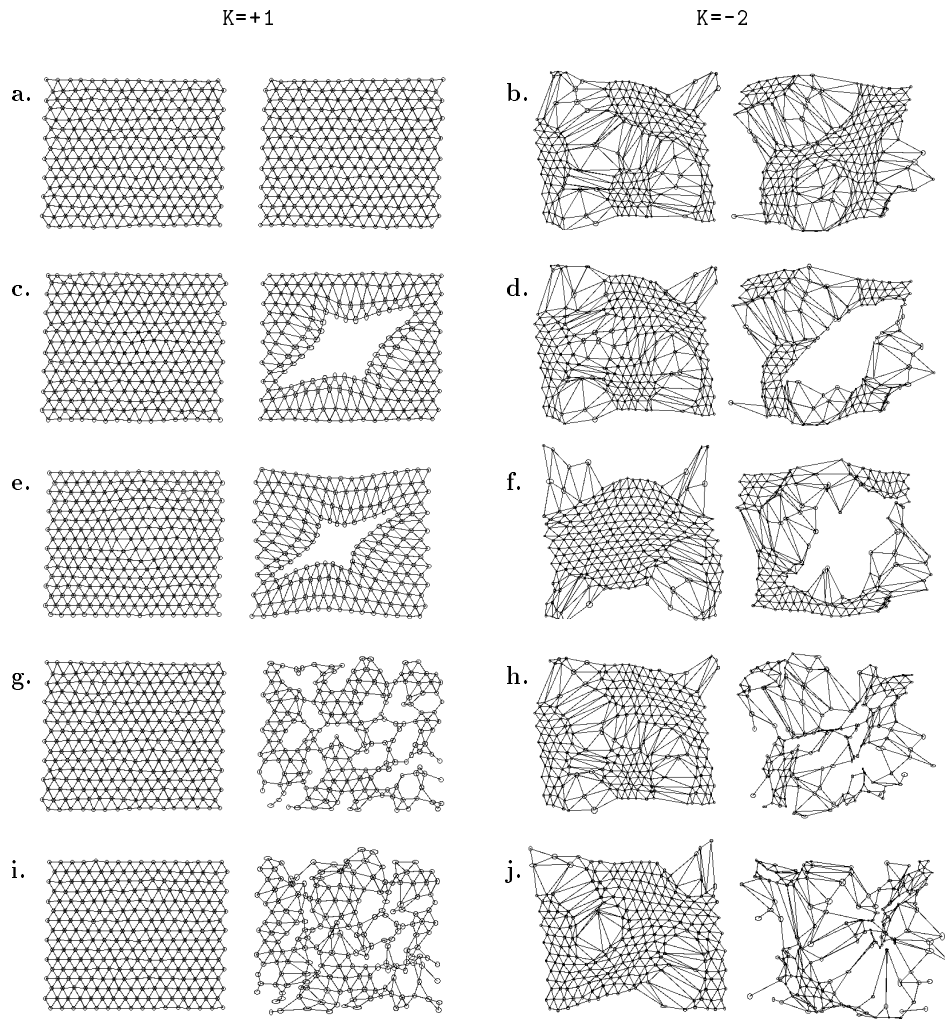Figure 5.1: Topographic maps in the two symmetric cortical regions: the left column corresponds to excitatory callosal strength $K = +1$, the right column to inhibitory callosal strength $K = -2$. **a, b** pre-lesion maps; **c, d** acute focal lesions; **e, f** chronic focal lesions; **g, h** acute diffuse lesions; **i, j** chronic diffuse lesions. All lesions are in the right hemispheric region and are of size 64.

Table 5.1: Variations of Intact Model Used for Lesion Study.

Asymmetry	Callosal strength	Organization Left	Right	Latera-lization	Mirror Symmetry	Mean Activation Left	Right
Symmetric	-2	0.39	0.45	0.06	-0.97	1.58	1.66
	-1	1.0	1.0	0.0	+1.0	1.76	1.76
	+1	1.0	1.0	0.0	+1.0	3.80	3.80
	-2	0.70	0.17	-0.53	-0.97	2.49	0.86
Excitability	-1	1.0	1.0	0.0	+1.0	2.36	1.16
1.05/1.0	+1	1.0	1.0	0.0	+1.0	3.84	3.84
Size 256/144	-2	0.73	0.23	-0.50	-0.87	2.55	1.23
	+1	1.0	1.0	0.0	+1.0	3.56	6.22
Connectivity	-2	1.0	0.16	-0.84	-0.69	3.34	4.34
radii 3/4	+0.5	1.0	1.0	0.0	+1.0	3.25	3.25

5.3 Nature of Topographic Map Response to Lesions

Fig. 5.1 shows representative examples of the effects of lesions in the maps observed during simulations in the symmetric case.

The lesions introduced into the cortical regions for the present study are illustrated in the right halves of topographic maps 5.1c–j. A *focal* lesion is represented graphically by a relatively large contiguous "hole" (c – f), and a *diffuse* lesion consists of a number of small "holes" (g – j). By recovery from a lesion we mean the changes in the receptive field maps that lead to the "closing" of the holes (or at least reduction in their size). Biologically, this is analogous to the well-known phenomenon where nearby surviving neurons move their receptive fields into the area previously represented by their dead neighbors [68]. Such recovery is illustrated in Fig. 5.1c and 5.1e, representing an acute focal lesion, and the same lesion after retraining (the latter state will be called chronic). Table 5.1 contains the values of our measures for the maps presented in Fig. 5.1.

5.4 Results of Systematic Lesioning Simulations

5.4.1 Symmetric Case

Simulated cortical lesions were done with symmetrical versions of the model in which all parameters in both cortical regions were identical except for the random initial weights. Because of the approximate symmetry, the results of left and right hemisphere lesions were essentially the same, so we only show them for right lesions here.

Figure 5.2 is a typical example that shows how organization in the two cortical regions in symmetric case changes with time after acute focal and diffuse lesions of size 64 are introduced at time 0 in the right cortical region (recall that the cortical regions have size 16x16=256

Table 5.2: Organization and Other Measures for Maps in Fig. 5.1

| Map	K^*	Lesion type	Organization Left	Organization Right	Latera-lization	Mirror Symm.	Mean Activation Left	Mean Activation Right	Mean Activation R.intact
a.	+1	None	1.0	1.0	0.0	+1.0	3.80	3.80	3.80
b.	-2	None	0.39	0.45	0.06	-0.97	1.58	1.66	1.66
c.	+1	Acute Focal	1.0	0.65	-0.35	+0.30	3.59	3.56	4.75
d.	-2	Acute Focal	0.43	0.25	-0.18	-0.97	2.14	1.07	1.43
e.	+1	Chronic Focal	1.0	0.89	-0.11	+0.78	3.74	3.74	4.98
f.	-2	Chronic Focal	0.59	0.29	-0.30	-0.97	2.17	1.22	1.62
g.	+1	Acute Diffuse	1.0	0.44	-0.56	-0.12	3.70	2.82	3.76
h.	-2	Acute Diffuse	0.50	0.12	-0.38	-1.0	2.20	0.98	1.30
i.	+1	Chronic Diffuse	1.0	0.44	-0.56	-0.11	3.82	2.91	3.88
j.	-2	Chronic Diffuse	0.62	0.11	-0.51	-0.99	2.33	0.98	1.31

$^*K$ = callosal strength.
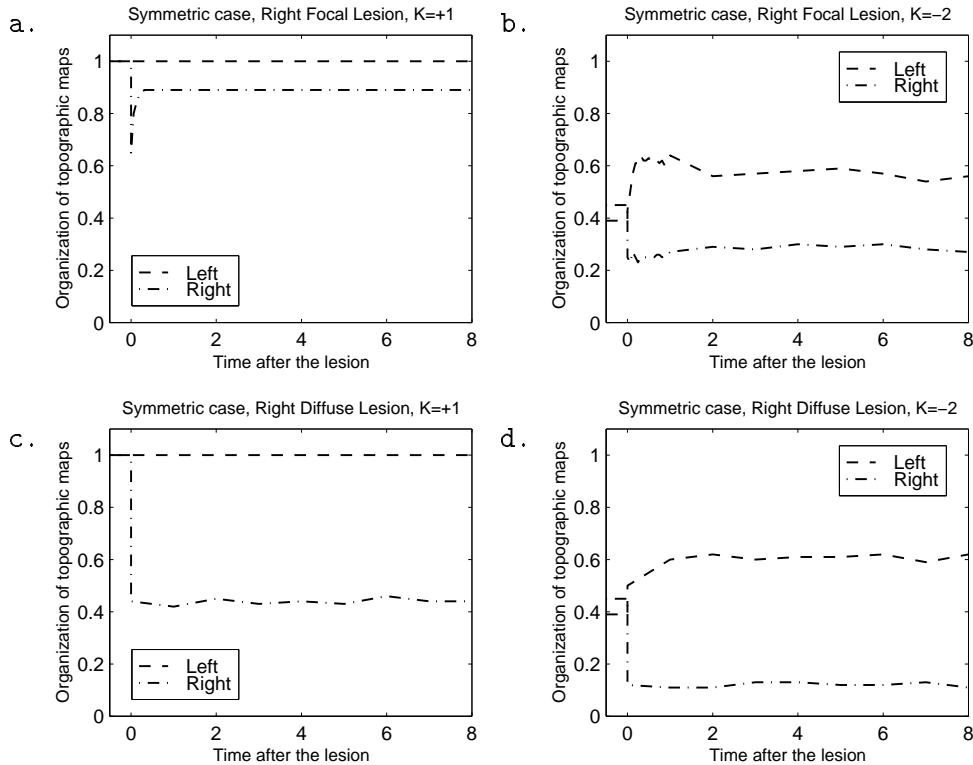
Figure 5.2: Time course for symmetric model recovery following 64-element right lesions. One time unit represents 32768 training inputs. The four graphs correspond to the cases of excitatory ($K = +1$, left column) and strongly inhibitory ($K = -2$, right column) callosal connections, focal (top row) and diffuse (bottom row) lesions.

elements, so a 64-element lesion removes a quarter of the region). As this representative example shows, there is always an initial drop in organization of the lesioned hemispheric region that persists, at least partially, and in general this drop is more pronounced with diffuse lesions. With inhibitory callosal influences, organization in the unlesioned left hemispheric region increases. Figure 5.1 shows the corresponding topographic maps before the lesions (Fig. 5.1a,b), right after the lesions (Fig. 5.1c,d,g,h), and after retraining (Fig. 5.1e,f,i,j), both for focal and diffuse lesions. The case of weak inhibitory connections ($K = -1$) was also studied, since in the intact model (chapter 4) it exhibited behavior more close to the excitatory case than to the strongly inhibitory case, and it was found that the lesioned model behaved very similarly to the case $K = +1$, so the results are not explicitly shown here.

Fig. 5.1 also illustrates that the damage in one cortical region causes a different reaction in the other one depending on the nature of their callosal connections. In case of *excitatory* callosal influences both regions have excellent maps prior to the lesion (Fig. 5.1a). After one region suffers damage, the other, intact, region remains unchanged acutely, although there may be a small change for the worse in the intact region's organization when the lesion is very large, and this may get slightly worse after retraining. This impairment is caused by the decrease in stabilizing effects due to loss of homotopic excitatory input from the damaged region. In the case of *inhibitory* connections, the contralateral effect of a lesion depends largely on its location as the two maps are typically complementary (Fig. 5.1b). If most of the damage occurs in the cortical elements not participating in the organized subregions of the lesioned cortical region, then organizations of both cortical regions experience practically no change. In contrast, if a substantial piece of an organized subregion is lesioned, the previously unorganized part in the opposite hemisphere becomes more organized immediately, and completely organized after retraining, so that organization in the damaged hemisphere decreases acutely and stays low, while the contralateral hemisphere gets better acutely and even better later (see Fig. 5.1b,d,f). The unlesioned hemisphere, released from the transcallosal inhibition of the lesioned hemisphere, clearly has a latent tendency for map organization that is normally suppressed.

Figure 5.2 also illustrates that recovery (if any is present) is fastest right after the lesion and then slows down significantly. This is similar to the actual pattern of recovery observed clinically after a stroke.

The way cortical elements adjacent to a focal lesion shift and enlarge their receptive fields immediately after the lesion (e.g. Fig. 2c,e for $K = +1$) and shift their receptive fields after retraining is very similar to the recovery pattern seen in the model of a single cortical region described in (Sutton et al.,1994) and also corresponds well to what is known to happen biologically [68]. Activations of the individual elements close to the lesion increase acutely and subside chronically, while the elements homotopic to the lesion in the contralateral hemisphere decrease their activation acutely and then restore most of it chronically. This is also biologically plausible.

When lesions of various sizes were applied, a "mass effect" (increased impairment due to larger lesions) was clearly seen in terms of organization of the lesioned cortical region in both acute and chronic cases, regardless of callosal connection strength. Figure 5.3 shows how organization of both cortical regions changes with variations in the size of a focal right-side lesion. The lesioned right hemispheric region's organization decreases acutely and remains
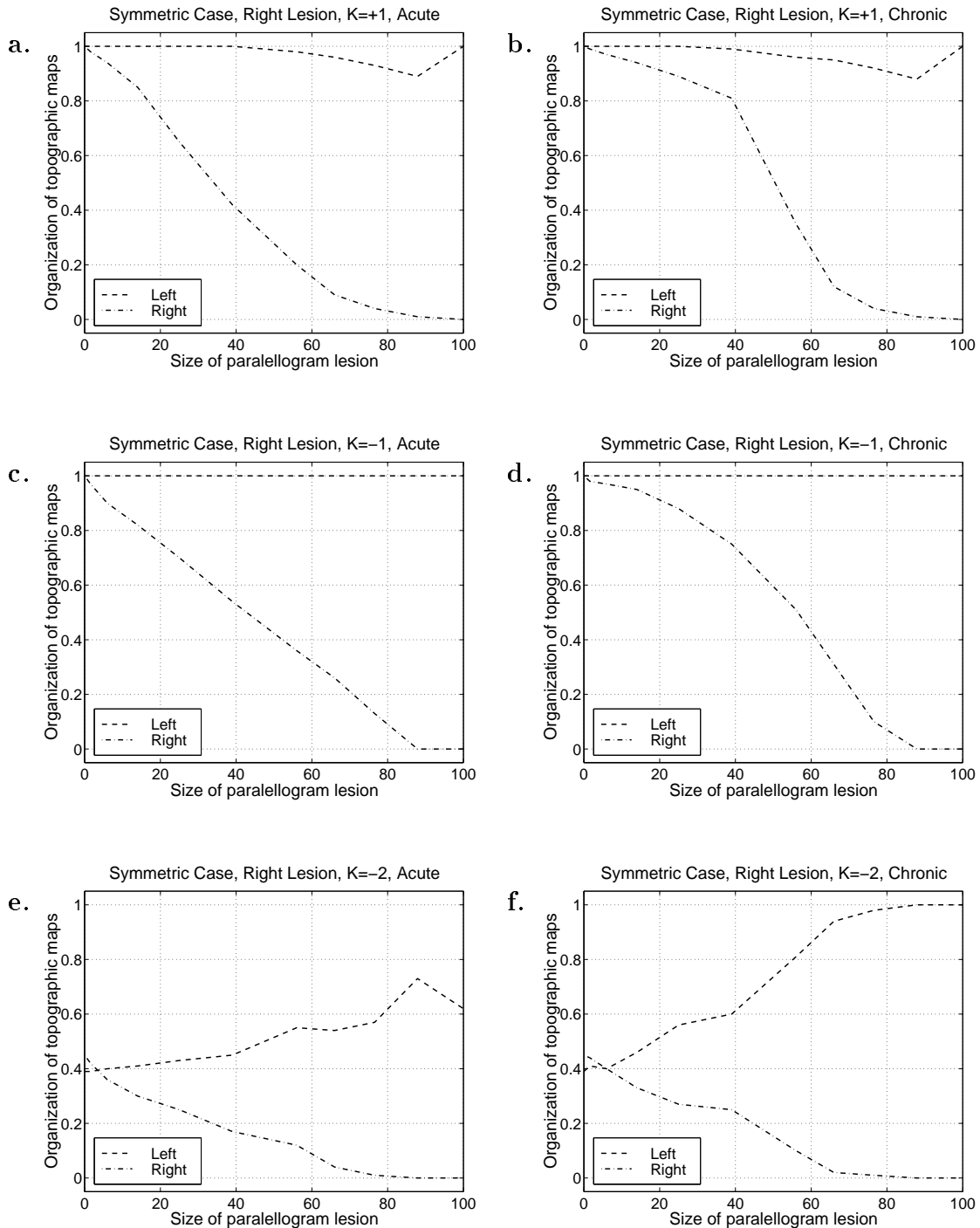
46

Figure 5.3: Organization versus lesion size in symmetric case for right focal lesions. Acute post-lesion organization measures are on the left; chronic measures following a recovery period are on the right. Top row: excitatory callosal influences, middle row: weakly inhibitory callosal influences, bottom row: strongly inhibitory callosal strength.

decreased even after retraining (for all callosal strengths). Recovery on the right is substantial for excitatory and weakly inhibitory connections but very small for strongly inhibitory connections. As noted above, the post-lesion changes in the left (intact) cortical region depend much more on the callosal strength. For $K = +1$, large right lesions cause some decrease in the left organization; for $K = -1$ the left organization is unaffected; and for $K = -2$ the improvement in left organization occurs acutely, especially with large right lesions, and gets even better after retraining.

The post-lesion changes in *mean activation* versus right-side lesion size are shown in Fig. 5.4, and differ qualitatively depending on whether callosal influences were excitatory or inhibitory. For excitatory callosal influences (Fig. 5.4a, b) the mean activation levels decreased bilaterally, and for larger lesions the decrease was more pronounced on the side of the lesion. Decreased activation on the right lesioned side was due to inactive lesioned elements, while in the intact left hemispheric region it was due to loss of transcallosal excitatory influences from the lesioned region. Surprisingly, the mean activation of just the remaining intact elements in the lesioned hemispheric region was increased (dotted line in Fig. 5.4a, b), in spite of decreased transcallosal excitation from the intact hemisphere. This was due effectively to the loss of intracortical lateral inhibitory influences from the lesioned area on the remaining cortex, and the competitive distribution of afferent activation.

In contrast, with inhibitory callosal influences (Fig. 5.4c-f), the mean activation also falls in the lesioned right hemispheric region. However, mean activation rises in the unlesioned left hemisphere, dramatically so with larger lesions. Note that activation in the remaining intact elements of the lesioned right hemisphere now decreases (e.g., Fig. 5.4e,f) due to increased inhibition from the more highly active unlesioned left hemispheric region.

Diffuse lesions are qualitatively similar in their effects to focal lesions, except they generally cause a more serious drop in organization and almost no recovery on the damaged side for all corresponding values of K. Unlike the focal case for $K = +1$, the other side always remains well-organized, even for large lesions. Mean activation levels post-lesion behave similarly to the focal case for $K = \pm 1$. For the case where $K = -2$, the undamaged side improves its organization after retraining slightly better than in the focal case, and mean activation of the impaired side decreases more than in the corresponding focal lesion case.

5.4.2   Asymmetric Cases

Now consider the results of introducing lesions into asymmetric models. In such cases lesions of left (dominant) and right (non-dominant) hemispheres may cause different effects, so consider both.

Asymmetric Excitability

As mentioned above, asymmetric excitability causes significant lateralization in the intact model when callosal influences are strongly inhibitory (the maps are complementary, but the side with higher excitability has a larger organized region), while for $K = \pm 1$ both cortical regions develop complete symmetric maps.
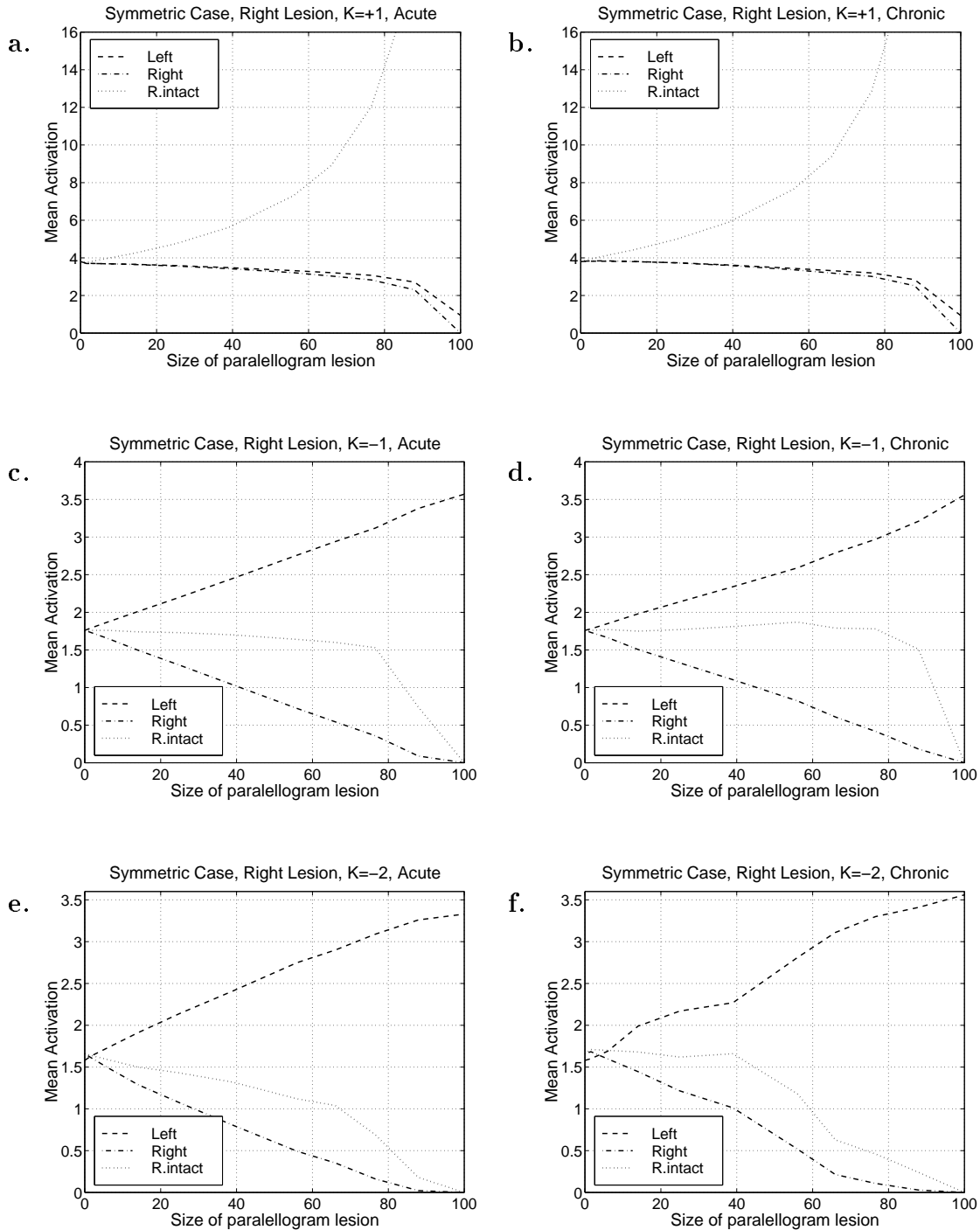
Figure 5.4: Mean activation versus lesion size in symmetric case for right focal lesions. Note that the vertical scales on these graphs differ. Same layout as Fig. 5.3. Shown are mean activation levels for the left (dashed line) and right (dash-dot line) hemispheric regions, and for just the right elements that remain intact following the lesion (dots).
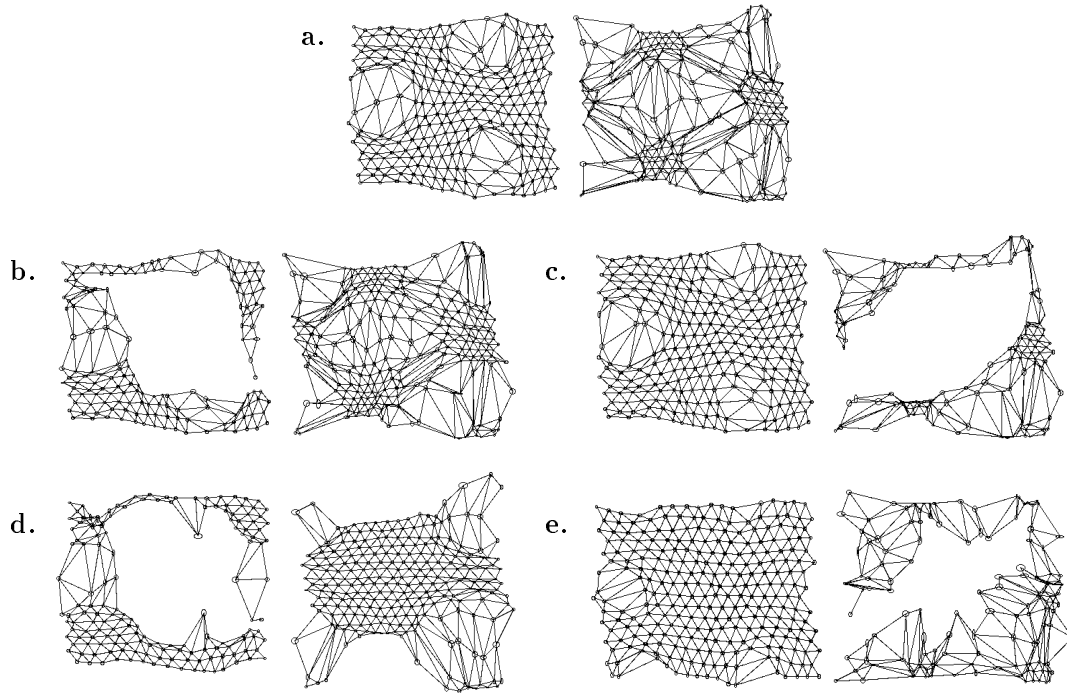
Figure 5.5: Pre-lesion (top) and post-lesion maps for asymmetric excitability case, $K = -2$. Left column: acute and chronic left-side 10x10 lesions, right column: acute and chronic right-side 10x10 lesions.

Table 5.3: Organization and Other Measures for Maps in Fig. 5.5. $K = -2$

Map	Lesion type	Organization Left	Right	Latera-lization	Mirror Symm.	Mean Activation Left	Right	intact
a.	None	0.70	0.17	-0.53	-0.97	2.49	0.86	*
b.	Left Acute Focal	0.30	0.29	-0.01	-0.98	1.30	1.93	2.13
c.	Right Acute Focal	0.75	0.07	-0.68	-0.97	2.93	0.43	0.71
d.	Left Chronic Focal	0.33	0.50	0.17	-0.97	1.46	1.87	2.40
e.	Right Chronic Focal	0.88	0.06	-0.82	-0.97	3.05	0.32	0.52
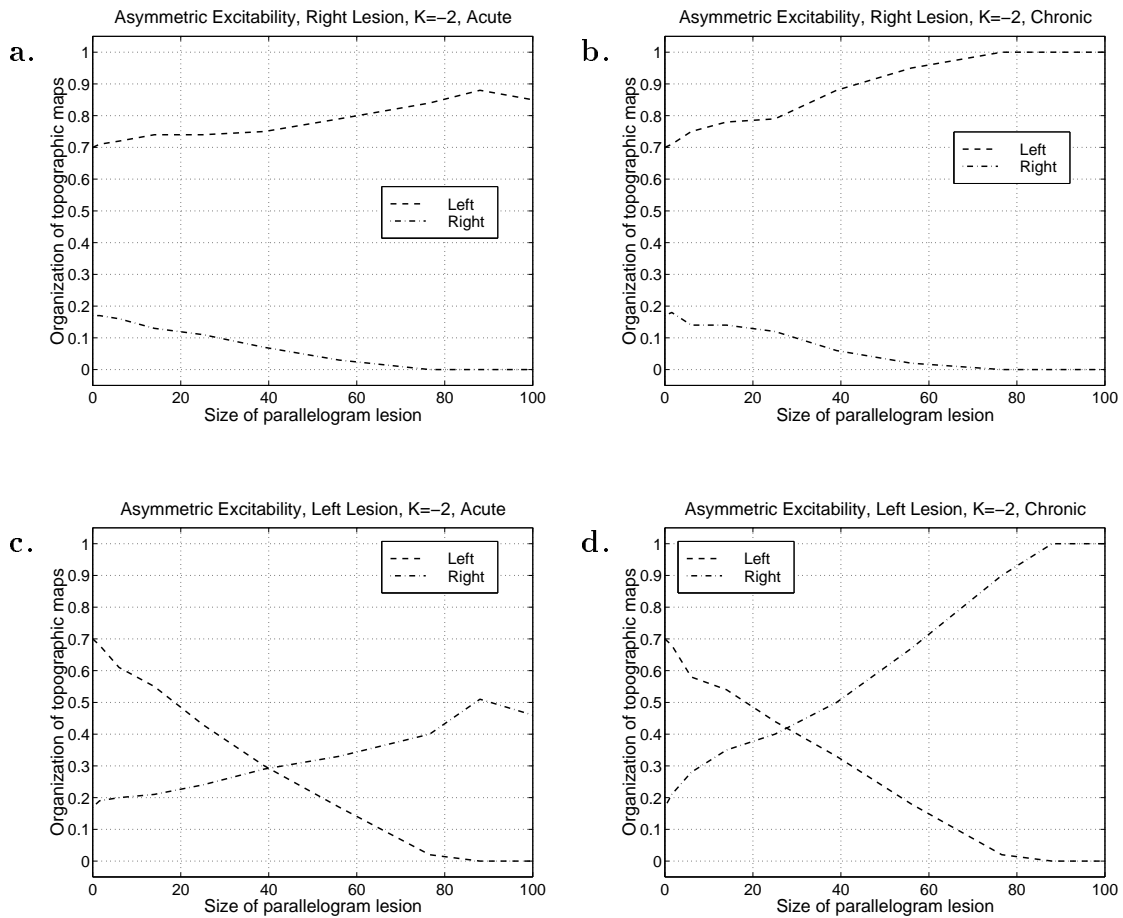
Figure 5.6: Organization versus lesion size in asymmetric excitability case for focal lesions and $K = -2$. The left side was dominant (most organized) before the lesion (see Table 5.1). Top row: acute and chronic lesions on the right, bottom row - lesions on the left.
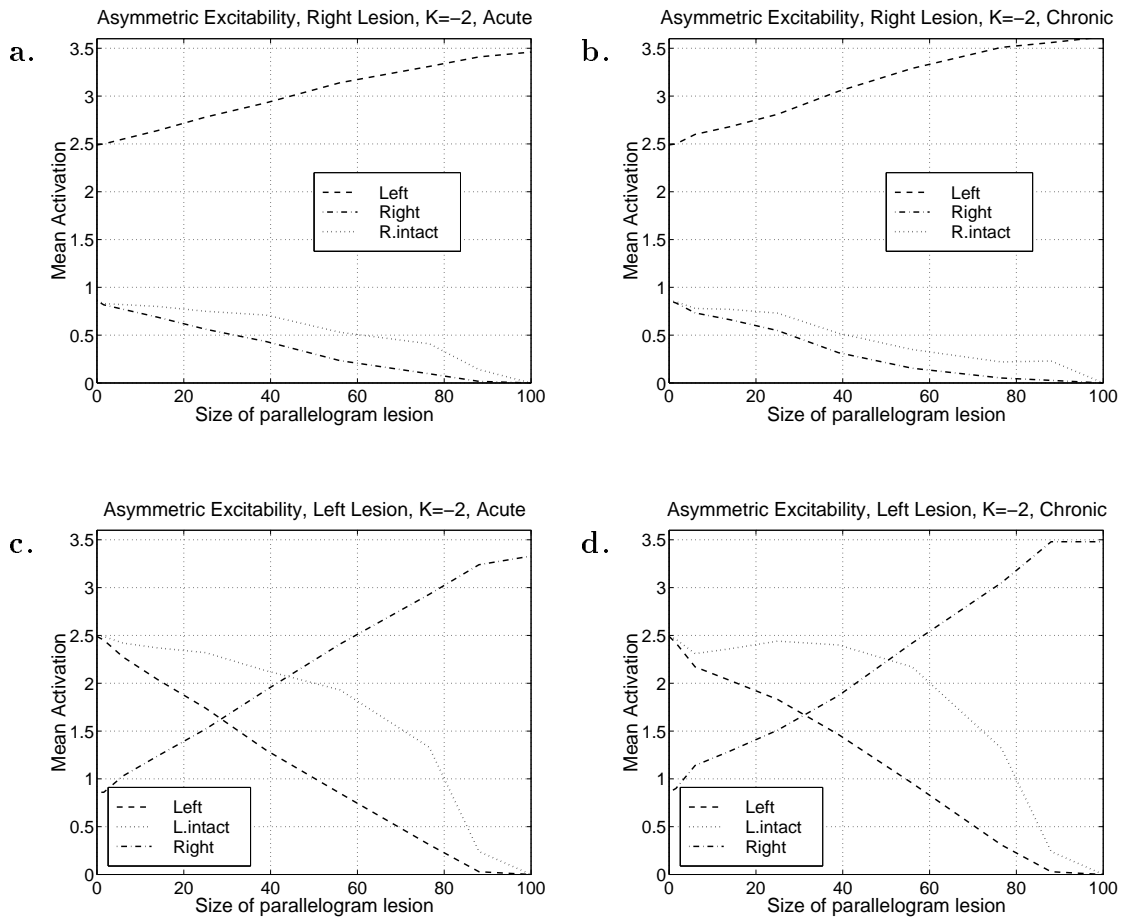
Figure 5.7: Mean activation level of each hemispheric region versus lesion size in asymmetric excitability case for focal lesions and $K = -2$. The left side was dominant before the lesion (see Table 5.1). Same layout as Fig. 5.6.

Figure 5.5 shows pre-lesion and post-lesion maps for simulations with asymmetric excitability due to higher input sensitivity on the left with callosal strength $K = -2$. Table 5.3 contains all metrics for those maps. Figures 5.6, 5.7 illustrate post-lesion organization and mean activation for this case both for lesions on the left and on the right side. For $K = +1$ and $K = -1$ the results of lesions on either side are very similar to the symmetric case described above (see Fig. 5.3a–d), so the graphs for these cases are not shown. For $K = -2$ all recovery happens in the intact side, independently of whether the dominant or non-dominant side is damaged. In general, the non-lesioned side increases its organization immediately following a lesion, and with time this increases progressively, especially with larger lesions. Mean activation of the damaged side goes down, and that of the intact side increases, these effects are more pronounced with larger lesions. Neither changes much during retraining. Diffuse lesions cause much more damage than comparable focal lesions.

Asymmetric Connectivity

Another type of asymmetry that causes significant lateralization in the intact model is asymmetric connectivity (see section 4.2.4). When each element of the input layer sends its output to elements of the left cortical set within radius 3 of its homotopic element (37 elements) and to the elements of the right cortical set within radius 4 (61 elements), after training the topographic map on the left becomes well organized while the map on the right remains largely disorganized even for slightly inhibitory callosal connections. The top row of Fig. 5.10 displays the maps developed by the intact model after initial training for $K = 0.5$ and $K = -2$. As before, excitatory callosal influence ($K > 0$) leads to complete symmetric maps in both cortical regions, while inhibitory callosal influence causes significant lateralization (good map on the left and no organized regions on the right).

Figures 5.8 and 5.9 illustrate simulation results for focal lesions for $K = +0.5$ and $K = -2$. When $K = +0.5$, the prelesion maps are full and symmetric. A lesion on either side causes the same loss of organization to the lesioned hemispheric region (Fig. 5.8a,b). In addition, loss of organization on the contralateral side is more pronounced than in any other case we have considered. During recovery the maps change quite unexpectedly (probably because of the small callosal radius in this case). The process of recovery is shown in Fig. 5.10. When a lesion is introduced in the center of the left hemispheric region, the center of the right region becomes slightly less organized immediately (due to the loss of transcallosal excitation). During additional training, as the "hole" in the left region becomes smaller, some map disturbance appears on its edges, and a much larger disturbance develops in the right hemispheric region, thus causing substantial decrease in contralateral organization. Mean activations for $K = +0.5$ (Fig. 5.9a,b) behave very similarly to the mean activations in symmetric case for $K = +1$ (Fig. 5.4a,b).

Like in other cases with excitatory callosal influences, a diffuse lesion causes more pronounced damage in the lesioned side and practically no damage in contralateral side.

For $K = -2$, a lesion in the non-dominant (right) hemispheric region causes no changes in the dominant one, even though mean activation of the remaining elements of the damaged hemispheric region increases dramatically with lesion size. Retraining improves organization on the lesioned right side very slightly and only for small lesions. In contrast, when the
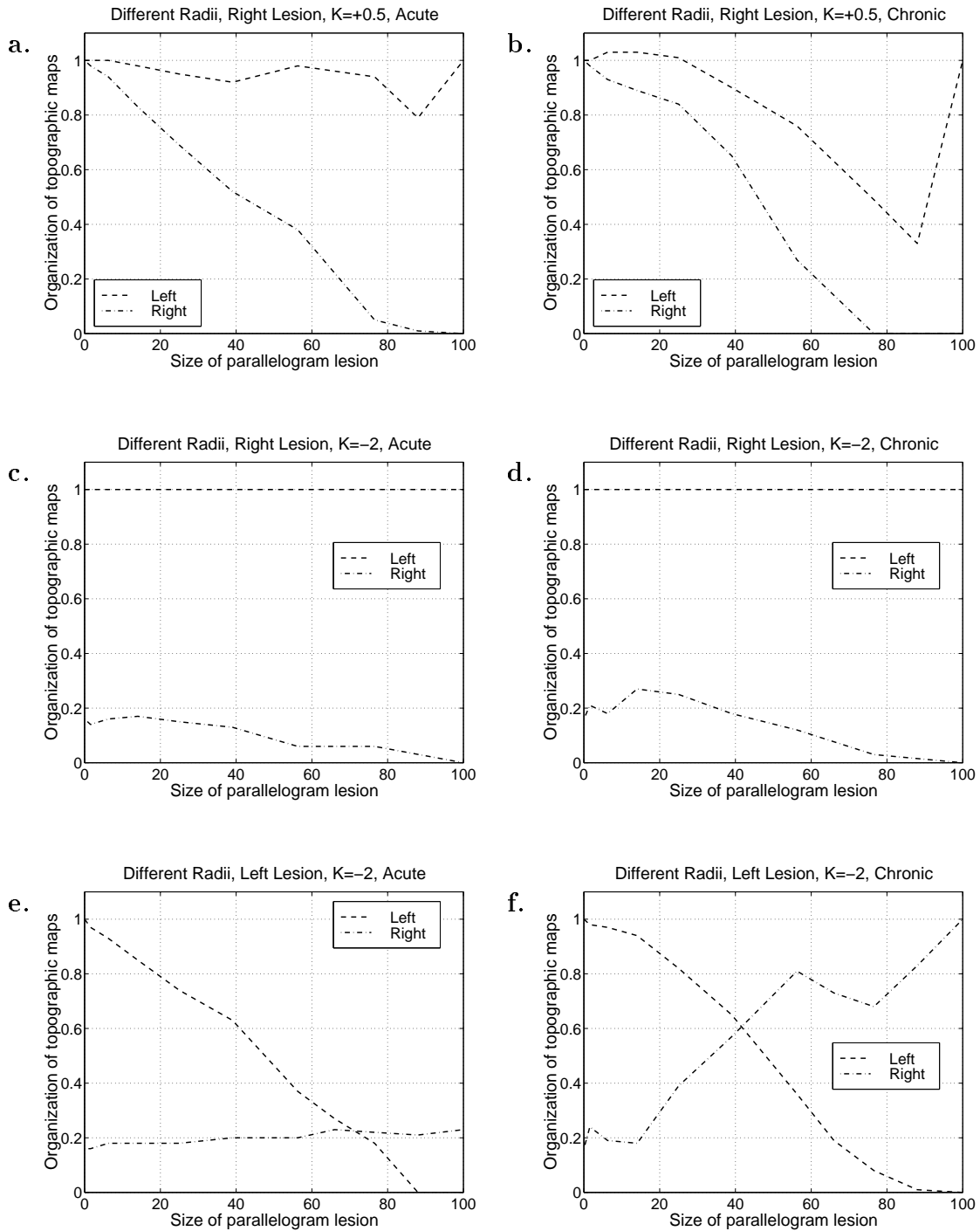
Figure 5.8: Organization versus lesion size in model with asymmetric connectivity for focal lesions. Left column: acute lesions, right column: chronic lesions. Top row: excitatory callosal strength; middle and bottom rows: strongly inhibitory callosal influences, right- and left-side lesions respectively. The left side was dominant in the intact model (see Table 5.1).
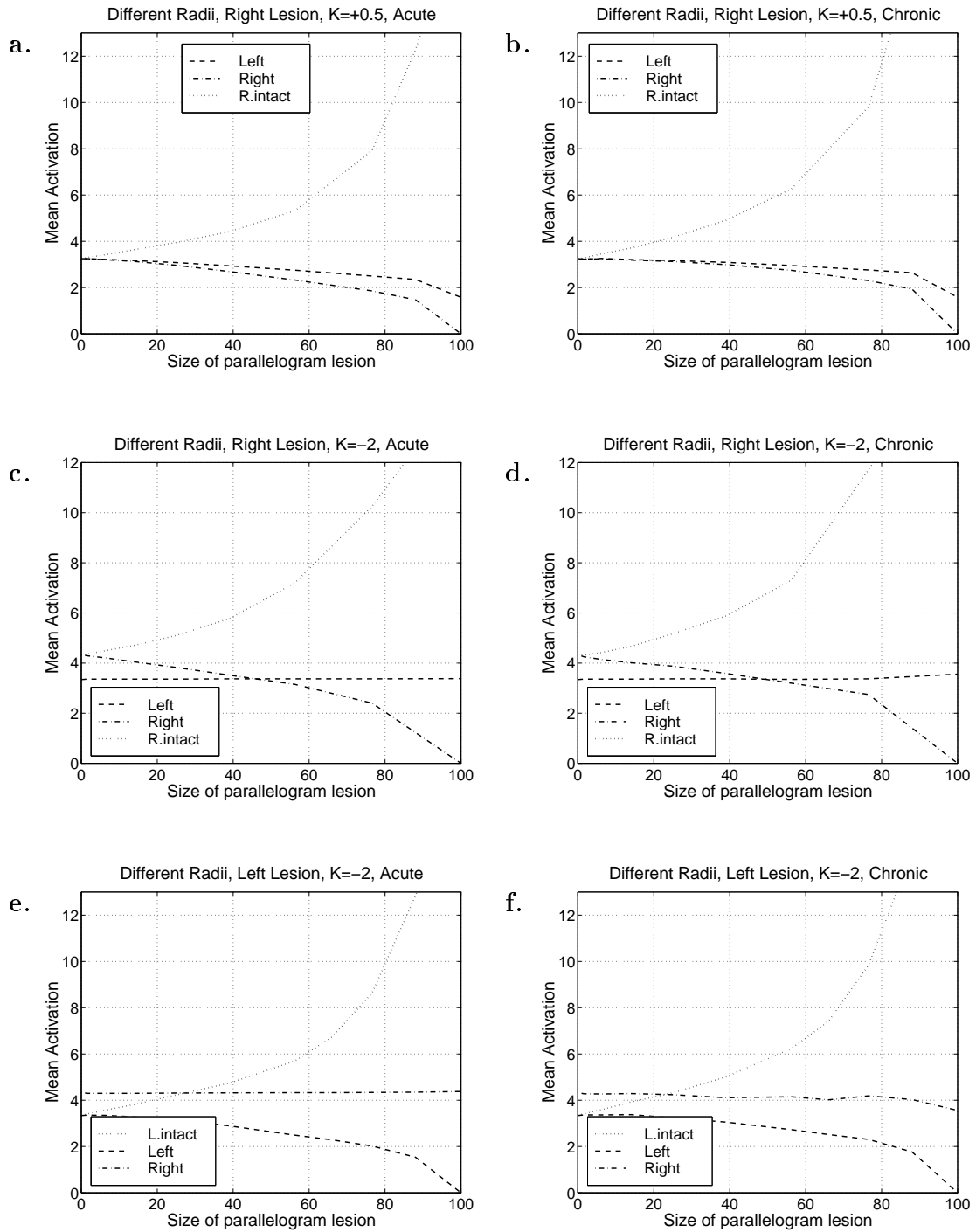
Figure 5.9: Mean activation versus lesion size in case of asymmetric connectivity for focal lesions. Same layout as Fig. 5.8.

Table 5.4: Organization and Other Measures for Maps in Fig. 5.10

Map	K^*	Lesion type	Organization Left	Organization Right	Latera-lization	Mirror Symm.	Mean Activation Left	Mean Activation Right	Mean Activation L.intact
a.	+0.5	None	1.0	1.0	0.0	+1.0	3.25	3.25	3.25
b.	-2	None	1.0	0.16	-0.84	-0.69	3.34	4.34	3.34
c.	+0.5	Acute Focal	0.83	0.98	0.15	0.69	3.13	3.17	3.64
d.	-2	Acute Focal	0.63	0.20	-0.43	-0.62	2.89	4.32	4.74
e.	+0.5	Focal	0.87	0.94	0.07	0.85	3.12	3.14	3.63
f.	-2	Focal	0.64	0.44	-0.20	-0.44	3.05	4.27	5.00
g.	+0.5	Chronic Focal	0.91	1.03	0.12	0.82	3.17	3.20	3.69
h.	-2	Chronic Focal	0.65	0.57	-0.08	-0.34	3.05	4.11	5.01

$^*K$ = callosal strength.

dominant (left) hemispheric region is lesioned and looses enough elements (about 20% or more), the contralateral side begins to improve after retraining (Fig. 5.10, right column). With asymmetric connectivity, unlike with any other case, for $K = -2$ the mean activation of the remaining (intact) elements in the damaged hemisphere (either one) *increases* with lesion size while the activation of the other side stays fixed. However, the overall mean activation of the damaged side is decreased with larger lesions.

Asymmetric Size Hemispheric Regions

Finally, the case when the two cortical regions had different numbers of elements is considered: the left had 16x16=256 elements while the right had only 12x12=144 elements. Pre-lesion maps were again complete and symmetric for $K = +1$ and complementary with pronounced lateralization to the left for $K = -2$. For excitatory callosal connections the changes caused by lesions were similar to those in the symmetric case (Fig. 5.3a,b, Fig. 5.4a,b), except for one interesting phenomenon related to the fact that in the intact model the mean activation of the elements of the smaller hemispheric region is higher than that of the larger hemispheric region (see Table 1). If the larger region is lesioned, the mean activation of its remaining (intact) elements is higher with larger lesions (just as before), and becomes approximately equal to the mean activation of the smaller hemispheric region when the number of remaining elements in it equals the number of elements of the smaller region. For larger lesions the mean activation of the remaining elements increases quite rapidly, similar to the symmetric case.

When the connections are strongly inhibitory, the model reacts to the lesions similar to the asymmetric excitability case described above (Figs. 5.6, 5.7). Namely, a lesion in either hemispheric region causes a drop in ipsilateral organization and some improvement in contralateral organization acutely, with additional contralateral improvement after retraining. All these phenomena are much more pronounced when the dominant hemisphere is lesioned, so that a lesion of about 35% or more causes lateralization to reverse. Mean activations of the two hemispheric regions behave similarly to corresponding organizations.
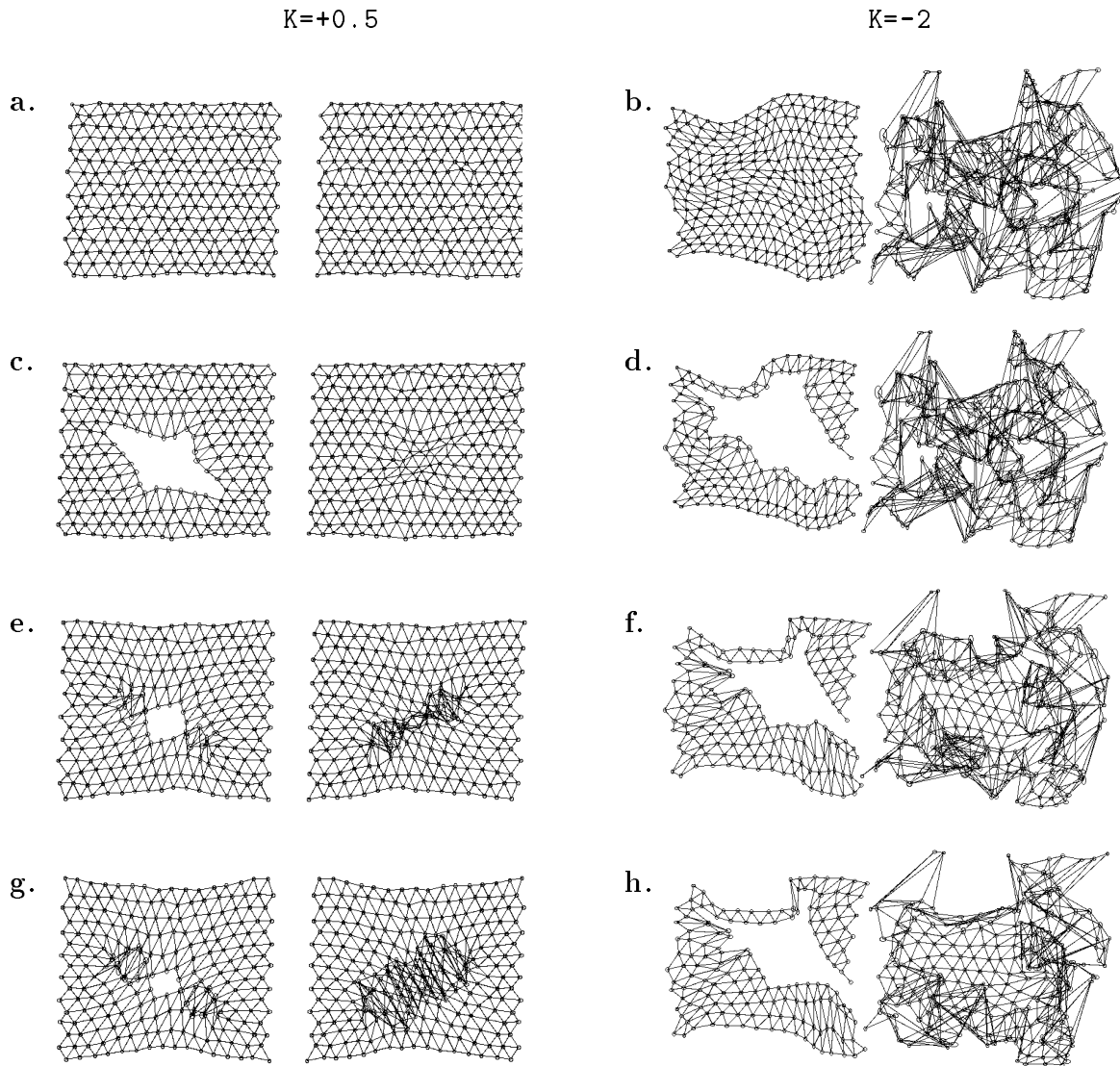
Figure 5.10: Snapshots of topographic map changes after focal lesions in the different connectivity case (**left column:** 6x6 lesion for excitatory connections, **right column:** 10x10 lesion for inhibitory connections). **Top row:** maps before the lesions; **second row:** acute lesions; **third row:** after short training (32768 inputs for $K = +0.5$, 98304 inputs for $K = -2$); **bottom row:** after longer training (131 thousand inputs for $K = +0.5$, 262 thousand inputs for $K = -2$).

5.4.3 Summary of Lateralization Results

Table 5.5 summarizes the results of simulations for lesions involving 56% of a hemispheric region. For focal lesions, this corresponds to a 12x12 lesion in the standard 16x16 hemispheric region, or to a 9x9 lesion in the smaller 12x12 cortical region in the case with size asymmetries. It presents the values of lateralization for focal and diffuse lesions of each side of the model right after the lesion and after retraining.

Table 5.5: Post-Lesion Lateralization Values

Case	Prelesion latera-lization	Focal				Diffuse			
		Left		Right		Left		Right	
		Acute	Chronic	Acute	Chronic	Acute	Chronic	Acute	Chronic
Symmetric									
$K = -2$	0.06	0.50	0.77	-0.43	-0.71	0.65	0.92	-0.63	-0.93
$K = -1$	0	0.64	0.49	-0.64	-0.49	0.92	0.98	-0.92	-0.98
$K = +1$	0	0.78	0.61	-0.78	-0.61	0.94	0.96	-0.94	-0.96
Excitability									
$K = -2$	-0.53	0.16	0.49	-0.76	-0.93	0.38	0.71	-0.89	-0.99
$K = -1$	0	0.59	0.50	-0.68	-0.50	0.92	0.98	-0.91	-0.97
$K = +1$	0	0.79	0.64	-0.78	-0.61	0.94	0.96	-0.94	-0.96
Size									
$K = -2$	-0.50	0.25	0.36	-0.77	-0.82	0.71	0.53	-0.89	-0.99
$K = +1$	0	0.80	0.70	-0.75	-0.69	0.97	0.97	-0.98	-0.98
Connectivity									
$K = -2$	-0.84	-0.17	0.45	-0.94	-0.88	0.14	0.21	-1.0	-1.0
$K = +0.5$	0	0.60	0.49	-0.60	-0.49	0.92	0.89	-0.92	-0.80

The table illustrates the following trends in lateralization changes after a lesion:

- diffuse lesion always causes larger damage in the ipsilateral side than a focal one of the same size, and hence smaller lateralization when the dominant side is lesioned and larger lateralization for a non-dominant side lesion;

- the amount of post-lesion lateralization depends not only on the size and shape of the lesion, but also on pre-lesion lateralization, callosal influences, and type of asymmetry in the model;

- retraining usually *reduces* lateralization when callosal influence is excitatory or weakly inhibitory and *increases* lateralization when callosal influence is strongly inhibitory.

5.5 Discussion

The work described in this chapter examined the effects of simulated lesions on cortical maps in versions of the S2 model. Both the details of the intact model (symmetric vs.

asymmetric regions, callosal influences, etc.) and of the lesions (number of cortical elements lost, focal vs. diffuse, etc.) have been systematically varied. This is the first investigation of how underlying cortical asymmetries and callosally-mediated hemispheric interactions might influence the recovery process and how the contralateral intact hemisphere might participate in recovery.

Simulations of sudden focal cortical lesions in this model showed that the larger the lesion, the greater the disruption of the maps on the lesioned side, regardless of the assumed role of callosal connections. This expected increase in disorganization with increase in lesion size was modulated by the degree of pre-lesion lateralization. Specifically, the more lateralized a model was initially, the more effect a left "dominant hemisphere" lesion had on overall map organization relative to an equivalent right "non-dominant hemisphere" lesion, regardless of the underlying cause of lateralization. The occurrence of increased organization deficits with larger lesion size and/or dominant hemisphere damage, and the rapid-then-slow temporal pattern of recovery, are encouraging in demonstrating that, however simplified the model is compared to reality, it does capture some expected fundamental aspects of post-lesion observations.

More interestingly, the model's post-lesion behavior gives some insight into two currently controversial issues concerning hemispheric interactions. First, as noted earlier in this dissertation, it is not clear today whether each hemisphere exerts primarily an overall excitatory or inhibitory influence on the opposite hemisphere via the corpus callosum. Most neurons sending axons through the corpus callosum are pyramidal cells, and these synapse mainly on contralateral spiny cells [55, 66]. Such excitatory synaptic *connections*, as well as transcallosal diaschisis and split brain experiments, suggest that the resultant transcallosal influences are mainly excitatory in nature [15]. However, this hypothesis is quite controversial [38]. Transcallosal monosynaptic postsynaptic potentials are subthreshold and of low amplitude, and are followed by stronger, more prolonged inhibition [125], suggesting to some that transcallosal inhibitory influences are much more important [34, 72]. Recent transcranial magnetic stimulation studies have also indicated that activation of one motor cortex region inhibits the contralateral one [45, 87], although it is difficult to know what this response to such a non-physiological stimulus implies for normal physiological hemispheric interactions.

The lesioning results with S2 model provide some support for the hypothesis that the overall effects of callosal connections are predominantly excitatory. In general, regardless of callosal influences, acutely after a focal lesion to one hemispheric region in the model, the activation levels in that hemispheric region decreased substantially, as occurs experimentally. However, the post-lesion changes in activation in the contralateral intact hemispheric region depended on callosal influences. With excitatory callosal influences, lesions generally resulted in an acute fall in averaged hemispheric activation in the intact, unlesioned hemisphere. In contrast, with versions of the model having inhibitory callosal influences, mean activation in the unlesioned hemisphere generally increased substantially acutely after lesions due to disinhibition. Experimental studies measuring regional cerebral blood flow and glucose metabolism have consistently demonstrated an acute fall in hemispheric activation following cortical lesions, not only on the lesioned side but also in the contralateral non-lesioned hemispheric region [88, 27, 40, 22]. Thus, to the extent that cerebral metabolism and blood flow are coupled to cerebral activation, the model results with excitatory callosal

connections best fit existing data. The increase in mean activation in the model's unlesioned hemisphere when callosal influences are inhibitory also appears to be inconsistent with this same data.

The second controversial issue concerning interhemispheric interactions for which this model has implications is the extent to which the non-lesioned hemisphere participates in recovery following a lesion. There is substantial recent evidence that the unlesioned hemisphere is responsible for a significant part of recovery from sensorimotor and language deficits following a stroke (e.g., [117, 118, 131, 132, 94, 27]). However, other studies have questioned the role of the contralateral hemisphere in the recovery process (e.g., [8, 57, 58]). Very little is currently known about this issue specifically with respect to sensory maps, although one study has found changes in receptive fields sizes contralateral to a partially denervated cortical region [26].

In many versions of S2 model, clear cut changes in contralateral maps occurred following lesions. When full symmetric maps were present initially, generally little change was seen in the map contralateral to the lesion. (An exception occurred when the hemispheric regions had asymmetric connectivity, and lesions caused increased disorganization in the contralateral map during the recovery period.) In such cases, there were two duplicate maps of the same sensory surface before lesioning, a fault-tolerant situation in which the built-in redundancy automatically compensates for the lesion. In contrast, when complementary/antisymmetric maps were present before lesioning, a single map of the full sensory surface was divided across the left and right hemispheric regions, similar to the mosaic maps found in some animal cortices [17]. In these cases, lesioning of one map generally resulted in increased map formation and organization in the contralateral, intact hemispheric region. These results represent testable predictions of the models that could readily be investigated using current electrophysiological methods similar to those in [17].

Finally, note that diffuse lesions in a cortical region generally had more pronounced effects than focal lesions of the same size. This finding is in accordance with theoretical predictions of post-lesion memory capacity changes in spatially-organized neural networks [113], and suggests that such theoretical predictions apply to a wider range of models than initially considered.

Chapter 6

S4 Simulator

This chapter presents a second model, called the S4 model, that more closely matches input connectivity in much of biological cortex primary sensory regions. This model of cortical maps is a generalization of the S2 simulator. The chapter describes the model and gives simulation results for the symmetric case and several model asymmetries. The results are qualitatively similar to those of the S2 simulator, but they also give insight into some important details of topographic map formation.

6.1   The Model
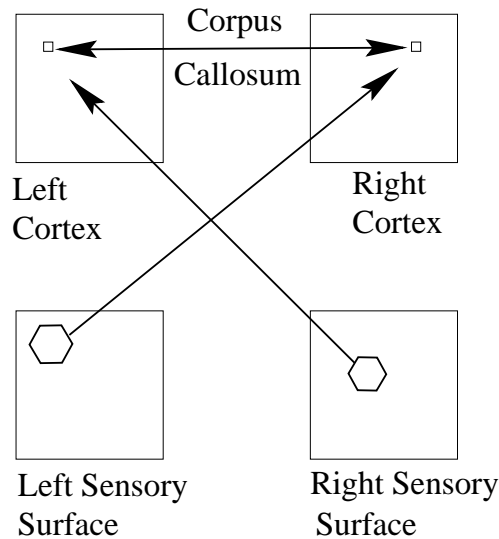
Figure 6.1: The model of two interacting cortical regions receiving inputs from two independent sources.

The S2 simulator was the first model of bihemispheric cortical maps. It had a single, shared sensory surface, and thus could represent only a small portion of real primary sensory cortex (i.e., midline regions). The primary sensory maps in the mammalian brain mostly receive inputs only from contralateral sensory surfaces, so in order to simulate them more closely

another model is needed. Figure 6.1 shows its high-level structure, which differs from the S2 model in having two sensory surfaces. This model uses the same internal structure, activation and learning rules as S2 simulator, but it allows independent (or dependent, but different) inputs to the two sensory sets. We refer to it here as the S4 simulator.

Receptive fields can be computed in two ways in the S4 simulator. One way of computing receptive fields, which seems most natural, is to give point stimuli to the left sensory surface (one at a time), record responses in the right cortex, and then compute receptive fields for the right cortex. Then a similar procedure is performed on the right sensory surface and left cortex. A second way of computing receptive fields mimics experiments described by Bianki [17], where he uses bilateral stimuli to find asymmetries in the sensory maps. This can be done by applying point stimuli in the corresponding nodes of both sensory sets at the same time and recording cortical responses in both cortical sets. Both ways of computing receptive fields are used in this study, and the results are compared with each other and with the S2 simulator.

Experimental methods and baseline parameters used for the S4 simulator were identical to those used for the S2 simulator, except the radius of input stimuli was 2 in most cases, and the two sensory surfaces gave an additional degree of freedom in considering independent, symmetric, or nearly symmetric input stimuli.

6.2   Results with the S4 Simulator

Fig. 6.2 shows a few representative examples of the kinds of maps that emerge during learning in the S4 simulator. The specific maps that appear depend, for example, on whether the two cortical regions have identical or different parameters (excitability, size, etc.), whether overall callosal influences are assumed to be excitatory or inhibitory, on the way of computing receptive fields, and on the training input stimuli overlap.

In general, the maps observed are similar to those with the S2 simulator. For example, the vertices (nodes) in the left picture in Fig. 6.2b represent the centers of the receptive fields of the left cortical region after training plotted in the space of the sensory surface, just as with the S2 model. The entire grid in this specific picture shows that a fairly organized map is present in both cortical regions (i.e., the sensory surface projects in a smooth fashion onto the two-dimensional cortex surface), the typical result found after learning when excitatory callosal influences are present. In contrast, Fig. 6.2d,i illustrate cases with strong inhibitory callosal influences where the well-organized parts of the right and left cortical regions after training are complementary (antisymmetric with respect to reflection in the vertical midline). Values for organization, lateralization, and mirror symmetry for the maps in Fig. 6.2 are given in Table 6.1.

It is interesting to note that Fig. 6.2g,h,i,j all represent the S4 simulator results for the symmetric case with $K = -2$. The only difference between them is the way of computing receptive fields (bilateral point stimuli for **g** and **i**, independent computation for **h** and **j**) and independent (for **g** and **h**) versus symmetric (for **i** and **j**) training inputs. All four pairs are clearly very different, with **h** having complete symmetric maps, **i** fully complementary with sharp boundaries between organized and unorganized subregions, and other two also
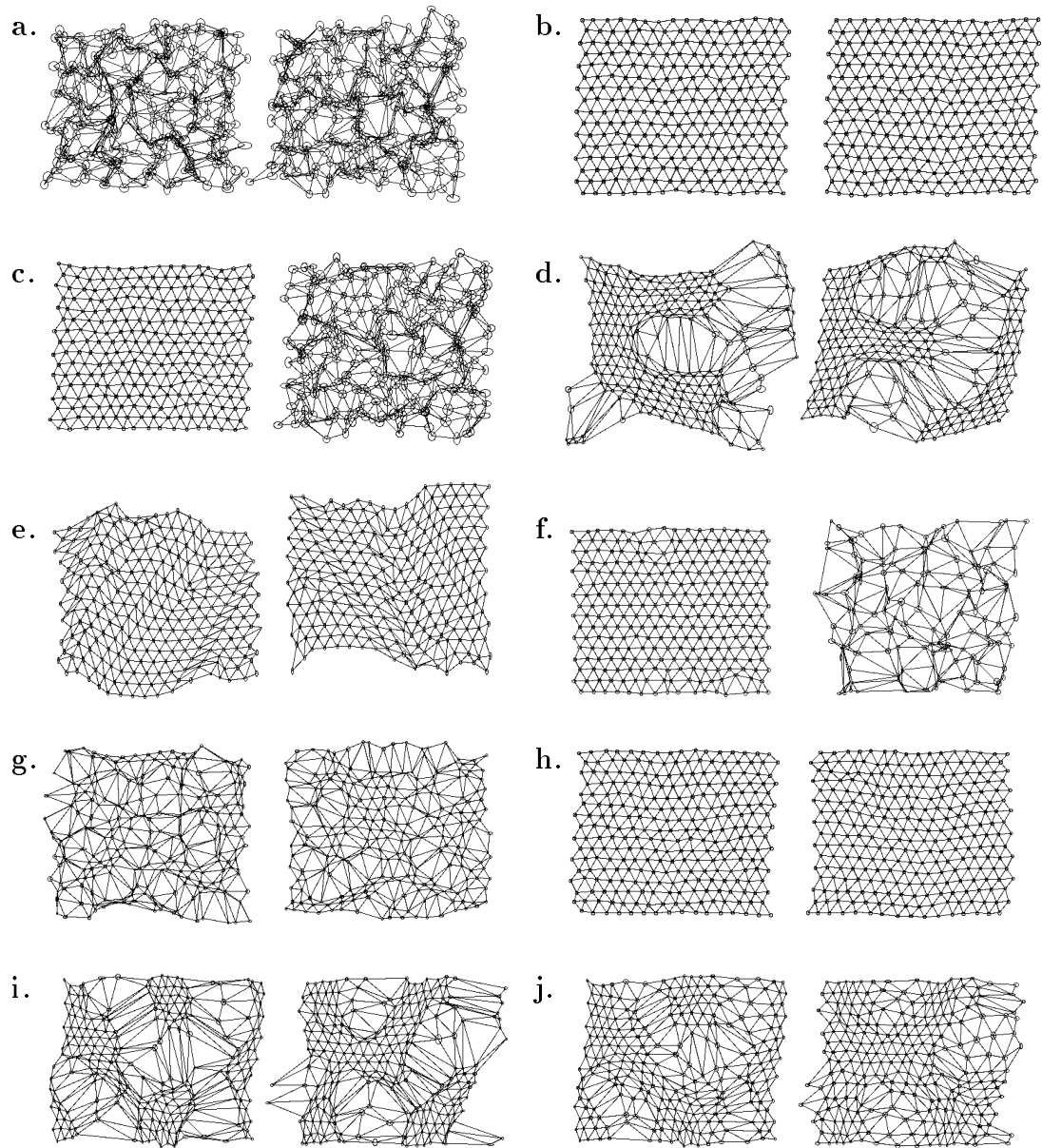
Figure 6.2: Receptive field maps produced by the S4 simulator: (a) the maps before training (unorganized); (b) bilaterally organized maps after training; (c) the left map is better organized than the right; (d),(i) organized regions are complementary; (e) maps are shifted and curved; (f) cortical regions have different size; (g–j) effects of different ways of computing receptive fields and different overlap of training input stimuli: (g), (h) independent stimuli, (i), (j) symmetric training stimuli, receptive fields were computed independently for (h) and (j), and with bilateral point stimuli for all other map pairs shown here.

Table 6.1: Values of Quantitative Measures for the Maps in Fig. 6.2

| map | sigmoid diff. (SD) | | organized area | | lateralization | mirror |
	left	right	left	right	based on SD	symmetry
a	0.01	0.00	0.02	0.05	0.0	undefined
b	0.98	0.99	1.0	1.0	0.01	1.0
c	0.97	0.15	1.0	0.0	-0.82	-1.0
d	0.67	0.66	0.40	0.38	-0.01	-1.0
e	0.75	0.74	0.47	0.47	-0.01	-0.39
f	0.97	0.20	0.93	0.01	-0.77	-1.0
g	0.39	0.57	0.12	0.22	0.18	-0.94
h	0.99	0.99	1.0	1.0	0.0	1.0
i	0.52	0.58	0.23	0.27	0.06	-1.0
j	0.68	0.73	0.46	0.50	0.05	-0.82

complementary, but the boundaries are very vague. We will return to the discussion of the these maps at the end of this chapter and in the next chapter, where the mechanics of map formation is considered in detail.

6.2.1 Varying Training Input Overlap

Since the main difference between the S4 and the S2 simulators is the ability of the S4 simulator to use different input stimuli for training, it is natural to look at how different degrees of training input overlap affect map formation (for simplicity, in the symmetric case). The term "training input overlap" can be defined as the number of sensory elements in the intersection of an input stimulus in the left sensory surface and the mirror image of the training stimulus (at the same time) in the right sensory surface. Recall that in the symmetric case the S2 simulator produced perfect maps for $K > -1.4$ and complementary ("mosaic") maps for $K < -1.4$. When the training inputs are independent in the S4 simulator, one would expect the activations in the two cortical layers not to interfere with each other most of the time, and so expect two complete maps to form quickly in both cortical layers for any K. With 100% overlap one would expect the S4 simulator to produce the same results as the S2 simulator. Hence the most interesting case to look at is $K < -1.4$, for instance, $K = -2$.

Figure 6.3 shows results for the symmetric case, $K = -2$, when the overlap of training inputs was varied from 0 to complete, with radii of the input patches 1 and 2. The reason radius 2 is used (a hexagonal patch of radius 2 includes 19 nodes; a patch of radius 1, only 7) is that with hexagonal radius 1 only a very limited number of overlap values is possible (0,1,2,4 and 7), and also with bigger training patches even independent random inputs have a higher chance of interacting, producing some interesting phenomena.

Fig. 6.3 has two columns, corresponding to the two different ways of computing receptive fields in this model, described in section 6.1. The left column is based on bilateral computa-

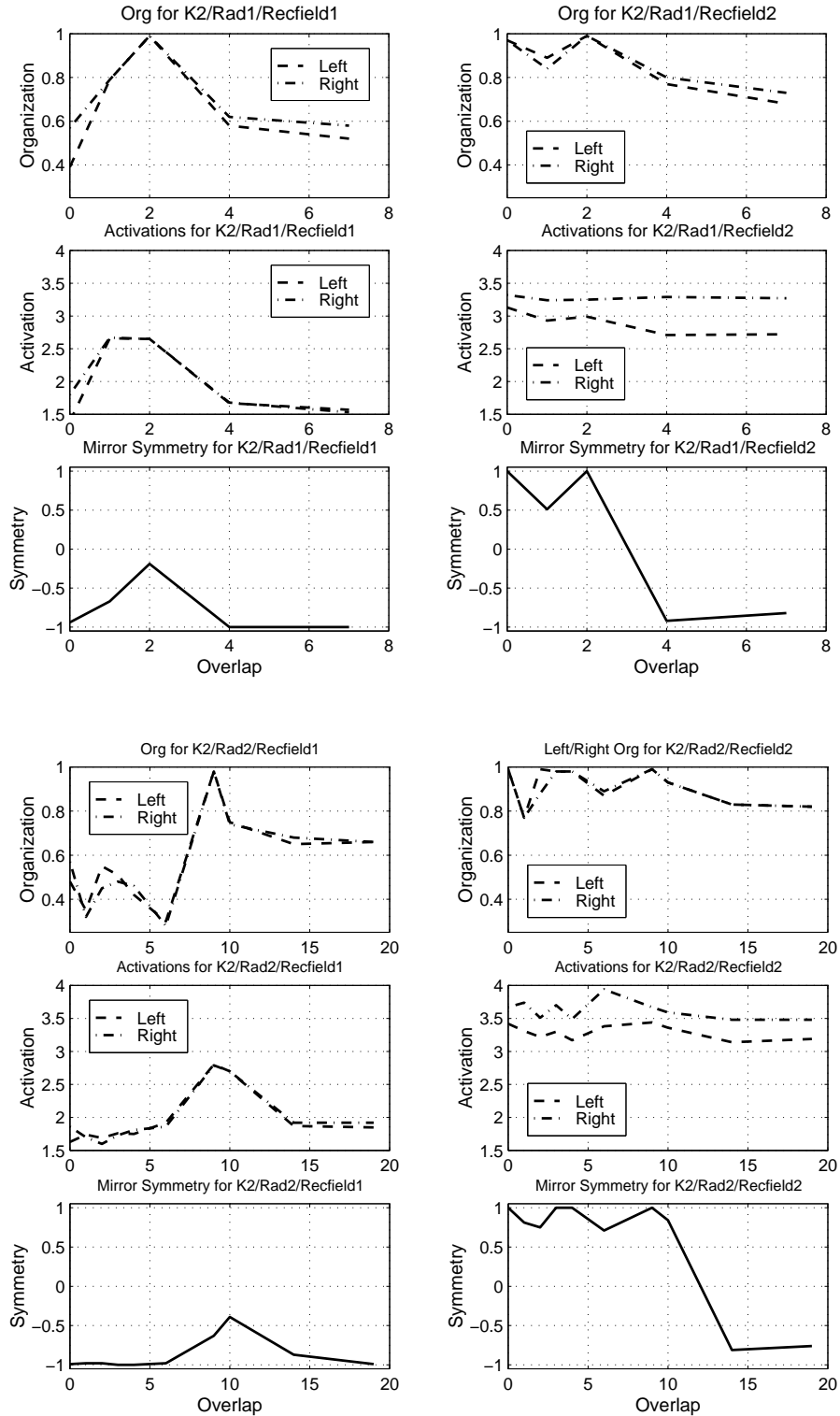Figure 6.3: Results of the S4 simulator for the symmetric case with varying training input overlap. Top: training inputs of radius 1, bottom: of radius 2. The horizontal axis is overlap of simultaneous left and right stimuli in every graph here. The left column corresponds to the bilateral method for computing receptive fields, the right column is based on independent computation of receptive fields.

tion of receptive fields, and the right column corresponds to independent point stimuli. The figure illustrates several important observations:

- results for radius 1 and 2 are qualitatively similar;

- the different ways of calculating receptive fields produce very different results, even though the same weight vectors are used;

- map complementarity is much more pronounced when the training input overlap is higher;

- for some input overlap (usually close to 50%) the simulator produces "shifted" maps, i.e. nearly perfect maps but shifted in different directions, such as in Fig. 6.2e.

6.2.2   Symmetric Case

Radius 2 input stimuli were used for the simulations described below, with three different training input overlap values: 0 for independent randomly-centered inputs, overlap 10 (nearly 50% overlap), and overlap 19 (perfectly symmetric training inputs). Figure 6.4 shows results for the symmetric case when K varied between -4 and 1. As in the S2 simulator, sharp transitions in organization and symmetry values appear between -1 and -1.5. No significant lateralization is present.

The sharp transitions appear both for independent and symmetric inputs, but for symmetric inputs they appear independently of the method used for receptive field calculation, while for independent inputs only bilateral point stimuli reveal the transition. This is related to the difference in weight changes, to be discussed in the next chapter.

6.2.3   Asymmetric Cases

Figure 6.5 shows results for the asymmetric excitability case. Lateralization is noticeable for inhibitory callosal connections, and is strongest when the training inputs are symmetric. Similar to the symmetric case, independent training inputs and independently computed receptive field maps produce perfect symmetric maps for all values of K, while the same weights and bilaterally computed receptive fields lead to some lateralization and asymmetry. Independent calculation of receptive fields after training with symmetric stimuli smoothes out most of the lateralization, but asymmetry persists.

Overall, significant lateralization and complementary maps were observed in the simulations with strongly inhibitory callosal influences and asymmetry in the size or excitability of the cortical regions. Asymmetric synaptic plasticity caused only transient (but very strong for some callosal strengths) lateralization (Fig. 6.2c) which disappeared after further training. Results for independent and symmetric training stimuli were in most cases surprisingly similar qualitatively. For asymmetric excitability though, lateralization was stronger for symmetric stimuli. Figure 6.6 summarizes results for the various kinds of model asymmetry favoring the left side that were studied. It presents plots of lateralization for varying callosal strength for the cases when training stimuli were symmetric and when they were
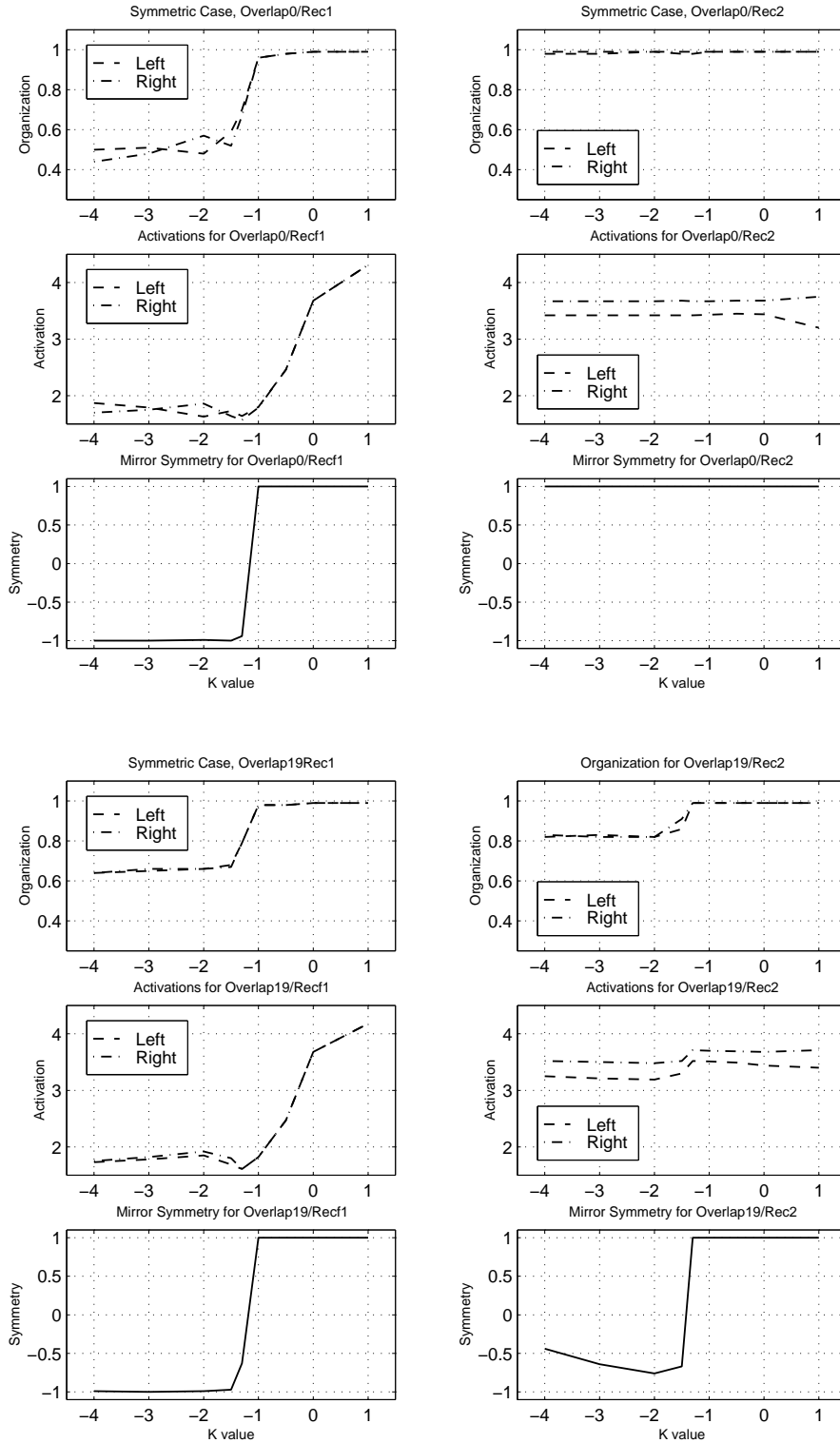
Figure 6.4: Results of the S4 simulator for the symmetric case. Top: independent training inputs, bottom: identical training inputs. The horizontal axis is the callosal influence K in every graph here. The left column corresponds to the bilateral method for computing receptive fields, the right column is based on independent computation of receptive fields.
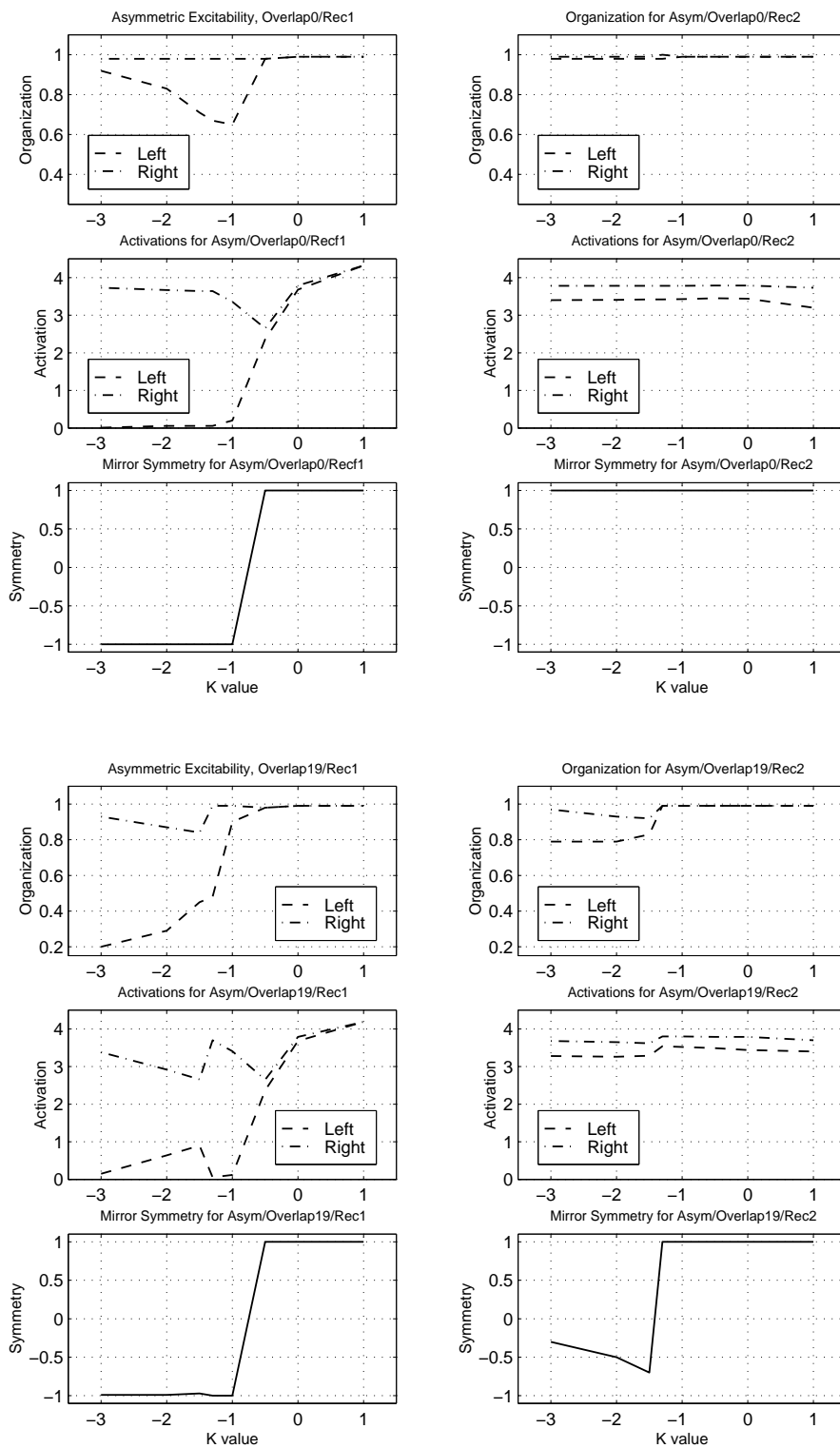
Figure 6.5: Results of S4 simulator for asymmetric excitability case. Same notation as in Fig. 6.4.

independent, but receptive fields were computed bilaterally for both cases. For the asymmetric synaptic plasticity case only lateralization after short training is presented. In fact, asymmetric synaptic plasticity was the only case producing lateralization with independent training inputs *and* independently computed receptive fields.
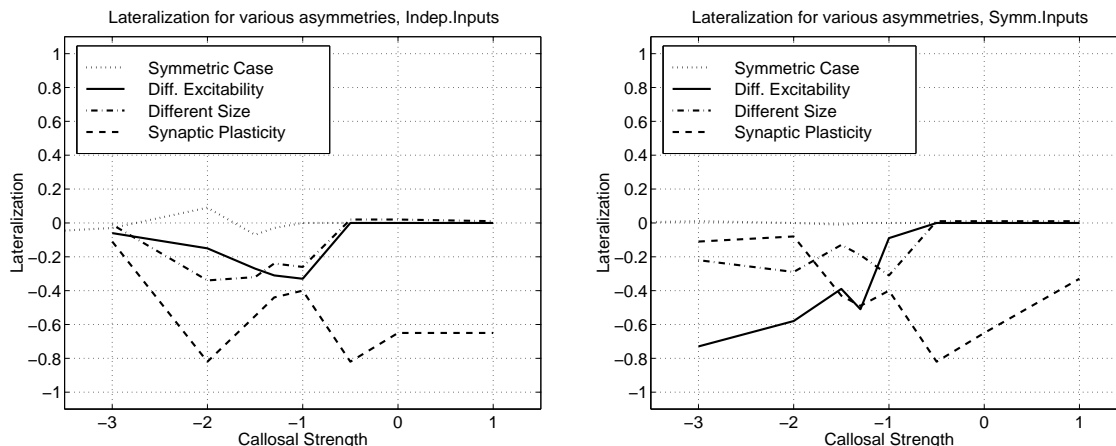

Figure 6.6: Summary of lateralization results for all model asymmetries for independent (left) and symmetric (right) training inputs.

6.3   Discussion

The S4 simulator described in this chapter allows independent inputs to the left and right cortical regions. This is similar to what happens in much of biological primary sensory maps, since each hemisphere of a real brain normally receives input mostly from the contralateral side of the body. The effects of various model asymmetries, excitatory and inhibitory callosal influences, and different degrees of training input overlap were studied systematically. The study of varying training input overlap shows that identical training inputs can produce most of the interesting phenomena observed, thus justifying using a simpler model (with only one sensory surface) as with the S2 simulator.

Observation of simulation results obtained with independent training inputs and with the different ways of computing receptive fields gives insight into the map formation process which the S2 simulator could not give. Namely, it shows that for strongly inhibitory callosal influences even when the incoming cortical weights are well-organized, the receptive field maps (computed bilaterally) are poorly organized. On the other hand, even when the weights are not so well organized, independent calculation of receptive fields may help to improve the map organization.

Consider a symmetric case with strongly inhibitory callosal connections. The four maps produced by the S4 simulator using symmetric and independent training inputs, bilateral and independent point stimuli during receptive field calculations are shown in Fig. 6.2**g–j**. The map **h** obtained with independent training stimuli and independent calculation of receptive fields is nearly perfect. The map **g**, based on the same weights, but computed

69
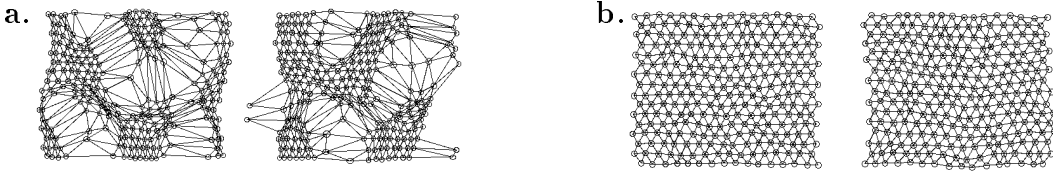
Figure 6.7: Incoming weight vectors after training for the symmetric S4 model with strongly inhibitory callosal influences: **a.** Symmetric training inputs; **b.** Independent training inputs.

with bilateral point stimuli, is quite different. The organization of both of its parts is very low (even lower than that of the complementary maps produced by the S2 simulator for symmetric case), and the symmetry measure is close to -1. The map **i** is a typical example of the S2 simulator result, and map **j** is its smoothed out version. Fig. 6.7 presents the incoming weight vectors after training with symmetric (a) and independent (b) stimuli. Clearly, the two plots are quite different (the weights in part **a** are very well organized, while in part **b** they are ready for producing complementary mosaic-type maps), and this difference is reflected in the receptive field maps. Thus, both the weights and the method of receptive field computation play an important role in determining final map organization.

Chapter 7

Theoretical Analysis

This chapter presents a mathematical analysis of some important aspects of the models described in this dissertation. First, a summary of previous results for similar models is given. Then, analysis of total hemispheric activations for the S2 simulator leads to the discovery of some bifurcations, and their role in the behavior of the model is explained. Another variation of the model, having even more competitive distribution of activation, is also considered and analysed. Further, results with the S4 simulator reveal the relationship between organization of the weights and of receptive field maps (depending on the way of computing receptive fields). This is also explained by the above bifurcation. Finally, it is shown that the activation patterns forming in the cortex in the beginning of training can predict the organization of the weights after training. Namely, the average dot product of activations in the cortex and sensory surface correlates quite well with the final organization of incoming weights. This is explained, and it is shown how this dot product, in turn, depends on the parameters of the model. Thus, the analysis makes it possible to predict map organization (given all model parameters) before training.

7.1   Past Related Work

This section briefly summarizes previous mathematical analysis of neural models using competitive distribution of activation.

Several researchers attempted mathematical analysis of the activation dynamics in S1 simulator and similar models. However, since the system of nonlinear equations (2.1) and (2.2) for all sensory and cortical elements is too complicated, various simplified versions were actually analysed. The ultimate goal of this research is the analysis of more complex models based on the S1 simulator, so it is important to list the existing results of the S1 simulator analysis here.

First we notice that the dynamics of activation of sensory nodes is not too hard to analyse since there are no lateral connections: the nodes receiving constant positive input quickly approach the maximum activation level Max, while the nodes with no input stay at activation level 0. These are the only two types of dynamics that can happen in the sensory layer.

Sutton [123] found that when no sensory input is present and all cortical nodes are

assumed to have the same activation, that activation has a stable fixed point at 0 provided that $c_s + c_{lf} Max < 0$.

Reggia and Edwards [107] considered a neural network with competitive distribution of activation, when the activation of node i is governed by

$$a_i(t + \delta) = a_i(t) + \delta[e_i(t) + r_i + \sum_{j \in N} c_{ij}(t)a_j(t)] \tag{7.1}$$

where $0 < \delta \leq 1$ represents the fineness of time quantization, $e_i(t)$ denotes the external input to node i at time t, r_i is a constant bias at node i, and $\sum_{i \in N} c_{ij}(t) = c$ for any j, where N denotes the whole network. Total external input is assumed to be constant (E) and defining $R = \sum_{i \in N} r_i$, they found two phase transitions for the total network activation $A(t) = \sum_{i \in N} a_i$: The total network activation asymptotically approaches a fixed point $A^* = -(E + R)/c$ whenever $-2/\delta < c < 0$ (as $t \to \infty$). For c outside this interval the total activation diverges, i.e. grows without bounds. Thus, $c = 0$ and $c = -2/\delta$ are two phase transitions. This result applied to the S1 simulator (where ODEs are replaced by Euler method approximations with time step δ) leads to the conclusion that the total activation converges when $c_s + c_{lf} < 0$ and $\delta < -2/(c_s + c_{lf})$. Of course, the convergence of the total activation is a necessary but not a sufficient condition for the convergence of activations of individual nodes.

McFadden, Peng and Reggia [85] found local conditions for boundedness and divergence of the entire activation vector in a more general model. In terms of model (7.1) their results can be formulated as follows: define positive, negative and self-gains associated with node j as

$$c_P^j = \sum_{i \in P_j} c_{ij}(t), \quad c_N^j = \sum_{i \in N_j} c_{ij}(t), \quad c_S^j = c_{jj}(t),$$

where P_j and N_j are the sets of nodes receiving positive and negative connections from the node j respectively. Then parameters

$$c^j = c_P^j + c_N^j + c_S^j \quad \text{and} \quad R^j = c_P^j - c_N^j$$

play a significant role in determining the behavior of the system. Namely, if the conditions $c_S^j < -R^j$ and $\delta(R^j - c_S^j) < 2$ hold for any j then the system (7.1) is bounded for all choices of initial values. Note that R^j is a Gershgorin radius derived from the jth column of the connection matrix. Another theorem from [85] implies that in model (7.1) with zero external input, if either $c_S^j > R^j$ or $c_S^j < -2/\delta - R^j$, then the system diverges for all nonzero initial values.

Benaim and Samuelides [14] found a Lyapunov function and used it to prove convergence for a competitive distribution model which was substantially different from the S1 model. Their result was based on LaSalle's invariance principle and Hirsch's theorem [62]. Although it is not directly applicable to the models considered here, the approach seems to be promising. In fact, McFadden [83] and Peng Wu [136] found Lyapunov functions for models which are closer to S1 simulator and also used Hirsch's theorem to prove convergence.

Finally, Yinong Chen and Reggia [32] considered a competitive distribution model very

close to the S1 simulator. Under some simplifying assumptions, such as the absence of lateral connections in the cortical layer and only one input node, they proved convergence of activations to a fixed point, coordinates of which were found explicitly.

7.2 Simplified S2 Model and Total Activations

In the simulations described in Chapters 4 and 6 a sudden transition occurs in model behavior at a specific callosal strength (roughly $K = -1.4$ in the symmetric case, $K = -1.2$ in the asymmetric excitability case). For K above this strength, symmetric, non-lateralized and highly organized maps occur, while for K below, lateralized and asymmetric mosaic pattern maps occur. What causes this transition or bifurcation in model behavior? Below the cause of a change in the dynamics of total hemispheric activations near $K = -1.4$ is shown and then an explanation on how it leads to asymmetry in map formation is given.

First, consider the difference in total activation of the left hemispheric region L versus the right R in the model. The activation dynamics described by (3.1)– (3.5) are highly nonlinear and difficult to analyze. However, as in [107], a "linearized" version of these equations gives insight into the model's dynamics. Consider equations

$$\frac{da_i^L}{dt} = c_s a_i^L + in_{Li}^+ + in_{Li}^-, \tag{7.2}$$

where a_i^L is the activation of element i in L, and in_{Li}^+ and in_{Li}^- are inputs to that element given by (3.2) to (3.5). By algebraic manipulations, for $j \in L$, $k \in S$, $m \in R$ we have

$$\sum_{i \in L} c_{ij}^{LL} = c_{lf}^L, \quad \sum_{i \in L} c_{ik}^{LS} = c_p^L, \quad \sum_{i \in L} c_{im}^{LR} = K^{LR}. \tag{7.3}$$

Analogous equations hold for the right hemispheric region R.

Consider a fixed input pattern. Denote the total activation in the left hemisphere by A_L, that in the right by A_R, and that in the sensory surface by A_S. Adding together the equations (7.2) for all elements i in the left hemisphere and using (3.2), (3.3) and (7.3) one obtains:

$$\frac{dA_L}{dt} = c_s A_L + c_{lf}^L A_L + c_p^L A_S + K^{LR} A_R \tag{7.4}$$

and a similar equation for the right hemisphere.

7.3 Symmetric Case

In the symmetric case, where $c_{lf}^L = c_{lf}^R = c_{lf}$, $c_p^L = c_p^R = c_p$ and $K^{LR} = K^{RL} = K$, subtracting dA_R/dt from dA_L/dt we have:

$$\frac{d(A_L - A_R)}{dt} = (c_s + c_{lf} - K)(A_L - A_R). \tag{7.5}$$

This indicates that when $K < c_s + c_{lf}$, an initial difference in activation levels of the two hemispheres will grow exponentially with time, while for $K > c_s + c_{lf}$, this difference will decay exponentially. With our baseline parameters this change is expected at $K = c_s + c_{lf} = -1.4$, precisely where the transition occurs in the symmetric case simulations (see Fig. 4.1). A more involved analysis given below shows that similar changes in asymptotic behavior of total hemispheric activations occur in a more general case for roughly the same K (e.g., when the two hemispheres have different excitation).

How does this change in activation growth affect symmetry and lateralization? With random initial weights, an input pattern quickly causes slightly different initial levels of activation in the two hemispheres. With time, this initial difference will either disappear (for $K > -1.4$) or grow (for $K < -1.4$). In the former case, both hemispheres will have nearly equal activation levels by the time a learning step occurs, and hence they will "learn" the input at about the same speed (assuming equal learning rates), hence eventually developing complete and symmetric maps. In the latter case, by the time of learning one hemisphere may be largely inactive while the other is highly active, so the input is more effectively learned by the more active hemisphere, resulting in local lateralization of map formation. Recalling that the hemispheric regions are homotopically connected, this competition occurs locally between mirror image sections of the cortex. Thus a small part of the map can become better organized on one side than the other. After a sufficiently long training period, a mosaic pattern is therefore likely to occur for $K < -1.4$. For symmetric hemisphere parameters by chance each hemisphere would be expected to be dominant on about the same number of input patterns as the other, and so complementary maps but almost no lateralization is expected. With asymmetric cortical excitability we would expect larger total activation more often on the more active hemisphere, so that hemisphere will develop a map covering a larger part of the sensory surface, which leads to lateralization.

Consider the general linearized case (7.2) where the hemispheric regions may be asymmetric. Denote $c_s + c_{lf}^L = c_L$, $c_s + c_{lf}^R = c_R$, $c_p^L A_S = B_L$, and $c_p^R A_S = B_R$, giving

$$\frac{dA_L}{dt} = c_L A_L + K^{LR} A_R + B_L, \quad \frac{dA_R}{dt} = K^{RL} A_L + c_R A_R + B_R. \tag{7.6}$$

This is a system of two linear differential equations, with matrix $\begin{pmatrix} c_L & K^{LR} \\ K^{RL} & c_R \end{pmatrix}$, whose trace is $c_L + c_R$ (negative in our model), and whose determinant is $c_L c_R - K^{RL} K^{LR}$; it thus has a unique fixed point unless $K^{RL} K^{LR} = c_L c_R$. The fixed point, which is asymptotically stable when $K^{RL} K^{LR} < c_L c_R$ and asymptotically unstable when $K^{RL} K^{LR} > c_L c_R$, is

$$A_L^* = \frac{-c_R B_L + K^{LR} B_R}{c_L c_R - K^{LR} K^{RL}}, \quad A_R^* = \frac{-c_L B_R + K^{RL} B_L}{c_L c_R - K^{LR} K^{RL}}. \tag{7.7}$$

In the symmetric case with baseline parameter values $c_L = c_R = -1.4$, $B_L = B_R = 7.0$, $K^{LR} = K^{RL} = K$, we have $A_L^* = A_R^* = 7/(1.4 - K)$, so for $K = 1.4$ activation grows without bound in the linearized model. However, the additional self-inhibition that we use for $K > 0$ in simulations prevents this problem: as stated earlier for positive K instead of $c_L = c_R = -1.4$ we use $c_L = c_R = -1.4 - 2.6K$, which makes the behavior of the fixed point

smooth for positive K (although it is not differentiable at $K = 0$): $A_L^* = A_R^* = 7/(1.4 + 1.6K)$. This fixed point remains asymptotically stable for all $K > 0$, facilitating symmetric map formation in both hemispheres. Thus, in the symmetric case the fixed point remains bounded, and is asymptotically stable for all $K > -1.4$ and asymptotically unstable for $K < -1.4$.

Thus, the following result has been justified:

Theorem 7.3.1. *In the symmetric case the system (7.4) has a bifurcation point at $K = c_s + c_{lf}$, and it causes a qualitative change in the behavior of the whole model.*

7.4 Different Excitability

In asymmetric cases, the coordinates of the fixed point behave more interestingly. For different input sensitivity constants ($c_p^L = 1.05$ makes $B_L = 7.35$, but $c_L = c_R$) the difference $A_L^* - A_R^* = (B_L - B_R)/(K - c_L)$ remains quite small for $K > -1$, but gets very large as K approaches $c_L = -1.4$. Different lateral feedback has a similar effect, except the bifurcation point changes slightly: when $c_L = -1.3$ the fixed point becomes unstable for a larger K ($K \approx -1.349$). The difference of the total activations at the fixed point is given by $A_L^* - A_R^* = B_L(c_L - c_R)/(c_L c_R - K^2)$ which is small for $K > -1$ and also goes up sharply near the bifurcation point. Fig. 7.1 shows the dependence of the fixed point on K for various cases. Here the additional self-inhibition for positive K is taken into account.
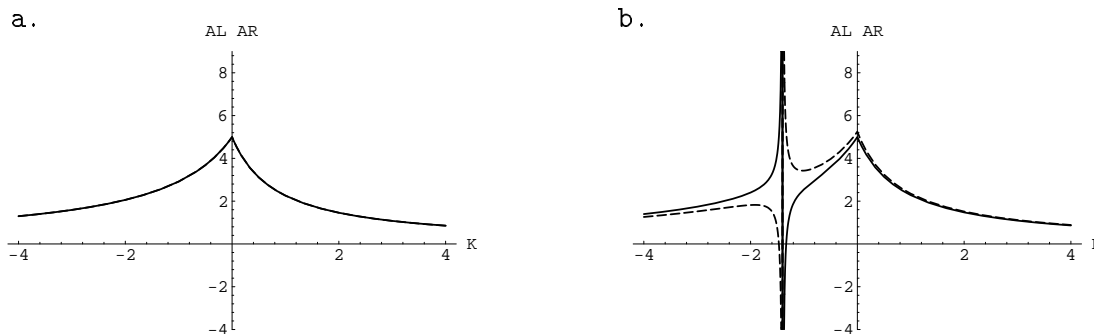

Figure 7.1: Fixed point of system (7.6) in (**a**) the symmetric case and (**b**) with asymmetric input sensitivities or lateral feedback coefficients. Dashed line is total activation for the left hemisphere, solid line for the right. In the symmetric case the values are equal and the two lines coincide; in the asymmetric case they are close except near $K = -1.4$.

Finally, asymmetric excitability actually causes *two* transitions in the model's dynamics. While the coordinates of the asymptotically stable fixed point remain close to each other (for $K \geq -1$) we have a situation similar to the symmetric case for $K > -1.4$, so complete symmetric maps form. But when the asymptotically stable fixed point coordinates have different orders of magnitude (as happens between $K = -1.2$ and $K = -1.4$, see Fig. 7.1b), then the activation levels in the two hemispheres will differ significantly (with the left hemisphere *always* much more active), and most of the learning will occur in the left hemisphere. Thus, the post-training organization level on the left stays close to 1, while on the right it

drops sharply. This also accounts for the "bumps" in the post-training activation levels in Fig. 4.2b and the sharp changes in lateralization and mirror symmetry in Fig. 4.2c. Finally, at $K < -1.4$ the fixed point becomes asymptotically unstable, and any initial difference in the activations of two hemispheres will grow exponentially (like in symmetric case for $K < -1.4$). However, due to the asymmetry in excitability the left hemisphere is more likely to have higher initial activation. This facilitates complementary map formation favoring the more active hemisphere.

Thus, the following theorem has been proved:

Theorem 7.4.1. *The system (7.6) has a bifurcation point when $K^2 = c_L c_R$, $K < 0$, and the whole model has another qualitative change in its behavior when K approaches this point from the right.*

7.5 Analysis of Another Variation of the Model, Using Competitive Distribution of Activation Between Two Cortices

Another variation of S2 simulator is a model with the same overall structure as S2 simulator (see Fig. 3.1), but with slightly different activation dynamics. Namely, each sensory node now distributes its output competitively not only to elements of each cortical set separately, but to elements in both sets simultaneously. Thus, instead of the first equation (3.4) we now have

$$c_{ik}^{LS} = c_p^L \frac{w_{ik}^L(a_i^L + q)}{\sum_n w_{nk}^L(a_n^L + q) + \sum_m w_{mk}^R(a_m^R + q)} \tag{7.8}$$

Yet another variation is obtained when the output of each sensory node is first divided among the left and right cortices proportional to their total activations at the moment, and then distributed competitively among the recipient nodes in each cortex within its quota. This last version also allows for interesting theoretical analysis.

When each sensory node distributes its activation competitively among the recipient nodes in *both* cortical sets, even the linearized model is very hard to study analytically. Indeed, the equation (7.8) will only let us get rid of the sum in the denominator if we add together activation equations for all elements in both cortical sets. In that case, assuming also that $c_p^L = c_p^R = c_p$, we get the following equation for the total activations:

$$\frac{d(A_L + A_R)}{dt} = c_s(A_L + A_R) + c_{lf}^L A_L + c_{lf}^R A_R + c_p A_S + K^{LR} A_R + K^{RL} A_L. \tag{7.9}$$

Clearly this allows analysis only for the symmetric case. The equation for the overall acti-

76

vation $A = A_L + A_R$ is simple:

$$\frac{dA}{dt} = (c_s + c_{lf} + K)A + c_p A_S.$$

As before, A will diverge (go to infinity) if $K > -(c_s + c_{lf})$, which is 1.4 for our baseline parameters. But again, this can be prevented if additional self-inhibition is used for positive K.

As mentioned above, the other variation of competitive distribution is when each sensory node's output is first divided proportional to the total activations of cortical sets and then within each set (we assume that the initial total activations are positive). The linearized version of this model leads to the following nonlinear system of ODEs for total activations (we again denote $c_s + c_{lf}^L = c_L$, $c_s + c_{lf}^R = c_R$, $c_p^L A_S = B_L$, and $c_p^R A_S = B_R$):

$$\frac{dA_L}{dt} = c_L A_L + K^{LR} A_R + B_L \frac{A_L}{A_L + A_R}, \quad \frac{dA_R}{dt} = K^{RL} A_L + c_R A_R + B_R \frac{A_R}{A_L + A_R}. \quad (7.10)$$

For this system the analysis becomes more interesting. As before, for the symmetric case the solution can be found explicitly. The fixed point is $A_L = A_R = -B/(2(c + K))$, which is asymptotically stable for $K < -c$, goes to infinity when K approaches $-c$, and becomes asymptotically unstable (and negative) for $K > -c$. It is important to note that even though the fixed point becomes unstable for large K, the difference $A_L - A_R$ will still converge to 0. This is easy to see if a change of variables is made: $x = A_L - A_R$, $y = A_L + A_R$, the system becomes:

$$\frac{dx}{dt} = x(c - K) + B\frac{x}{y}; \quad \frac{dy}{dt} = y(c + K) + B.$$

From the second equation $y = \alpha \exp((c + K)t) - B/(c + K)$, and from the first equation $dx/dt = x(c - K + B/y)$. For $K > -c$, $y(t) \to \infty$ as t grows, hence $c - K + B/y$ becomes negative very quickly even if it was positive at the beginning, so $x(t) \to 0$. The consequence of this result is the absence of sharp transitions in the model's behavior for this kind of model for $K > 0$. In particular, the symmetry measure is expected to stay close to 1 in the symmetric case for all $K > 0$ despite the competitive distribution of activation. Simulations have confirmed this prediction.

However, for the asymmetric case the problem gets harder. It is still possible to find the coordinates of the fixed point explicitly, but the expressions are too big to offer any help in understanding of the dynamics. But using the idea of continuation method [97] can help. In all model variations the parameters usually differ from the symmetric case only slightly, and so we can analyse the behavior of the fixed point in an asymmetric case by starting from the fixed point in a close symmetric case and then varying a parameter a little at a time. No bifurcations are observed in the parameter space except when $K^{RL}K^{LR} = c_L c_R$, and so this approach should work well.

7.6   Analysis of S4 simulator

The S4 simulator, described in Chapter 6, is a generalization of the S2 simulator. In particular, it is equivalent to the S2 simulator when symmetric training inputs are used and the receptive fields are computed with bilateral point stimuli. Thus, in such a case the analysis given in the previous sections applies to the S4 simulator as well.

When the training stimuli applied to the left and right sensory surfaces are independent, the incoming weights for both cortices usually organize fairly well for all callosal strengths (except, perhaps, the case with asymmetric learning rates and short training), but the organization and symmetry of receptive field maps depends very strongly on their way of calculation. Calculated independently, the maps are nearly perfect, so there is nothing interesting to analyse. When calculated from bilateral point stimuli, the maps are less organized and asymmetric for strong inhibitory callosal influences, which is explained easily by Theorem 7.4.1, since this asymmetry is again the result of asymmetric activation dynamics (recall that receptive fields are computed using activations of cortical elements in response to sensory point stimuli).

7.7   Activation Patterns and Weight Changes

The results with the S4 simulator show that in the bihemispheric models, weights are not the only factor affecting organization of receptive fields. This is a very important observation for the current study. It implies that one should look not only at the process of changing weights, but also at activation dynamics during receptive field calculation. Of course, the weight changes are very important.

Strong lateralization observed in the S2 simulator for even slightly inhibitory callosal connections when the *connection radii* were different suggest that the *shapes of activation patterns* forming in the cortices during training are extremely important for weight organization and topographic map formation. In this section an attempt is made to measure the shape of an activation pattern so that would be predictive of map formation (or at least weight organization) after training. First, a way to measure "goodness" of activation patterns is suggested, and then it is shown how it correlates with resulting map and weight organization. Intuitively, the measure should give a high value to a bell-shaped, or at least to a "convex" activation pattern, and a low value to a centrally-depressed activation pattern, as well as non-contiguous or simply very low activation.

In fact, the importance of the shape of activation patterns for map formation was first pointed out by Armentrout in [5], when he was studying the noncompetitive version of the S1 simulator. He showed that "bell-shaped activity islands are required for topographic map formation". Armentrout proved that in a "one-dimensional Kohonen network the ordered states are absorbing if and only if the symmetric neighborhood function is non-increasing with distance". Being absorbent means that "once weights become ordered subsequent learning will not change this ordering" and is very desirable for good map formation. His analysis and simulations (using noncompetitive version of the S1 simulator) showed that "centrally-depressed or non-contiguous ... activation patterns do not promote topographic

map formation as nearby input vectors are mapped to separate output regions".

Figure 7.2 presents some typical activation patterns found in the cortical regions under various combinations of model parameters for the S2 simulator. The top row shows activations in the sensory surface (part a), left (center) and right (right) cortical regions when all model parameters except random initial weights are symmetric, and callosal strength is 0. Good activation patterns form in both cortical regions, and very good symmetric maps form in them very quickly. The second row contains activation patterns for the symmetric case with strongly inhibitory callosal influences. Supporting the analysis above, one cortical region (left here) has very little activation, while the other (right in this figure) has a good activation pattern. Similar situations happen in asymmetric excitability case with strong inhibitory connections.

Finally, the bottom row of Fig. 7.2 shows activations for the asymmetric connectivity case, when the radius of connections from the sensory surface to the right cortical region is 4, and to the left one 3, with callosal radius 1 and input stimulus radius 2 (similar figure with input radius 1 is given on page 37). A "good" activation pattern (roughly bell-shaped) occurs in the left cortical region, and a "bad" one (centrally-depressed) in the right cortical region. Such a situation leads to strong lateralization as a well-formed map does not appear in the left cortical region.

Several approaches to evaluating the shape of activation patterns were tried. It turned out that a simple dot product of cortical and sensory activations (averaged over first 50 inputs) is a fairly good predictor of weight and map organization after training. The dot product is computed by adding together the products of activation levels in corresponding elements of one cortex and the sensory layer from which it receives input. Since the activation level of a sensory element is either 0 or 1, the dot product is effectively the total activation of the cortical elements directly corresponding to the active elements of the training stimulus. Figure 7.3 shows this dependence for training inputs of radius 1 (parts a, c) and 2 (parts b, d), based on results of many simulations with various model asymmetries (except different size, since it's hard to compute the dot product of activations for different size regions, and different learning rates, since the rates affect map formation, but do not affect activation patterns in the beginning of training). The figure has 2 points for each simulation, corresponding to left and right cortices.

Taking into account the previous discussion of the effect of a bilateral way of computing receptive fields on map formation when the training stimuli were independent (see Chapter 6), results of S4 simulator with independent training stimuli are used only for parts c and d, where weights are shown.

Some scattering of the points is probably due to the fact that normally tens or hundreds of thousands of training inputs are needed for map formation, so perhaps the first 50 may not be a sufficient sample. The figures show that most points fall into the 95% confidence interval around the parabola computed as the least squares fit. For higher levels of dot product the parabolas level off, showing that once the dot product is high enough, a good map will form (recall that map organization values are limited by 1). The graphs for training input radii 1 and 2 are given separately because it is not clear how to normalize the results so that they could be given together. Simple division by the number of elements in the training
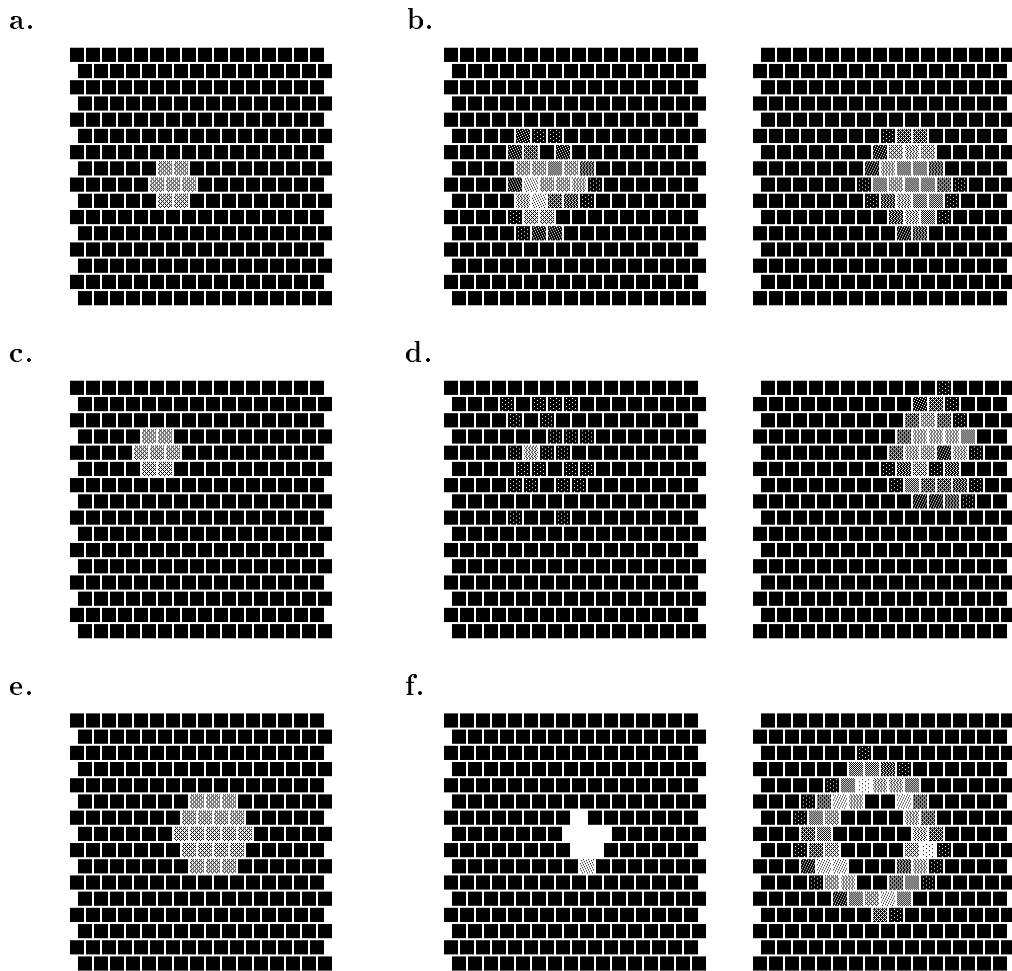
Figure 7.2: Activation in the (**a, c, e**) sensory surface and (**b, d,f**) the two cortical regions when (**a, b**) symmetric case, no callosal connections, "good" activation patterns in both cortical regions; (**c, d**) symmetric case, strongly inhibitory callosal connections, "good" activation pattern in the right cortical region, almost no activation in the left cortical region; (**e, f**) radii from the sensory surface to cortical regions are 3 and 4, callosal radius 1, inhibitory callosal connections, "good" pattern in the left and "bad" one in the right cortical region.

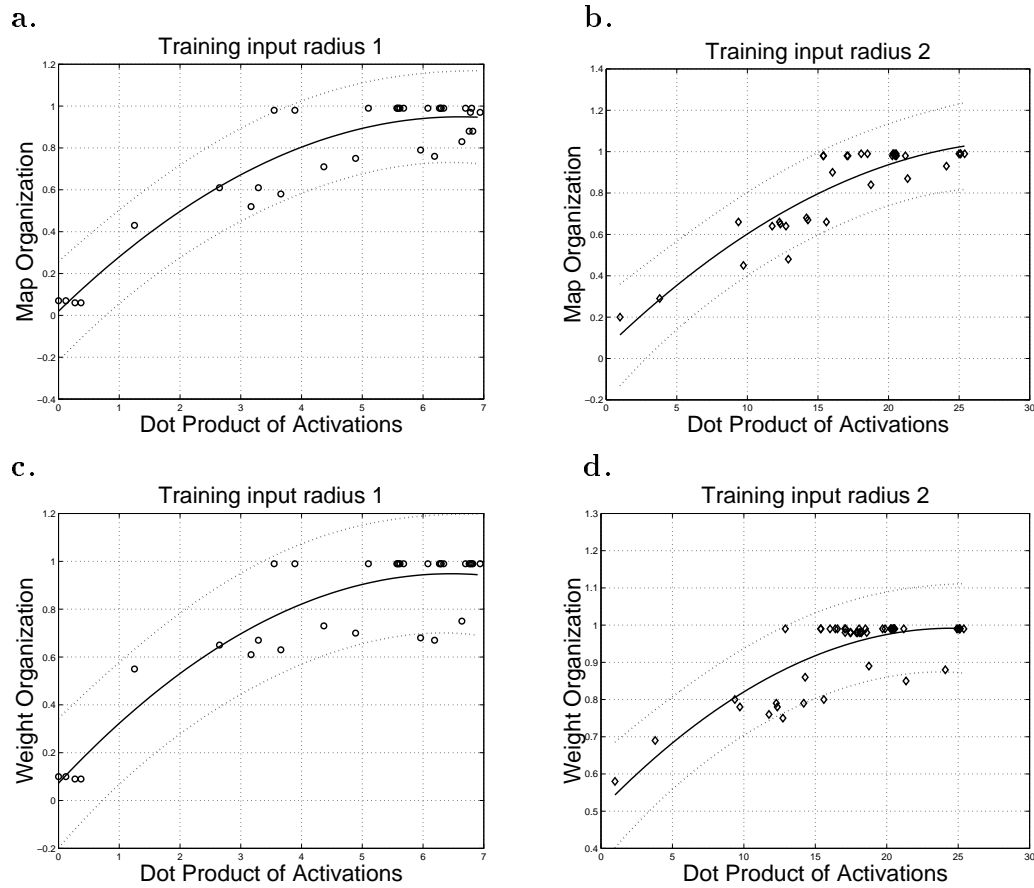Figure 7.3: Organizations of topographic maps and incoming weights (vertical axes) after training depend on dot product of activations of cortical and sensory elements before training (horizontal axes). The least squares quadratic approximation and 95% confidence intervals are also shown. (a, b) Map organization, (c, d) incoming weight organization; (a, c) training inputs of radius 1; (b, d) training inputs of radius 2.

patch does not work well, since the activation dynamics is highly nonlinear.

7.8   Factors Affecting Activation Patterns

Here an analysis of activation dynamics in individual nodes is undertaken, in order to see how the model parameters affect the resulting dot product of activations in sensory and cortical layers. In order to minimize the size of the nonlinear system of ODEs, the one-dimensional case is considered here. A small version of a one-dimensional S2 simulator has been implemented in Matlab, using its ODE solver ode23, which implements Runge-Kutta method with adjustable time step. The small version has only 8 elements in each cortical set, and only 2 input nodes, each sending input to 5 elements in each cortical set. Callosal radius is 1. The additional self-inhibition for positive K was not used, since all the most interesting phenomena happen for negative K anyway. While it is a minimal configuration that can be considered for analysis of activation patterns, it still has 16 nonlinear ODEs. The initially random weights create an additional problem, since they play an important role in activation dynamics.

Numerous computations show that after initial active changes, solutions of the ODE system converge to fixed points for all values of K considered. Fig. 7.4 shows the behavior of individual element activations as time goes from 0 to 40 that was observed for various parameter sets. The fixed points stay nearly unchanged for most negative values of K, as shown in Fig. 7.5, where elements 1 through 8 correspond to the left cortical set, and 9 through 16 to the right one.

For negative $K < -0.5$, usually only two elements (forming a cluster) on each side remain active after sufficient time has passed, and these elements on the left and right sides tend to be in different locations. This makes the dot product of cortical and sensory activations low, in fact, it is usually 0 on one side and around 1.2 on the other (see Fig. 7.6). Complete dominance of one side over the other (as could be expected from the analysis of total activations above) does not happen here because the callosal radius is too small.

For $K > -0.5$, as the inhibition gets weaker, the clusters of active elements on both sides become wider, more active and more symmetric, so that the dot products increase (up to around 4 for $K = 1$) and become close to each other.

Fig. 7.6 presents the dependence of dot product of cortical and sensory activations on K. For various initial weights and parameter variations this figure remains amazingly similar, with only small changes near $K = -0.5$. Of course, for the symmetric case either left or right cortex can have higher dot product with sensory surface, while for the asymmetric excitability case usually the left cortex (having higher excitability) has higher dot product.

When the sensory-cortical radii are asymmetric and callosal influences inhibitory, the activation pattern on the side with larger radius (right side here) is split into two parts with zeros in the middle (the middle here corresponds to the position of the input stimulus in the sensory layer). This split is caused by stronger inhibition from the other (left) side exactly in the middle. Indeed, the elements in the middle of the right side receive inhibition from practically all active elements on the left, while the positive activation from the input nodes is distributed (competitively!) over a larger number of right side elements, and those farther
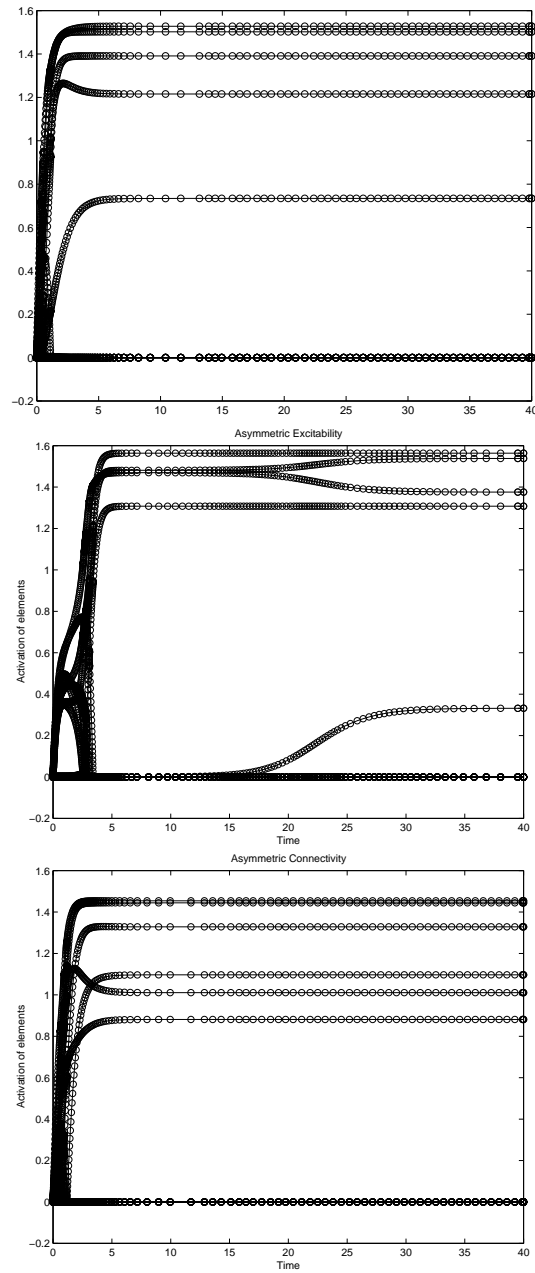
Figure 7.4: Changes in activations of individual cortical elements in a simple model with time, $K = -2.1$. Top: the symmetric case; middle: asymmetric excitability; bottom: asymmetric connectivity. All activations converge to fixed points after some time.
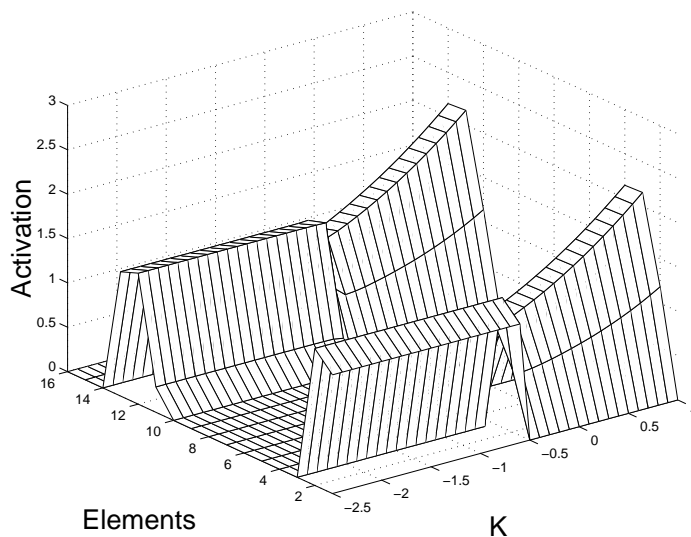
Figure 7.5: Fixed points of the system of 16 nonlinear ODEs as a function of K.

away from the middle get less inhibition. This leads to the centrally-depressed activation pattern on the right side and makes its dot product with the sensory layer activation zero. At the same time, the activation cluster on the left side is closer to the center, thus making the dot product much higher than in other cases. Strong lateralization inevitably follows. A similar argument also applies to the two-dimensional model when callosal radius is small. This explains strong lateralization even for weakly inhibitory callosal influences described in section 4.2.4.

7.9 Discussion

The models described in the previous chapters have been analyzed here from various points of view. The analysis of a simplified ("linearized") version of the S2 simulator helps to explain the sudden transitions in organization and symmetry observed in many simulations, as well as lateralization and the "bumps" in post-training activation for the asymmetric excitability case. It is shown how these phenomena depend on the stability and behavior of a fixed point of a linear ODE system for total hemispheric activations. The behavior of the S4 simulator is also explained by the above analysis.

Another variation of the model, using competition for activation between the two cortical regions, is also considered and analyzed. For this model the ODEs for total activations are also nonlinear. It is shown that no sharp transitions in the model's behavior should be expected, and highly symmetric maps should form for positive K. Simulations have confirmed this prediction.

Finally, it is demonstrated how activation patterns forming in the cortex in the beginning of training can predict weight and map organization after training. It is discovered that the dot product of activations in the cortical and sensory layers before training correlate with the
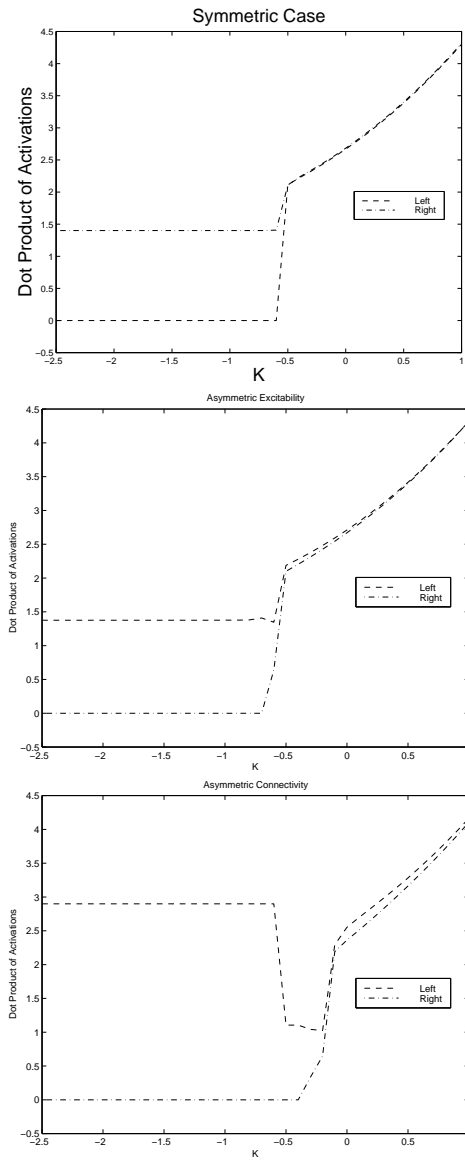
Figure 7.6: Dot product of activations as a function of K. Top: the symmetric case; middle: asymmetric excitability; bottom: asymmetric connectivity.

final (after training) weight organization (and map organization in certain cases). Formation of those activation patterns under various combinations of parameters is also discussed.

Chapter 8

Conclusions

8.1   Results of this Research

Lateralization and asymmetries in the brain have been a subject of research in biology, psychology, cognitive science, and other disciplines for over a century. However, computer models of interacting left and right hemispheric regions have appeared only recently and have been very limited. Very few of them examined the effects of callosal connections and various asymmetries on spontaneous lateralization, and none considered lateralization and asymmetries in cortical maps. In this dissertation, several mathematical models of lateralization and asymmetry in cortical maps have been created and analysed both computationally and theoretically. The recurrently-connected neural models considered here are, of course, simplified from biological reality. None the less, they do capture several key aspects of real hemispheric regions. They have a spatial organization that permits examination of maps, their interconnections are roughly homotopic, and they self-organize using unsupervised (Hebbian) learning.

The main achievements described in this dissertation are as follows:

1. The first models of left and right cortical maps interacting via a simulated corpus callosum have been created and analyzed. The models are based on the ideas of self-organizing maps, competitive distribution of activation, and competitive learning.

2. Metrics for objective quantitative evaluation of topographic map organization, lateralization and mirror symmetry have been introduced and analyzed. The metrics not only have desired formal mathematical properties, but also correlate well with people's subjective estimates of map organization, lateralization, and mirror symmetry.

3. The study of the effects of various model asymmetries on map lateralization has determined that most of the asymmetries can cause lateralization, supporting the hypothesis that lateralization is a multifactorial phenomenon.

4. A systematic study of the effects of callosal influences on map formation in the symmetric case and in the presence of model asymmetries shows that most lateralization and map asymmetry occurs with inhibitory callosal influences, while symmetric well-organized maps develop when callosal influences are weak or excitatory. There are also

sharp transitions in organization, lateralization, and mirror symmetry as the callosal influences become more inhibitory. These findings support the hypothesis that callosal influences are functionally inhibitory.

5. In contrast, lesioning studies lead to the conclusion that diaschisis is most faithfully reproduced with excitatory callosal influences. The effects of lesions on map formation have been studied both acutely (immediately after the lesion) and chronically (after a retraining period), for several model variations, having excitatory and inhibitory callosal connections.

6. Further, the intact hemisphere participates in the recovery process mostly with inhibitory callosal influences. This may indicate that current theories of lateralization are inadequate, but the experimental literature is ambiguous on these issues.

7. Analysis of a bifurcation point of an ODE system explains the sudden transitions in the model's behavior, and analysis of the shapes of activation patterns shows how to predict post-training organization based on the pre-training activation patterns. For a slightly simplified S2 model, a system of linear ordinary differential equations (ODE) for total hemispheric activations was obtained and analyzed. In most cases the system has one fixed point, which is asymptotically stable for excitatory and slightly inhibitory callosal connections, and asymptotically unstable for strongly inhibitory connections. The explanation of the effects of this change on map formation is given. Deeper analysis of activation patterns helps to explain some cases not explained by the first approach. It is shown how activation patterns observed in the cortical regions in the beginning of training can predict weight and map organization after training, and how the activation patterns depend on model parameters. Theoretical analysis of the model's dynamics explains the key computational findings and helps to better understand the roles of various model parameters in the map formation and lateralization.

8.2   Future Work

Several directions of possible expansion for this research can be suggested.

One is finding another way of measuring activation patterns that works better in predicting ultimate map organization than the dot product of activations used in this research. It is not clear at this point whether such a way exists.

Another is further analysis of the behavior of the ω-limit set (in particular, the fixed point) of the system of nonlinear ODEs for activations. Possible existence of bifurcations of various kinds for the one-dimensional model can be checked by a continuation method, or using specialized software packages. Similar analysis for the two-dimensional case is desirable, but it is not clear how to approach it.

Yet another direction is analysis of the relationship between the shape of activation pattern, learning rate, and final weight and map organization. In this dissertation the effect of activation shape on map formation was considered only for a fixed learning rate. But simulations with different learning rates suggest that for some activation shapes smaller

or larger learning rates may actually improve weight organization and map formation. It would be interesting to find an optimal learning rate for each value of goodness of activation pattern.

Finally, other models can also be considered. The models described in this dissertation display lateralization for inhibitory callosal strengths and diaschisis after a lesion (see Chapter 5) only for excitatory callosal connections. Thus, a more complex model is needed which would have both of the above effects with the same callosal strength.

BIBLIOGRAPHY

[1] Afifi A., Bergman R. *Functional Neuroanatomy*, McGrow Hill, 1998.

[2] Alvarez S., Levitan S., Reggia J. Metrics for Cortical Map Organization and Lateralization, *Bull. Math. Biol.*, 60, 1998, 27–47.

[3] Anninos P.A., Argyrakis P., Skouras A. A Computer Model for Learning Processes and the Role of the Cerebral Commissures, *Biol. Cybern*, 50, 1984, 329–336.

[4] Anninos P.A., Cook N. Neural Net Simulation of the Corpus Callosum, *Intl. J. Neurosci*, 38, 1988, 381–391.

[5] Armentrout S.L. *A Computational Theory of Map Reorganization.* Ph.D. thesis, University of Maryland at College Park, 1994.

[6] Armentrout S.L., Reggia J.A., Weinrich M.A. A Neural Model of Cortical Map Reorganization Following a Focal Lesion, *Artificial Intelligence in Medicine*, 6, 1994, 383–400.

[7] Bates E., Thal D., Janowsky J. Early Language Development and Its Neural Correlates, *Handbook of Neuropsych*, 7, S. Segalowitz & I. Rapin (eds.), Elsevier, 1992, 69–110.

[8] Belin P, Van Eeckhout P, Zilbovicius M, et al. Recovery From Nonfluent Aphasia After Melodic Intonation Therapy: A PET Study, *Neurol.*, 47, 1996, 1504–1511.

[9] Benaim M. A stochastic model of neural network for unsupervised learning. *Europhysics Letters*, 19, 1992, 241–246.

[10] Benaim M. Convergence Theorems for Hybrid Learning Rules, *Neural Computation*, 7, 1995, 19–24.

[11] Benaim M. On Invariant Hypersurfaces of Strongly Monotone Maps, *J. of Differential Equations*, 137, 1997, 302–319.

[12] Benaim M., Hirsch M.W. Asymptotic Pseudo trajectories and Chain Recurrent Flows, with Applications. *J. of Dynamics and Differential Equations*, 8, 1996, 141.

[13] Benaim M., Samuelides M. Inhibition virtuelle dans les reseaux multicouches de diffusion competitive. *Proc. Neuro Nimes 89 Intern. workshop Neural Networks & Applications*, 1989, 333–345.

[14] Benaim M., Samuelides M. Dynamical Properties of Neural Nets Using Competitive Activation Mechanisms. In *Proc. Int. Joint Conf. on Neural Networks*, 1990, vol.3, 541–546.

[15] Berlucchi G. Two Hemispheres But One Brain, *Behav. Brain Sci.*, 6, 1983, 171–173.

[16] Berndt R, D'Autrechy C & Reggia J. Functional Pronunciation Units in English Words, *J. Exp. Psych: Learning, Memory and Cognition*, 20, 1994, 977–991.

[17] Bianki V.L. *The Mechanism of Brain Lateralization*, Gordon & Breach, 1993.

[18] Biddle F.G., Eales B.A. The Degree of Lateralization of Paw Usage (Handedness) in the Mouse is Defined by Three Major Phenotypes. *Beh. Genet.* 26 (4), 1996, 391–406.

[19] Bisazza A., Rogers L.J., Vallortigara G. The Origins of Cerebral Asymmetry: a Review of Evidence of Behavioral and Brain Lateralization in Fishes, Reptiles, and Amphibians. *Neuroscience & Biobehavioral Reviews*, 22, 1998, 411–426.

[20] Blakemore C., Cooper G. Development of the Brain Depends on the Visual Environment, *Nature* (London), 228, 1970, 477–478.

[21] Blakemore C., Mitchell D. Environmental Modification of the Visual Cortex and the Neural Basis of Learning and Memory, *Nature* (London), 241, 1973, 467–468.

[22] Bowler J, Wade J, Jones B, et al: Contribution of Diaschisis to the Clinical Deficit in Human Cerebral Infarction, *Stroke*, 26, 1995, 1000–1006.

[23] Bullmore E., Brammer M., Harvey I., Ron M. Against the Laterality Index as a Measure of Cerebral Asymmetry. *Psychiatry*, 61, 1995, 121–124.

[24] Burgess C & Lund K. Modeling Cerebral Asymmetries in High-Dimensional Semantic Space, in *Right Hemisphere Language Comprehension*, M. Beeman & C. Chiarello, Erlbaum, 1998, 215-244.

[25] Cabeza R & Nyberg L. Imaging Cognition: An Empirical Review of PET Studies, *J. Cog. Neurosci.*, 9, 1997, 1–26.

[26] M. Calford, R. Tweedale, Interhemispheric Transfer of Plasticity in the Cerebral Cortex, *Science* 249, 1990, 805–807.

[27] Cappa S, Perani D, Grassi F, et al. A PET Follow-UP Study of Recovery After Stroke in Acute Aphasics, *Brain and Lang*, 56, 1997, 55–67.

[28] Caselli R. Bilateral Impairment of Somesthetically Mediated Object Recognition in Humans, *Mayo Clin. Proc.*, 66, 1991, 357–364.

[29] Cessac B., Doyon B., Quoy M., Samuelides M. Mean-field equations, bifurcation map and route to chaos in discrete time neural networks, *Physica D.*, 74, 1994, 24–44.

[30] Chen Y. *A Motor Control Model Based on Self-Organizing Feature Maps*, Ph.D. thesis, University of Maryland at College Park, 1997.

[31] Chen Y., Reggia J., Alignment of Coexisting Cortical Maps in a Motor Control Model, *Neural Computation*, 8, 1996, 731–755.

[32] Chen Y., Reggia J., The Temporal Correlation Hypothesis for Self-Organizing Feature Maps, *International Journal of Systems Science*, 1999, in press

[33] Cho S., Reggia J., Map Formation in Proprioceptive Cortex, *International Journal of Neural Systems*, Vol 5, 1994, 87–101.

[34] Cook N. *The Brain Code*, Methuen, 1986.

[35] Cook N., Beech A. The Cerebral Hemispheres and Bilateral Neural Nets, *Int. J. Neurosci.*, 52, 1990, 201–210.

[36] Davidson R.J., Hugdahl K. (eds.) *Brain Asymmetry*, MIT Press, Cambridge, MA, 1995.

[37] Dauce E., Quoy M., Cessac B., Doyon B., Samuelides M. Self-organization and dynamics reduction in recurrent networks: stimulus presentation and learning. *Neural networks*, 11, 1998, 521–533.

[38] Denenberg V. Micro and Macro Theories of the Brain, *Behav. Brain. Sci.*, 6, 1983, 174–178.

[39] Dennis M. & Whitaker H. Language Acquisition Following Hemidecortication. Linguistic Superiority of Left Over Right Hemisphere, *Brain and Language*, 3, 1976, 404–433.

[40] J. Dobkin, R. Levine, H. Lagreze, et al. Evidence for Transcallosal Diaschisis in Unilateral Stroke, *Arch. Neurol.* 46, 1989, 1333–1336.

[41] Doyon B., Cessac B., Samuelides M. On bifurcations and chaos in random neural networks. *Acta biotheoretica.* 42, 1994, 215.

[42] Feeney D. & Baron J. Diaschisis, *Stroke*, 17, 1986, 817–830.

[43] Felleman D. and Van Essen D. Distributed Hierarchical Processing in Primate Cerebral Cortex, *Cerebral Cortex*, 1, 1991, 1–47.

[44] Fendrich A., Wessinger C.M., Gazzaniga M.S. Nasotemporal overlap at the retinal vertical meridian: Investigations with a callosotomy patient, *Neuropsychologia*, 34, 1996, 637–646.

[45] Ferbert A., Priori A., Rothwell J.C. Interhemispheric Inhibition of the Human Motor Cortex, *J. Physiol.*, 453, 1992, 525–546.

[46] Gazzaniga M. Principles of Human Brain Organization Derived From Split-Brain Studies, *Neuron*, 14, 1995, 217–228.

[47] Geschwind N. & Galaburda A. *Cerebral Lateralization*, MIT Press, Cambridge, MA, 1987.

[48] Geschwind N. & Levitsky W. Left-Right Asymmetries in Temporal Speech Region, *Science*, 167, 1968, 186.

[49] Golden R.M. *Mathematical Methods for Neural Network Analysis and Design*, MIT Press, Cambridge, MA, 1996.

[50] Goodall S; Reggia J, et al. A Computational Model of Acute Focal Cortical Lesions, *Stroke*, 28, 1997, 101–109.

[51] Gordon B. Confrontation Naming: Computational Model and Disconnection Simulation, in *Neural Models of Language Processes*, M. Arbib et al, Academic, 1982, 511–530.

[52] Grajski K., Merzenich M. Hebb-Type Dynamics is Sufficient to Account for the Inverse Magnification Rule in Cortical Somatotopy, *Neural Computation*, 2, 1990, 71–84.

[53] Gur R.C., Packer I.K., Hungerbuhler J.P., et al. Differences in Distribution of Gray and White Matter in Human Cerebral Hemispheres, *Science*, 207, 1980, 1226–1228.

[54] Hale J., Kocak H. Dynamics and Bifurcations. New York: Springer-Verlag, 1991.

[55] Hartenstein V., Innocenti G. The Arborization of Single Callosal Axons in the Mouse Cerebral Cortex, *Neurosci Letters*, 23, 1981, 19–24.

[56] Hebb D.O. *The Organization of Behavior*, New York: Wiley, 1949.

[57] Heiss W, Karbe H, et al. Speech-Induced Cerebral Metabolic Activation Reflects Recovery From Aphasia, *J. Neurol. Sci.*, 145, 1997, 213–217.

[58] Heiss W, Kessler J, Karbe H, Fink G, & Pawlik G. Cerebral Glucose Metabolism as a Predictor of Recovery From Aphasia in Ischemic Stroke, *Arch. Neurol.*, 50, 1993, 958–964.

[59] Hellige J. *Hemispheric Asymmetry*, Harvard University Press, Cambridge, MA, 1993.

[60] Hertz J.A., Krogh A.S., Palmer R.G. *Introduction to the Theory of Neural Computation*, Reading, MA: Addison-Wesley, 1991.

[61] Hirsch H., Spinelli D. Visual Experience Modifies Distribution of Horizontally and Vertically Oriented Receptive Fields in Cats, *Science*, 168, 1970, 869–871.

[62] Hirsch M. Convergent activation dynamics in continuous time networks, *Neural Networks*, Vol. 2, 1989, 331–349.

[63] Hubel D., Wiesel T. Receptive Fields of Cells in Striate Cortex of Very Young, Visually Inexperienced Kittens, *Journal of Neurophysiology*, 26, 1963, 994–1002.

[64] Hubel D., Wiesel T. Receptive Fields and Functional Architecture of Monkey Striate Cortex, *Journal of Physiology* (London), 195, 1968, 215–243.

[65] Hustler J., Loftus W., Gazzaniga M. Individual Variation of Cortical Surface Area Asymmetries. *Cerebral Cortex*, 8, 1998, 11–17.

[66] Innocenti G. General Organization of Callosal Connections in the Cerebral Cortex, *Cerebral Cortex*, Vol 5, E. Jones & A. Peters (eds.) Plenum, 1986, 291–353.

[67] Jacobs R., Kosslyn S. Encoding Shape and Spatial Relations, *Cognitive Science*, 18, 1994, 361–386.

[68] Jenkins W., Merzenich M. Reorganization of Neocortical Representations After Brain Injury: a Neurophysiological Model of the Bases of Recovery from Stroke, in *Progress in Brain Research*, vol. 71, 1987, Seil F., Herbert E., Carlson B. (eds), Elsevier, 249–266.

[69] Jenkins W., Merzenich M., Ochs M., Allard T., Guic-Robles E. Functional Reorganization of Primary Somatosensory Cortex in Adult Owl Monkeys After Bahaviorally Controlled Tactile Stimulation, *Journal of Neurophysiology*, 63, 1990, 229–231.

[70] Kaas J. Plasticity of sensory and motor maps in adult mammals, *Ann. Rev. Neurosci.*, 14, 1991, 137–167.

[71] Kempinsky W. Experimental Study of Distant Effects of Acute Focal Brain Injury, *Arch. Neurol. Psych.*, 79, 1958, 376–389.

[72] Kinsbourne M. (ed.) *Asymmetrical Function of the Brain*, Cambridge, 1978.

[73] Knopman D, Rubens A, Selnes O, Klassen A, & Meyer M. Mechanisms of Recovery from Aphasia, *Ann. Neurol.*, 15, 1984, 530–535.

[74] Kohonen T. *Self-Organizing Maps*, Springer-Verlag, Berlin, 1995.

[75] Kosslyn S, Chabris C, et al., Categorical Versus Coordinate Spatial Relations: Computational Analyses and Computer Simulations, *J. Exper. Psych: Human Perception and Performance*, 18, 1992, 562–577.

[76] Kosslyn S, Sokolov M & Chen J. The Lateralization of BRIAN, in *Complex Information Processing*, D. Klahr & K. Kotovsky (eds.), Erlbaum, 1989, 3–29.

[77] Lee H, Nakada T, Deal J, et al. Transfer of Language Dominance, *Ann. Neurol.*, 15, 1984, 304–307.

[78] Levitan S., Reggia J.A. A Computational Model of Lateralization and Asymmetries in Cortical Maps, 1999, submitted.

[79] Levitan S., Reggia J.A. Interhemispheric Effects on Map Organization Following Simulated Cortical Lesioning, *Artificial Intelligence in Medicine*, 1999, accepted.

[80] Levitan S., Stoica I., Reggia J.A. A Model of Lateralization and Asymmetries in Cortical Maps, *Proceedings of IJCNN99*, Washington D.C., July 1999.

[81] Loftus W.C., Tramo M.J., Thomas C.E., et al. Three-Dimensional Quantitative Analysis of Hemispheric Asymmetry in the Human Superior Temporal Region, *Cerebral Cortex*, 3, 1993, 348–355.

[82] Macdonell R., Shapiro B., Chiappa H. et al. Hemispheric Threshold Differences for Motor Evoked Potentials Produced by Magnetic Stimulation, *Neurol.*, 41, 1991, 1441–1444.

[83] McFadden F. Competitive Learning and Competitive Activation in Cortical Map Formation, *Ph.D. thesis, University of Maryland at College Park* 1993.

[84] McFadden F. Convergence of Competitive Activation Models Based on Virtual Lateral Inhibition, *Neural Networks*, 8, 1995, 865–875.

[85] McFadden F., Peng Y., Reggia J.A. Local Conditions for Phase Transitions in Neural Networks With Variable Connection Strengths, *Neural Networks* 6, 1993, 667–676.

[86] Merzenich M., Kaas J., et al. Topographic Reorganization of Somatosensory Cortical Areas 3b and 1 in Adult Monkeys Following Restricted Deafferentation, *Neuroscience*, 8, 1983, 33–55.

[87] Meyer B.-U., Röricht S., Gräfin von Einsiedel H. et al. Inhibitory and Excitatory Inter-hemispheric Transfers Between Motor Cortical Areas in Normal Humans and Patients with Abnormalities of Corpus Callosum, *Brain*, 118, 1995, 429–440.

[88] Meyer J. Changes in Local CBF and Lambda Values Following Regional Cerebral Infarction in the Baboon, *Adv. Biosci.*, 43, 1982, 153–165.

[89] Meyer J, et al. Clinical and Experimental Studies of Diaschisis, in *Cerebral Blood Flow*, J. Wood (ed.), 1987, 481–502.

[90] Meyer J, et al. Diaschisis, *Neurol. Res.*, 15, 1993, 362–366.

[91] Monoghan P. & Shillcock R. The Cross-Over Effect in Unilateral Neglect, *Brain*, 121, 1998, 907–921.

[92] Nudo R., Jenkins W., Merzenich M. et al. Neurophysiological correlates of hand preference in primary motor cortex of adult monkeys, *J Neurosci*, 12, 1992, 2918–2947.

[93] Obermayer K., Ritter H., Schulten K. A Neural Network Model for the Formation of Topographic Maps in the CNS: Development of Receptive Fields, *Proceedings of International Joint Conference on Neural Networks, Vol. II*, 1990, 423–429. San Diego, CA.

[94] Ohyama M, Senda M, Kitamura S, et al. Role of the Nondominant Hemisphere and Undamaged Area During Word Repetition in Poststroke Aphasics, *Stroke*, 27, 1996, 897–903.

[95] Oja E. A Simplified Neuron Model As a Principal Component Analyzer. *Journal of Mathematical Biology*, 15, 1982, 267–273.

[96] Orban G. *Neuronal Operations in the Visual Cortex*, Springer-Verlag, 1984.

[97] Ortega J.M., Rheinboldt W.C. Iterative Solution of Non-linear Equations in Several Variables. New York: Academic Press, 1970.

[98] Pandya D. & Seltzer B. The Topography of Commissural Fibers, in *Two Hemispheres - One Brain*, F. Lepore et al. (eds.), Alan Liss, 1986, 47–73.

[99] Papanicolaou A et al. Evoked Potential Correlates of Right Hemisphere Involvement in Language Recovery Following Stroke, *Arch. Neurol.*, 44, 1987, 521–524

[100] Papanicolaou A, Moore B, Deutsch G, Levin H & Eisenberg H. Evidence for Right-Hemisphere Involvement in Recovery From Aphasia, *Arch. Neurol.*, 45, 1988, 1025–1029.

[101] Pearson J., Finkel L., Edelman G. Plasticity in the Organization of Adult Cerebral Cortical Maps: A Computer Simulation Based on Neuronal Group Selection, *Journal of Neuroscience*, 7, 1987, 4209–4223.

[102] Polani D. Organization Measures for Self-Organizing Maps. In: T. Kohonen, ed. *Proceedings of the Workshop on Self-Organizing Maps (WSOM'97)*, Helsinki University of Technology, 1997, 280–285.

[103] Pouget A. & Sejnowski T. Lesion in a Brain Function Model of Parietal Cortex, *Parietal Lobe Contribution in Orientation in 3D Space*, Thier, P. & Karnath, H. (eds.), 1997, 521–538.

[104] Reggia J. Symmetries of Natural and Artificial Neural Networks, *Symmetry: Culture and Science*, 6, 1995, 446–449.

[105] Reggia J.A., D'Autrechy C., Sutton G. & Weinrich M. A Competitive Distribution Theory of Neocortical Dynamics, *Neural Computation*, 4, 1992, 287–317.

[106] Reggia J., Berndt R. and D'Autrechy L. Connectionist Models in Neuropsychology. In *Handbook of Neuropsychology*, Volume 9, 1994, 297–333.

[107] Reggia J.A., Edwards M. Phase Transitions in Connectionist Models Having Rapidly Varying Connection Strengths, *Neural Computation* 2, 1990, 523–535.

[108] Reggia, J., Ruppin, E., and Berndt, R. (eds.) *Neural Modeling of Brain and Cognitive Disorders*, World Scientific, 1996.

[109] Reggia J.A., Goodall S., Shkuro Y. Computational Studies of Lateralization of Phoneme Sequence Generation, *Neural Computation*, 10, 1998, 1277–1297.

[110] Reggia J, Ruppin E & Glanzman D. *Brain, Behavioral and Cognitive Disorders: The Neurocomputational Perspective*, Elsevier, 1999, Forthcoming

[111] Revett K, Ruppin E, Goodall S & Reggia J. Spreading Depression in Focal Ischemia, *J. Cerebral Blood Flow and Metab.*, 18, 1998, 998–1007.

[112] Ringo J., Doty R., Demeter S. & Simard P. Time Is of the Essence: A Conjecture that Hemispheric Specialization Arises from Interhemispheric Conduction Delay, *Cerebral Cortex*, 4, 1994, 331–343.

[113] E. Ruppin, J.A. Reggia, Patterns of Functional Damage in Neural Network Models of Associative Memory, *Neural Computation* 7, 1995, 1105–1127.

[114] Scheibel A, et al. Differentiality Characteristics of the Human Speech Cortex, in *The Dual Brain*, D. Benson & E. Zaidel (eds), Guilford, 1985, 65–74.

[115] Shevtsova N.A., Reggia J.A. A Neural Network Model of Lateralization During Letter Identification, *J. Cognitive Neurosci.*, 1998, in press.

[116] Shevtsova N.A., Reggia J.A. Interhemispheric Effects of Simulated Lesions in a Neural Model of Letter Identification, 1999, submitted.

[117] Silvestrini M, Troisi E, Matteis M, Cupini L & Caltagirone C. Involvement of the Healthy Hemisphere in Recovery From Aphasia and Motor Deficits in Patients with Cortical Ischemic Infarction, *Neurology*, 45, 1995, 1815–1820.

[118] Silvestrini M, Troisi E, Matteis M, Razzano C. & Caltigirone C. Correlations of Flow Velocity Changes During Mental Activity and Recovery From Aphasia in Ischemic Stroke, *Neurology*, 50, 1998, 191–195.

[119] Sober S, Stark D, Yamasaki D & Lytton W. Receptive Field Changes After Stroke-like Cortical Ablation, *J. Neurophys.*, 78, 1997, 3438–3443.

[120] Springer S. & Deutsch G. *Left Brain, Right Brain*, W. H. Freeman, 1993.

[121] Stoer J., Bulirsch R. Introduction to Numerical Analysis. 2nd edition. New York: Springer-Verlag, 1993.

[122] Stone J., Leicester J, & Sherman S. Naso-Temporal Division of the Monkey's Retina, *J. Comp. Neur.*, 150, 1973, 333-348.

[123] Sutton G.G. *Competitive Learning and Map Formation in Artificial Neural Networks using Competitive Activation Mechanisms*, PhD thesis, University of Maryland at College Park, 1992.

[124] Sutton G.G., Reggia J.A., Armentrout S., D'Autrechy C. Cortical Map Reorganization as a Competitive Process, *Neural Computation* 6, 1994, 1–13.

[125] Toyama K., Tokashiki S., Matsunami K. Synaptic Action of Commissural Impulses upon Association Efferent Cells in Cat Visual Cortex, *Brain Res.*, 14, 1969, 518–520.

[126] Tucker D. & Williamson P. Asymmetric Neural Control Systems in Human Self-Regulation, *Psychol. Review*, 91, 1984, 185–215.

[127] Udin S., Fawcett J. Formation of Topographic Maps, *Annual Review of Neuroscience*, 11, 1988, 289–327.

[128] Van Kleek M. & Kosslyn S. Use of Computer Models in the Study of Cerebral Lateralization, *Cerebral Laterality: Theory and Research*, F Kitterle (ed), Erlbaum, 1991, 155–174.

[129] Von der Malsburg C. Self-Organization of Orientation Sensitive Cells in the Striate Cortex. *Kybernetik*, 14, 1973, 85–100.

[130] Wang P.Y., Seidman S.B., Reggia J.A. Analysis of Competition-based Spreading Activation in Connectionist Models, *Int. J. of Man-Machine Studies*, 1988, v.28, 77–97.

[131] C. Weiller, et al. Functional Reorganization of the Brain in Recovery from Striatocapsular Infarction in Man, *Annals of Neurology* 31, 1992, 463–472.

[132] Weiller C, et al. Recovery from Wernicke's Aphasia: A PET Study, *Ann. Neurol.*, 37, 1995, 723–732.

[133] Weinrich M., Sutton G., Reggia J.A. and D'Autrechy C., Adaptation of Non-competitive and Competitive Neural Networks to Focal Lesions, *Journal of Artificial Neural Networks*, Vol 1, 51–60 (1994)

[134] White E. *Cortical Circuits*, Birkhauser, 1989, pp. 69–79.

[135] Wood C. Variations on a Theme by Lashley: Lesion Experiments on the Neural Model of Anderson, Silverstein, Ritz and Jones. *Psychol. Rev.*, 87, 1980, 474–476.

[136] Wu P. Convergent Dynamics in a Network with Competitive Activation Mechanism, Scholarly paper for MA degree in MAPL, University of Maryland at College Park, 1997.

[137] `http://www.m-w.com/cgi-bin/dictionary` The on-line Webster dictionary.